Evaluation of DNA Damage and Endoplasmic Reticulum Stress in Cancer Patients in a Phase 1b Dose-Escalation Trial of Selenium Compounds

A thesis

submitted in fulfilment

of the requirements for the degree

of

Master of Science in Research in Molecular and Cellular Biology

at

The University of Waikato

by

Craig Burns

THE UNIVERSITY OF
WAIKATO
Te Whare Wānanga o Waikato

2025

Abstract

Selenium (Se) is an essential trace element needed in a healthy human diet. Past clinical trials have shown Se to be a promising co-drug for cancer patients undergoing treatment to minimise the effect of the cancer treatment on non-malignant cells. This project is a continuation of a 2019 Phase 1 clinical study "*Comparative Safety, Pharmacokinetic and Pharmacodynamic Evaluation of Three Oral Selenium Compounds in Cancer Patients*", that set out to analyse which Se compound and what dosage point is recommended for use in a Phase 2 clinical trial at the Waikato Hospital, New Zealand.

Nine cancer patients were recruited into the trial from Waikato Hospital with informed consent. They were randomised to take one of three Se compounds, the organic compounds Seleno-L-methionine (SLM) or Se-methyl-selenocysteine (MSC), or the inorganic compound sodium selenite (SS), at a starting dose of 1600 mcg/day for 28 days and then a higher dosage of 6400 mcg/day for another 28 days. Patients were then taken off the compounds and watched for the last 28 days of the trial. Patients were asked to keep a diary and record any adverse events (AEs) that they experienced while on the trial. Western blot methods were used to investigate ER stress, and the LORD-Q assay was used to investigate the genotoxicity of the three compounds. Samples were also sent away for Se speciation studies.

Out of the three compounds, patients on MSC experienced the fewest AEs, with five Grade 1 and two Grade 2 events. SS patients experienced seven Grade 1 and two Grade 2 events. Patients on SLM reported the highest number of AEs, with six Grade 1 and five Grade 2 events. Notably, one case of encephalopathy was observed in the SLM cohort.

In the LORD-Q assay the three Se compounds exhibited sustained mtDNA protection throughout the trial. SLM exhibited fluctuating nDNA lesions at the lower dose. As the concentration increased, no measurable nDNA damage was detected. However, a transient spike in nDNA damage was later observed, followed by a decrease towards the end of the trial. Both SS and MSC exhibited an increase in nDNA relative to the baseline which was sustained throughout the trial.

Western blot analysis was performed in two out of the nine patients to provide a preliminary point of evaluation of ER stress. The western blot data showed a sustained decrease in protein expression of eIF2α and sXBP1 throughout the trial. In contrast, GRP78 decreased throughout the lower dosage phase and then increases in expression at the higher dose point.

The preliminary findings of this thesis suggest that MSC should be the compound recommended to be used in the Phase 2 trial. This is based on findings on adverse events, genotoxicity, and total Se plasma levels. It is important to note that further results are required to elucidate this recommendation.

Acknowledgements

I would first like to thank Dr. Linda Peters for taking me under her wing and allowing me to undertake my Masters. Thank you for your guidance throughout this research, the knowledge and techniques that I have learnt will be carried with me onto future endeavors. Secondly, thank you to Dr. Micheal Jameson for allowing me to join the research team of the Phase 1b Dose-escalation Trial of Selenium Compounds in Cancer Patients, knowing that this research will have real world outcomes has been a big motivation, and to know that I played a small part in the direction future research is a privilege.

No clinical trial can run without the support of research nurses and staff; I would like to extend my gratitude to the people who work behind the scenes. Most importantly thank you to the patients who volunteered to be on this study, your contribution and selfness is appreciated greatly.

Thank you to Dr Geetanjali Rai and Dr. Judith Burrow for their help with any issues, or questions that I had regarding the PC1 and PC2 labs. Thank you for keeping the labs in order and ordering any reagents or supplies that I needed.

Thank you to Cat Turnbull who was the co-adviser on this project. Thank you for teaching me the western blot and the LORD-Q PCR protocol. Your experience and expertise were vital for the outcomes of this project. I don’t just take away your teachings, but I also take away a lifelong friend.

Thank you, Renee Goodall, and Deb Yung, for your support. Thank you for the coffee dates and wordle lunchtimes, they were a perfect reprieve from the pressures of this project. Thank you for the laughs when times got tough. Thank you for your guidance when I was lost.

Thank you to my team leaders at Hill Labs, thank you for being accommodating with my hour changes and allowing me time off when I needed to focus on this project.

And lastly, massive thank you to my partner Anson. Your unwavering support and belief in me during this project were crucial to me starting this chapter in my life. Thank you for taking over the housework while I was busy in the lab or at my computer. Thank you for encouraging me when I felt overwhelmed. Thank you to my wider friends and family for always supporting me and encouraging me to be the best I can be.

Table of Contents

List of Figures

List of Tables

List of Equations

List of Abbreviations

AE	Adverse Events
bZIP	Basic Leucine Zipper
CHOP	C/EBP Homologous Protein
Cys	Cysteine
DMSO	Dimethyl Sulfoxide
dNTPs	Deoxynucleoside Triphosphates
ECL	Enhanced Chemiluminescence
eIF2a	Eukaryotic Initiating Factor 2 alpha
ER	Endoplasmic Reticulum
FBS	Foetal Bovine Serum
GAPDH	Glyceraldehyde-3-phosphate Dehydrogenase
GRP78	Glucose Regulatory Protein 78
HRP	Horseradish Peroxidase
Hsp70	Heat Shock Protein 70
LORD-Q PCR	Long-Run Real Time Polymerase Chain Reaction
Met	Methionine
MSA	Methylseleninic acid
MSC	Methylselenocysteine
mtDNA	Mitochondrial DNA
nDNA	Nuclear DNA
NPC	Nutritional Prevention of Cancer
NZ	New Zealand
TP53	Tumour Protein 53
PBMC	Peripheral Blood Mononuclear Cells
PBS	Phosphate Buffered Saline
PVDF	Polyvinylidene Difluoride
ROI	Region Of Interest
ROS	Reactive Oxygen Species
RT	Room Temperature
S	Sulphur
SDS-PAGE	Sodium Dodecyl Sulphate Polyacrylamide Gel Electrophoresis

Se	Selenium
Sec	Selenocysteine
SECIS	Selenocysteine insertion sequence
SELECT	Selenium and Vitamin E Cancer prevention Trial
SelP	Selenoprotein P
SeMet	Selenomethionine
SLM	Seleno-L-methionine
SS	Sodium Selenite
sXBP1	Spliced x-box binding protein
TBS	Tris-buffered Saline
TBST	Tris-buffered saline with Tween 20
tRNA	Transfer RNA
UPR	Unfolded Protein Response
UTR	Untranslated Region
UVC	Ultraviolet C
VEGF-a	Vascular endothelial growth factor alpha
UoW	University of Waikato
RI	Relative Integrity

Chapter 1 Literature Review

1.1 Introduction

1.1.1 Overview of Cancer

Cancer is a disease which is characterised by the abnormal growth of cells and is defined by six fundamental hallmarks: sustained proliferative signalling, evasion of growth suppressors, resistance to cell death, replicative immortality, induction of angiogenesis, and activation of invasion and metastasis. In addition, two emerging hallmarks have been identified: deregulating cellular metabolism and evasion of immune destruction. These hallmarks are further enabled by two key underlying features- genomic instability within tumour cells and tumour-promoting inflammation (Hanahan & Weinberg, 2000, 2011). Major risk factors for cancer include sun exposure, diet, chemical exposures from pollution, tobacco, or alcohol use (Ames et al., 1995). In malignant tumours these abnormal cells can metastasise to other parts of the body, but benign tumours do not metastasise (National Cancer Institue, 2021).

The indigenous population of New Zealand (NZ), Māori, continue to have poorer survival than non-Māori. The extent of this disparity ranges from 12% to 156% higher mortality risk in the 23 out of 24 most common causes of Māori cancer death. The greatest disparity is in the colon patient group with 46% of Māori patients being more likely to die than non-Māori patients (Gurney, 2020). There were 10,536 cancer deaths recorded in 2022 (TeWhatuOra, 2024). Obertová et al. 2015 noted that Māori men with prostate cancer have a lower survival rate than non-Māori men, with these lower survival rates noticeably lower in the rural areas of NZ (Obertová et al., 2015). New Zealand is known to have low levels of soil Selenium (Se). Se supplementation trials conducted in populations with low baseline Se have shown promising anti-cancer benefits.

The debate on whether Se is a cancer preventative agent, a therapeutic agent, or a carcinogen remains ongoing. Cai et al. (2016). conducted a meta-analysis of high Se exposure and found that elevated Se levels in plasma, serum, or toenails were associated with a reduced cancer risk. However, Se supplementation did not appear to mirror this protective effect. More recently Krannich et al. (2024). performed a systematic review examining Se as a complementary treatment in cancer patients. It was reported that Se supplementation offered no benefit in patients with sufficient baseline Se levels, but those with low baseline Se experienced reduced treatment-related toxicities (Krannich, 2024). Given that low Se intake has been linked to increase cancer incidence and mortality, its relevance in prevention is clear. Equally important, however, is its potential role alongside cancer therapies to reduce toxicity and possibly improve treatment efficacy-an area that forms the focus of this research (Cai et al., 2016).

1.1.2 What is the Purpose of Selenium?

Se is a trace element that was discovered by Jons Jacob Berzelius and Johan Gottlieb in 1817. Berzelius considered Se to be toxic, however, in 1957 Klaus Schwarz, a nutrition scientist found it to be an essential trace element (Kuganesan et al., 2019; Mojadadi et al., 2021; Zeng et al., 2020). As Se cannot be naturally produced in the human body, it needs to be obtained through the diet through the soil plant food chain (Minch, 2022).

New Zealand is known to have low levels of Se in its soil, which can lead to Se deficiencies in the general population (Combs, 2001). New Zealand men have a baseline Se serum level of approximately 112 ng/mL when compared to a population of American men that have Se serum levels of approximately 140 ng/mL (Karunasinghe, 2019). Increased risk of mortality, poor immune function, and cognitive decline are outcomes of Se deficiencies (Rayman, 2012). Thus, Se supplementation can be beneficial to increase Se levels so that it can be incorporated into selenoproteins i.e. any protein that includes a selenocysteine (Sec, U, Se-Cys) amino acid residue. This mechanism of action will be discussed in more detail in **Section 1.2**.

Se is found naturally in organic forms, such as seleno-L-methioine (SLM) and Se-methyl-selenocysteine (MSC) or inorganic forms such as sodium selenite (SS), selenates and selenides. This study investigates two organic compounds SLM and MSC and one inorganic compound SS (**Figure 1**). These compounds were chosen as they have been studied in previous preclinical and supplement studies.

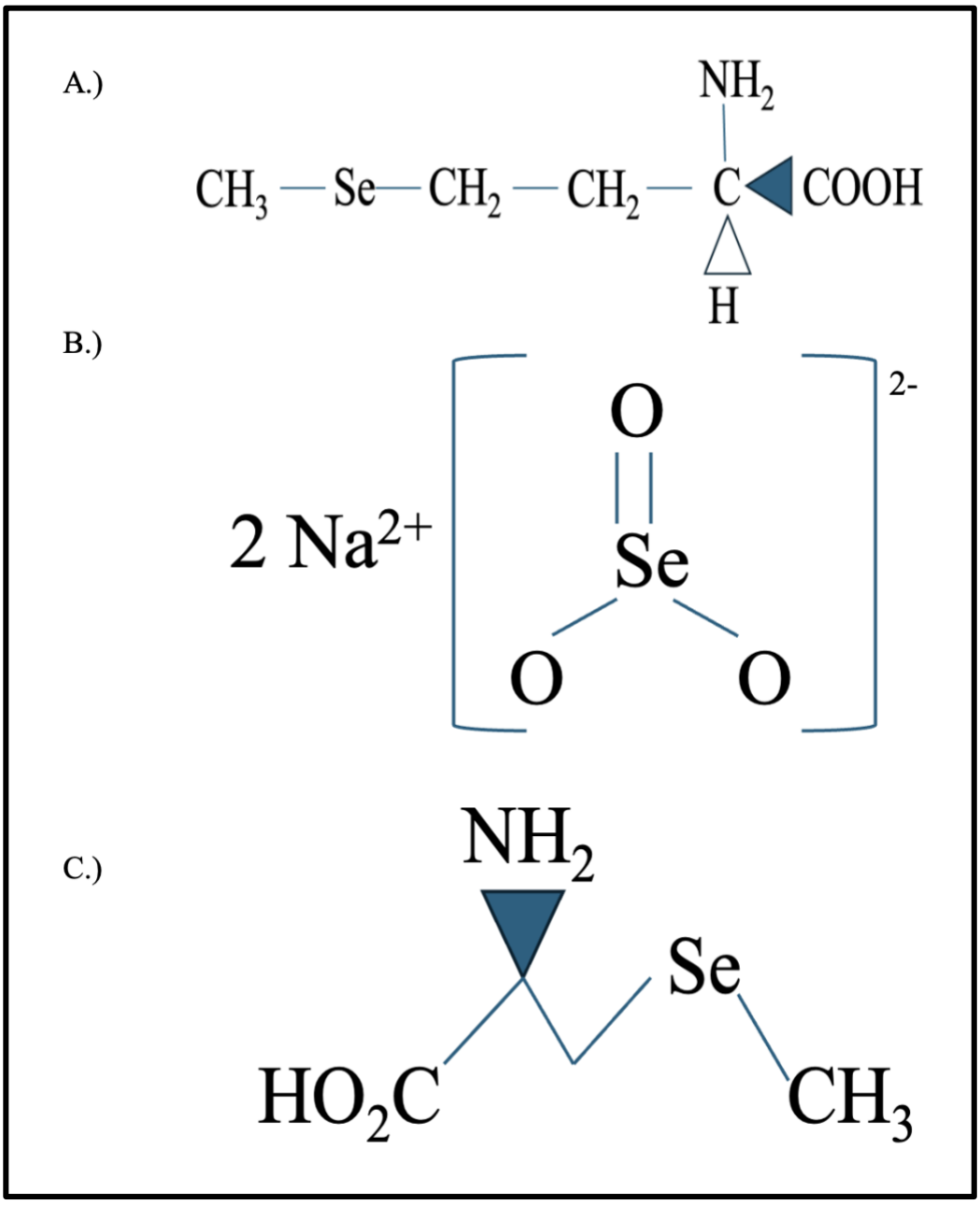

Figure 1 Schematic of the Se compounds used in this study.

A. seleno-L-methioine B. Sodium Selenite C. Se-methylselenocysteine.

1.1.3 Importance of Se in Human Health

The recommended daily dose of Se for the USA population is 55 mcg of Se per day for both men and women (National institutes of Health, 2024). However, the recommended levels are much

higher in NZ populations; 70 mcg/day for men and 60 mcg/day for women (Thomson et al., 2008). Dietary recommendations are based on the Se intake needed to reach the maximum activity of glutathione peroxidase in plasma. Due to the lower availability of Se available in the soil New Zealand has a higher recommended daily dose to compensate this and achieve the same effect of glutathione peroxidase. A 2010 dose escalation study by Hurst et al. (2010) investigated the optimal Se intake in 119 healthy men and women in the United Kingdom, based on total Se plasma levels and levels of selenoprotein P (SelP). They were given either 50, 100, or 200 μg/day capsules of selenised yeast. The mean baseline of total Se plasma levels in participants was 95 ng/mL. Levels of Se plasma increased to 118, 152, and 177 ng/mL with the respective Se doses. SelP baseline was 4.99 μg/mL and increased to 6.17 μg/mL, 6.73 μg/mL, and 6.59 μg/mL based on the respective dosages (Hurst et al., 2010). The findings support the hypothesis of a plateau of 7 mg/L as the doses of 100 and 200 μg/day do not increase above this. This study was also conducted on a population with typically low Se similar to New Zealand.

Se is known to have a U-shaped toxicity curve (**Figure 2**), meaning it has adverse health effects at both low and high levels (Rayman, 2012). A study conducted in 2008 analysed the Se serum levels in a USA population, which already has a higher baseline Se intake. It was found that both low and high levels of serum Se levels exhibited higher mortality rate. In the intermediate levels, approximately 120-130 μg/L mortality was found to be the lowest (Bleys, 2008).

The PRECISE study conducted in Denmark, a region with low Se levels in its soil, gave 491 participants 100 μg/day, 200 μg/day, and 300 μg/day doses of selenised yeast over a period of five years. The study identified that a long-term dose of 300 μgSe/day in the form of selenised yeast increased cancer and cardiovascular mortality (Rayman et al., 2018). It is important to note that these three supplementary studies are investigating Se doses in healthy populations.

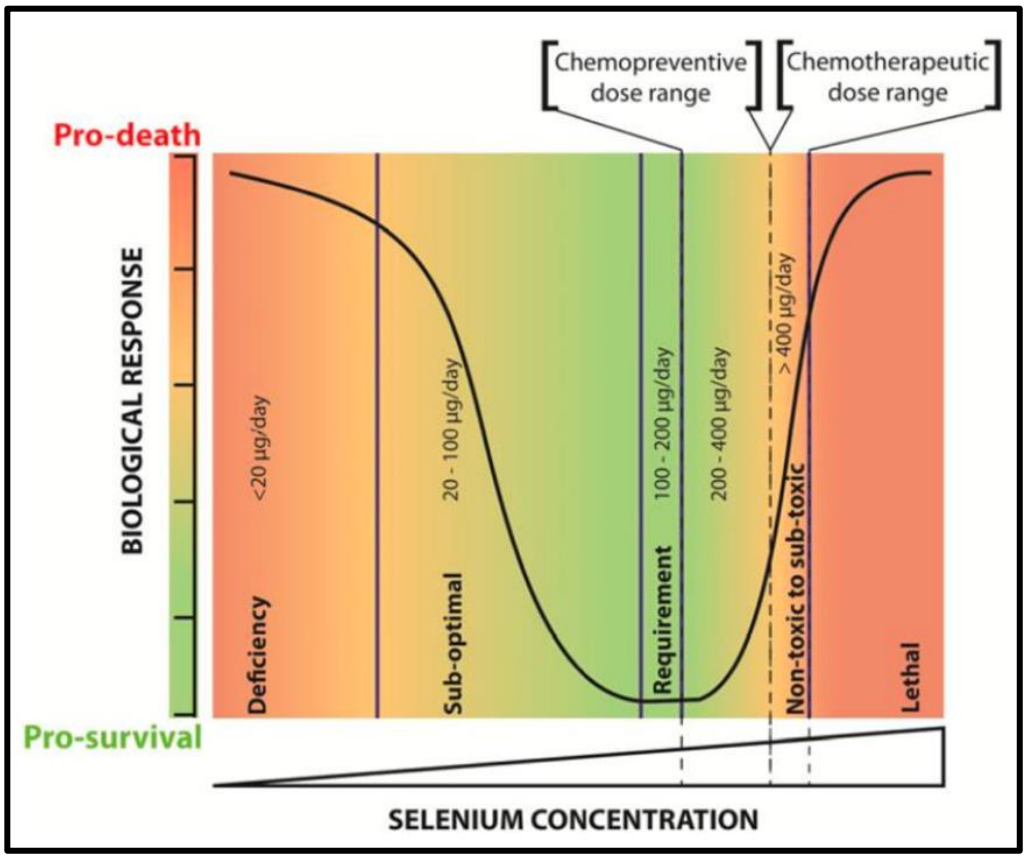

Figure 2 Se tolerances.

Chart shows Se tolerances from pro-survival (green) to pro-death (orange) and the U-shaped curve showing optimal Se at 100-200 mg/day. (Wallenberg et al., 2014).

There are also indications that organic Se is more bioactive than its inorganic counterpart. Animal studies suggest that inorganic Se is more genotoxic than the organic compounds which are not only safer but are more effective (Mojadadi et al., 2021). In addition, excessive Se intake in humans can cause development of Type 2 diabetes, fertility issues, garlicky breath, and hair loss (Hadrup & Ravn-Haren, 2023).

Risks that are associated with severe Se deficiency include Keshan disease (cardiomyopathy, a heart muscle disorder), Kashin-Beck disease (arthritis), male infertility, dysregulation of selenoproteins that trigger a higher production of reactive oxygen species (ROS) which impairs cellular growth, and male and female fertility (Wang, 2023).

1.2 The Synthesis of Selenium Proteins

1.2.1 Absorption of Se

Se is absorbed in the cecum of the large intestine and in the duodenum of the small intestine. The absorption has three different modes depending on the Se compound. For example, the inorganic selenites are absorbed by simple diffusion, whereas selenides are absorbed by secondary active transport also known as cotransport (Mehdi et al., 2013). Organic Se is absorbed by active transport, for example, SLM uses a sodium-dependent pump similar to the way methionine (Met) is absorbed (Schrauzer, 2000).

1.2.2 Metabolism of Se

Organic and inorganic Se is converted to selenide. It is from there that it is further incorporated into selenoproteins (Mojadadi et al., 2021). Organic Se is metabolised by class 4 enzymes γ or β lyase. These enzymes cleave the bonds of C-C, C-O, and C-N. They do this differently from the usual methods of oxidation and hydrolysis (Medicine, 2025). In comparison, inorganic Se is reduced by glutathione and glutathione reductase.

There are four different pathways by which Se compounds are converted into hydrogen selenide and the pathway depends on the compound. The four main pathways are shown below in **Figure 3**. Firstly, SLM is converted to selenocysteine where it is converted to hydrogen selenide by selenocysteine β-lysase (del Castillo Busto et al., 2024; Rataan et al., 2022).

Selenite can undergo two different pathways to produce hydrogen selenide; (1) reduction via thioredoxin reductase and thioredoxin to produce hydrogen selenide; (2) conversion into glutathioselenol where it is converted into hydrogen selenide (del Castillo Busto et al., 2024; Rataan et al., 2022). MSC once absorbed is transformed into methylselenol which is an important

anticancer metabolite. Methylselenol can undertake two pathways, it can either be methylated to form the volatile Se compounds dimethylselenide which is excreted by the breath, which is the noted garlic breath or trimethylselenouim ion which is excreted through urine (Marshall et al., 2017). Alternatively, it can be demethylated to form hydrogen selenide (del Castillo Busto et al., 2024) which is then converted into selenophosphate by the enzyme selenophosphate synthetase and this can be incorporated into the synthesis of selenoproteins (Rataan et al., 2022; Tobe & Mihara, 2018). Hydrogen selenide is then phosphorylated to form selenophosphate. Selenophosphate then converts pser-tRNA to sec-tRNA with selenocysteine synthase (Manta et al., 2022).

These metabolic differences are important to understand the distinct safety and efficacy profiles observed in this trial. The efficiency that MSC has to convert to the anti-cancer metabolite methylselenol and the efficiency that both MSC and SS have to convert to hydrogen selenide will be observed in the results.

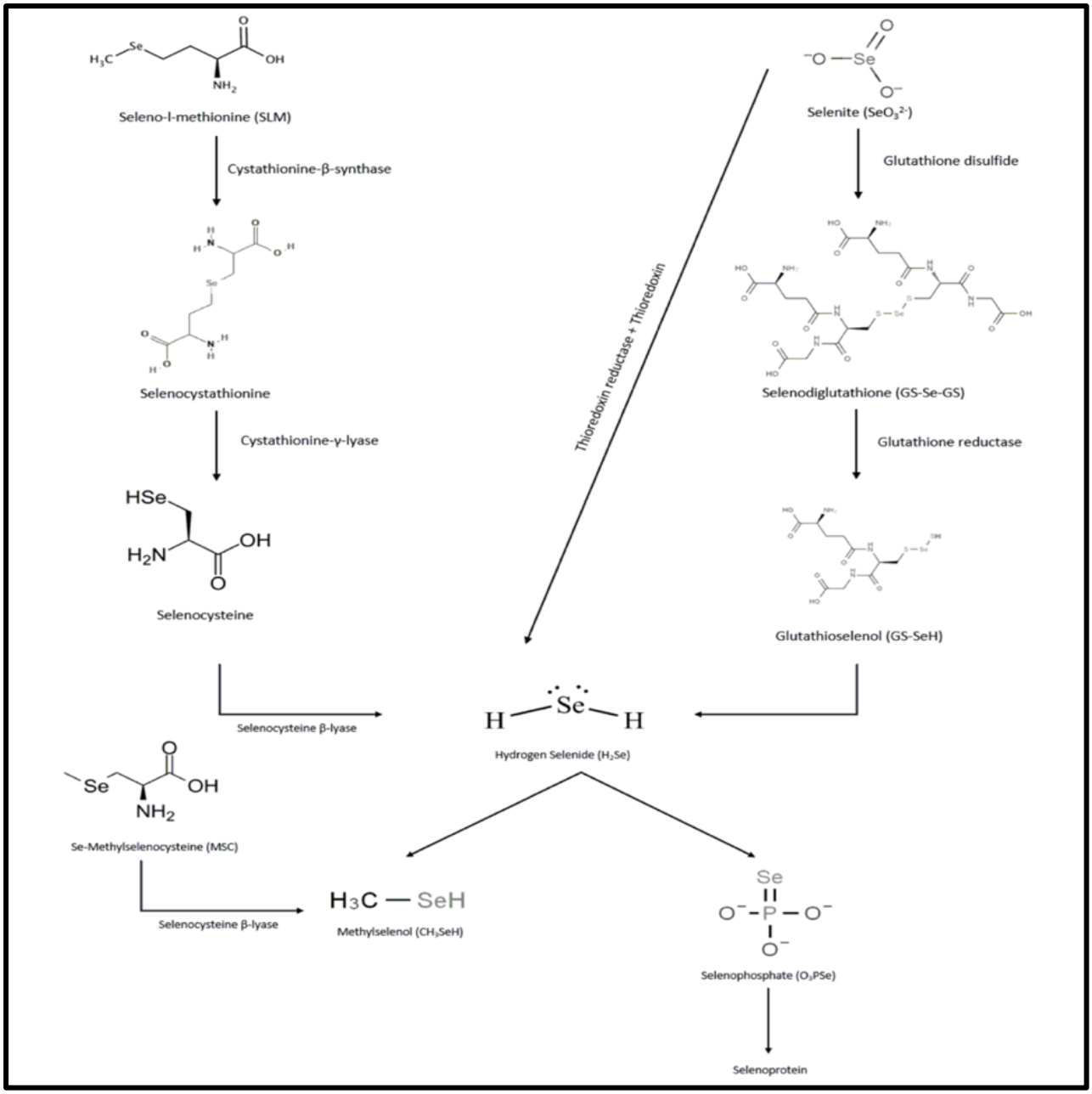

Figure 3 Biochemical pathway of MSC, SLM, and SS.

Figure shows the biochemical pathway of each of the Se compounds of interest. (Rataan et al., 2022).

1.3 Selenoproteins

1.3.1 Selenoprotein formation

Selenium proteins (selenoproteins) are any protein that contains a selenosysteine (Sec, U, Se-Cys) amino acid residue. Sec is a proteinogenic amino acid, which are amino acids that are biosynthetically incorporated into proteins. Sec is homologous to the amino acid cysteine (Cys), they both share the same structure however Cys contains a S atom in the place of a Se atom. Because they are so similar in structure Sec can substitute Cys during protein synthesis. This substitution can result in either an increase or decrease in enzymatic activity of the enzyme in question (Kim & Gladyshev, 2005).

Two important motifs are involved in the synthesis of Selenoproteins; (1) sec-tRNA$^{[ser]sec}$ and (2) selenocysteine insertion sequence (SECIS). The sec-tRNA$^{[ser]sec}$ is a specialised transfer RNA (tRNA) that contains an anticodon complementary to the UGA codon (**Figure 4**). While the UGA codon typically serves as a stop codon, in this context, it functions as the codon site for the sec-tRNA$^{[ser]sec}$. Firstly tRNA^{sec} is converted to ser-tRNA^{sec} by seryl-tRNA synthetase (SerRS). ser- tRNA^{sec} is then phosphorylated by phosposeryl-tRNA^{sec} kinase (PSTK). Then, sep- tRNA;sec tRNA synthetase (sepsecs) converts the SerP complex to Sec (**Figure 4**). The elongation factor ser (EFser) then allows the sec-tRNA$^{[ser]sec}$ to localise and bind to the UGA codon (Bulteau & Chavatte, 2015; Wright & O'Donoghue, 2023).

The SECIS forms a stem-loop-stem-loop structure of approximately 100 nucleotides in the 3'untranslated region (UTR) of the mRNA. This structure creates a hairpin loop located downstream of the Sec-encoding UGA codon. The hairpin loop extends outwards, providing a binding site for the Sec insertion sequence binding protein 2 (SECISP2) to bind. This protein also interacts with the EFser protein and co-localises the tRNA$^{[ser]sec}$ to the UGA codon (Kalimuthu et

al., 2022; Wright & O'Donoghue, 2023). The below diagram shows the formation of these motifs (**Figure 4**).

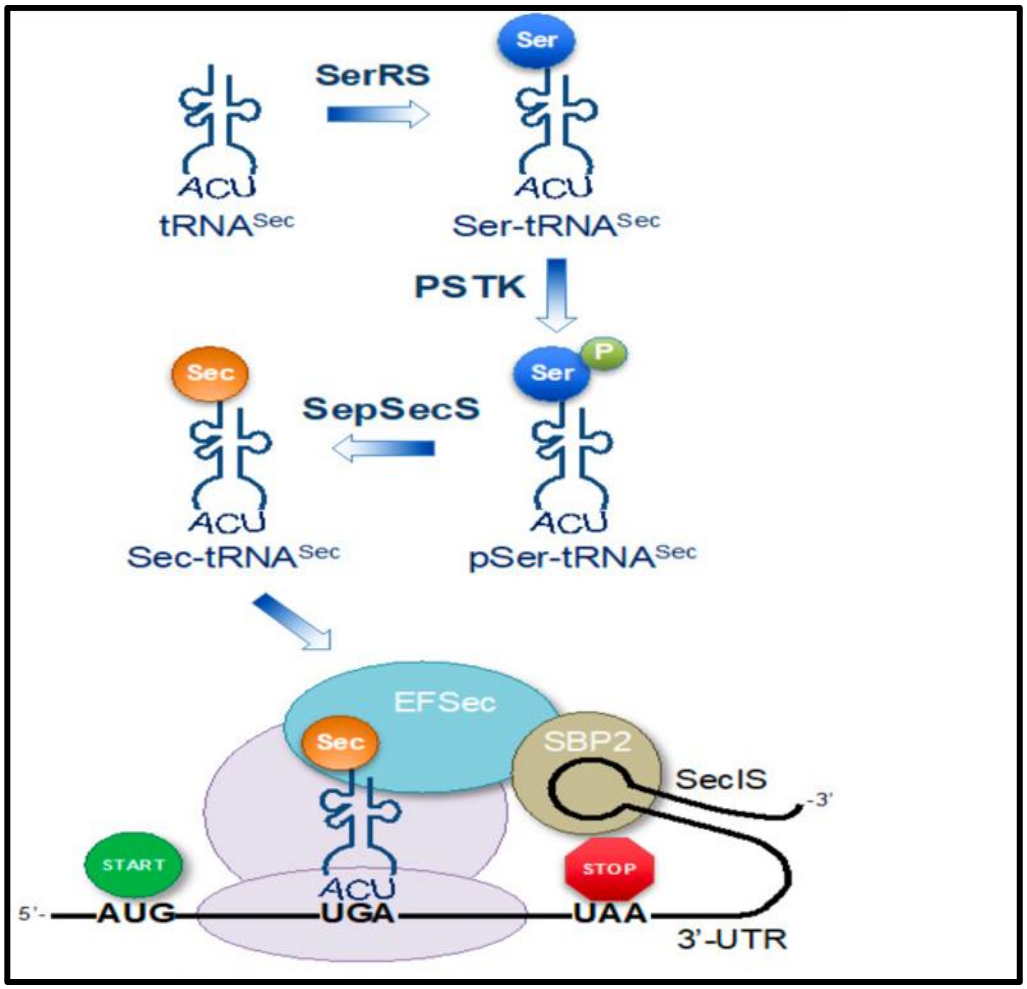

Figure 4 Schematic diagram of the incorporation of Sec into a protein.

(Wright & O'Donoghue, 2023).

Shetty et al. demonstrated the importance of the SECIS sequence by deleting the pre-and inter-SECIS in the SELENOP mRNA sequence. SelP was chosen as the candidate for this study because it contains two SECIS instead of the usual one plus it has ten Sec codons. The researchers found that the polypyrimidine tract binding protein (PTBP1) plays a crucial role in the biosynthesis of SelP by binding to the conserved region of the interSECIS and making the translation of SelP more efficient. Additionally, they also observed that deleting the inter-SECIS

region led to a decrease in SelP mRNA levels, whereas the pre-SECIS cells showed only a smaller decrease when compared to the wild type cells (Shetty et al., 2022).

UGA recoding is still being widely studied and is not fully understood. Many other elements are still being discovered and elucidated. There are many complex components to selenoprotein synthesis. Some of those components are nucleolin, L30, EIF4A3, and PTBP1. These components are still being studied to elucidate their full functions (Copeland & Howard, 2021).

1.3.2 Types of Selenoprotein

There are currently 25 known selenoproteins in the human body. **Table 1** summarises the selenoprotein with respect to the abbreviation, function, Sec location and protein molecular weight. For the purposes of this study, we will focus on 11 selenoproteins (in bold) including the first protein to be discovered, Glutathione Peroxidase 1 (GPx1) in 1957 (Pei et al., 2023).

Table 1 Summary of the 25 Selenoproteins.

Adapted from (He et al., 2025).*Selenoproteins relevant to this research study are highlighted in bold.

Selenoprotein*	Abbreviation	Function	Sec Location	Protein Size (kDa)
Glutathione peroxidase 1	GPx1	Metabolises hydrogen peroxide (H_2O_2) and some organic hydroperoxides	47	201
Glutathione peroxidase 2	GPx2	Antioxidant activity in gastrointestinal tissues	40	190
Glutathione peroxidase 3	GPx3	Reduces H_2O_2, fatty acid hydroperoxides, and phospholipid hydroperoxides in the plasma and thyrocytes	73	226
Glutathione peroxidase 4	GPx4	Reduces phospholipid- and cholesterol-hydroperoxides by using GSH	73	197
Glutathione peroxidase 6	GPx6	Reduces olfactory organs H_2O_2	73	221
Thioredoxin reductase 1	TrxR1	Antioxidant activity and regenerate reduction of thioredoxin	498	499

Selenoprotein*	Abbreviation	Function	Sec Location	Protein Size (kDa)
Thioredoxin reductase 2	TrxR2	Regenerates reduced thioredoxin in mitochondria	655	656
Thioredoxin reductase 3	TrxR3	Redox regulation	522	523
Iodothyronine deodinase 1	DIO1	Production of T3 in thyroid and peripheral tissues	126	249
Iodothyronine deodinase 2	DIO2	Production of T3 in peripheral tissues	133,266	273
Iodothyronine deodinase 3	DIO3	Inactivates thyroid hormone	144	278
Methionine-R-sulfoxide reductase	MSRB1	Restores oxidatively damaged methionine (Met-sulfoxide) to native configurations	95	116
Selenophosphate synthetase 2	SEPHS2	Sec synthesis	60	448
Selenoprotein F	SelF	Oxidoreductase that may assist in disulfide formation and protein folding/Correcting misglycosylated	93	162
Selenoprotein H	SelH	Cell cycle regulation & cancer prevention	38	116
Selenoprotein I	SelI	Phospholipid biosynthesis	387	397
Selenoprotein K	SelK	Antioxidant activity/immunity/inflammation	92	94
Selenoprotein M	SelM	Maintenance of Ca^{2+} ions/Antioxidant activity	48	145
Selenoprotein N	SelN	Growth and development of muscles	428	556
Selenoprotein O	SelO	Regulation of redox reactions	667	669
Selenoprotein P	SelP	Transportation of Se to brain and other tissues of the body	59,300,318,330, 345, 352, 367, 369, 376, 378	381

Selenoprotein*	Abbreviation	Function	Sec Location	Protein Size (kDa)
Selenoprotein S	SelS	Deletes the misfolded proteins in endoplasmic reticulum (ER) and responds to ER stress	188	189
Selenoprotein T	SelT	Regulation of endocrine secretion/Ca^{2+} mobilisation	36	182
Selenoprotein V	SelV	Expression of taste/Regulation of redox reactions	273	346
Selenoprotein W	SelW	Oxidative stress regulation, Bone remodeling	48	145

1.3.3 Thioredoxin Reductase

One selenoprotein that has been widely studied is thioredoxin reductase (TrxR). These enzymes are part of the thioredoxin system, which is known for its major antioxidative role in defending against oxidative stress (Ryuta et al., 2012). TrxR catalyses the NADPH-dependent reduction of thioredoxin (Trx) and other oxidised dithiols (**Figure 5**). Two enzymes that belong to the TrxR family are Thioredoxin reductase 1 (TR1) and Thioredoxin reductase 2 (TR2), and they are expressed in the cytosol and mitochondria.

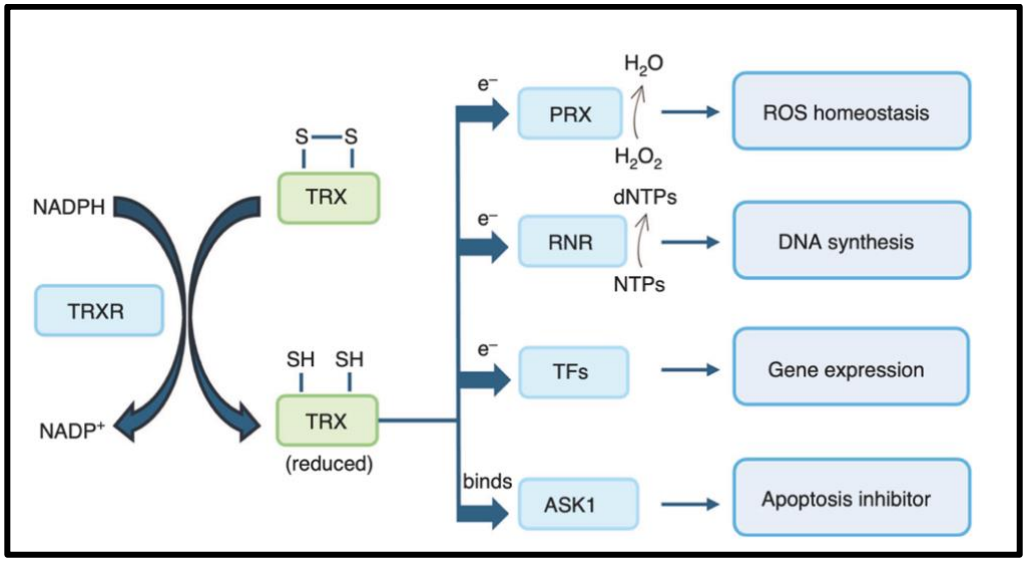

Figure 5 The biochemical reaction of thioredoxin reductase.

(Sudhadevi & Harijith, 2024).

These enzymes play a role in a wide range of functions, including transcription, cell proliferation, embryogenesis, DNA repair, angiogenesis, and cell signalling (Ryuta et al., 2012). Although TR1 has a broad range of substrates, it is the only enzyme capable of reducing Trx. TR1 has two main active sites that are positioned in the N-terminal and the C terminal site. The N terminal site contains two Cys resides at amino acid positions 59 and 64. The C terminal site contains a Cys and sec at sites 497 and 498, respectively. Because the C terminal contains a Sec residue, it is more reactive and has a higher substrate specificity (Jackson-Rosario & Self, 2010; Lee et al., 2000). The Sec is located at amino acid position 498 and lies beneath the side chain of Tyr-116.

Once reduced, the Sec is repositioned toward a solvent exposed orientation which is closer to the active site, which aligns with the enzyme's functionality (Cheng et al., 2009).

TR1 is a crucial component for the P53 pathway. TR1 reduces TrxR which in turn reduces redox factor 1. Redox factor 1 in its reduced form induces the transcription factor Tumour Protein P53 (TP53) that serves as a critical barrier to carcinogenesis by activating the target gene *p21* which is important in regulating cell cycle and progression and the DNA damage response (Seemann, 2005). The TP53 pathway has been shown to supress tumour development (Boutelle & Attardi, 2021) and inactivation of this gene is a key contributor to sporadic cancers (Olivier et al., 2010).

TP53 functions as a cellular stress sensor. In unstressed cells, TP53 is degraded by the nuclear-localised E3 ubiquitin ligase MDM2 Proto-Oncogene enzyme (MDM2); however, in stressed cells, MDM2 is relieved from TP53, allowing TP53 to bind to DNA and activate the transcriptional machinery. TP53 promotes G1 cell cycle arrest, facilitating either DNA repair or apoptosis to eliminate damaged cells (Boutelle & Attardi, 2021).

TR1 is highly expressed in many tumour cells (Yoo et al., 2006). Due to the antioxidant properties of this enzyme, tumours upregulate its expression to combat the high levels of ROS generated in the tumour microenvironment. A study on the mouse lung carcinoma cell line (LLC1), demonstrated that knocking down *Tr1* using RNA interference resulted in a dramatic reduction in tumour growth and metastasis (Yoo et al., 2006).

A study by Hedstrom et al. (2009) investigated the effects a low molecular weight molecule known as RITA. It was found that RITA forms a complex with TR1, inhibiting the enzymes antioxidant properties. As a result, ROS levels increased, leading to apoptosis in tumour cells

(Hedström et al., 2009). Thus, with this interaction of TR1 within the tumour microenvironment it was considered to be a good biomarker for cancer research.

TR1 has a duality when it comes to oncology. It is a vital component in cancer suppression with its role in the TP53 pathway but is also being studied as a therapeutic target in cancer patients.

1.3.4 Glutathione Peroxidase

Another member of the selenoprotein family is the glutathione peroxidase (GPx). One well-studied member of this family is glutathione peroxidase 4 (GPx4). The catalytic cycle of GPx4 is carried out in two steps: an oxidation reaction followed by a reduction reaction. In the oxidation step, the Sec residue is oxidised into selenic acid. This step reduces toxic lipid hydroperoxides to their respective alcohols. Notably, this reaction takes place without forming a typical enzyme-substrate complex. The reduction phase occurs in two steps; (1) the first glutathione molecule reduces selenic acid, forming the intermediate selenium-glutathione and releasing water as a by-product; (2) a second reduced glutathione molecule further reduces the intermediate, regenerating the selenol form of the enzyme and producing glutathione disulphide as a by-product. After this step the GPx4 protein is ready to repeat the catalytic cycle. (**Figure 6**) (Weaver & Skouta, 2022).

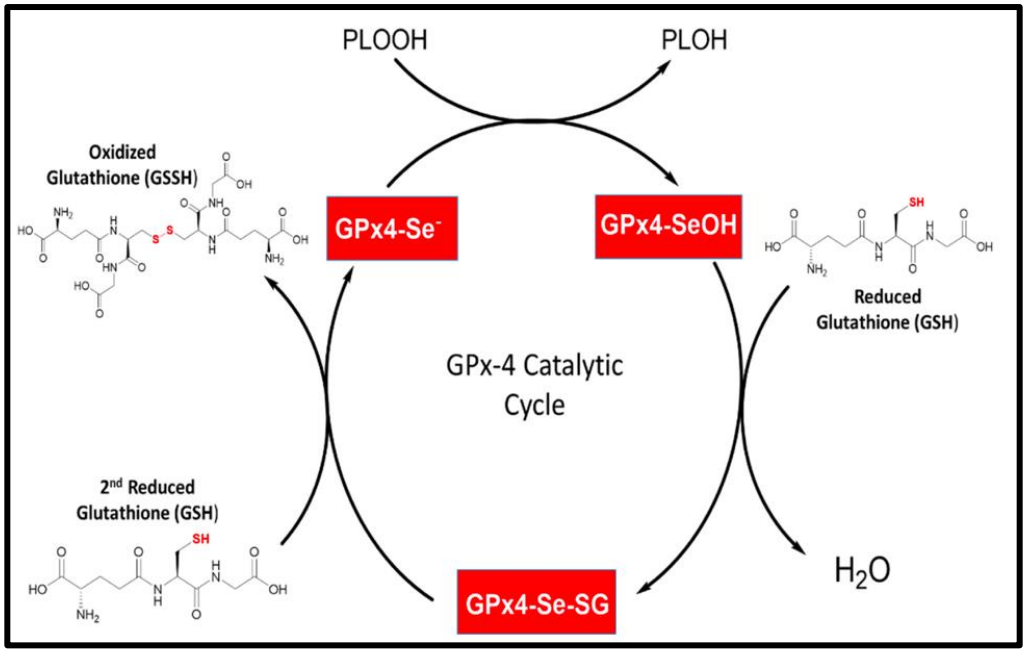

Figure 6 The catalytic cycle of GPx4.

(Weaver & Skouta, 2022).

GPx4 has dual effects on cancer treatment. Cancer cells express high levels of GPx4 as an antioxidant to combat oxidative stress in the microenvironment. A 2023 study investigated GPX4 expression levels in thyroid cancer tissues. When compared to normal tissues, thyroid cancer tissues expressed higher levels of GPX4. When GPX4 is knocked down supressed proliferation and ferroptosis is induced in thyroid cancer cells. It was also noted that cancer patients with over-expressed GPX4 had poorer survival outcomes to those with lower GPX4 levels (Chen, 2023).

A 2024 study investigated Se as a co-treatment alongside cisplatin. The aim was to determine whether increased GPX4 expression from Se supplementation could alleviate one of cisplatin's side effects, acute kidney injury, in which ferroptosis, a type of programmed cell death dependent on iron, is believed to play a role. The study found that using Se co-treatment elevated GPX4 levels, which in turn counteracted ferroptosis and alleviated the side effects of cisplatin (Li, 2024).

Both these studies show how levels of GPX4 can have different outcomes depending on if the target cell is malignant or non-malignant. GPX4 is needed to be knocked down in malignant cells for better outcomes whereas GPX4 needs to be elevated in non-malignant cells to protect against chemotherapy treatments.

A 2022 study by Liu et al. (2022) demonstrated that overexpression of *GPX4* negatively regulates ferroptosis in colorectal cancer cells. The researchers overexpressed a microRNA (miR-15a-3p), which in turn repressed *GPX4* by binding to its 3-untranslated end. This repression reduced ferroptosis in the cancer cells (Liu et al., 2022), supporting the hypothesis that excessive Se intake can be detrimental to human health. Furthermore, Sekhar et al. 2022 investigated the relationship between GPx4 and ferroptosis in thyroid cancer cells. They found that inhibiting *GPx4* activity with a small molecule, RSL3, induced ferroptosis (Sekhar et al., 2022). These studies highlight that raising GPX4 using Se supplementation can be harmful in cancer and beneficial in non-cancer cells.

1.3.5 Iodothyronine Deiodinases

Iodothyronine deiodinase are transmembrane selenoprotiens that regulate thyroid hormone levels by catalysing the removal of iodine atoms from thyroid hormones. The organ with the highest amount of Se per unit of tissue is the thyroid gland (Köhrle et al., 2005). There are three isoforms; DIO1 (29kDa), DIO2 (33kDa), and DIO3 (34kDa) and they share a fold structure similar to TrxR (Rodriguez-Ruiz et al., 2022). The main function of DIO1 and DIO2 is to convert the inactive thyroxine (T4) to the biologically active triiodothyronine (T3). DIO1 and DIO2 catalyse the reaction in the outer ring (**Figure 7**) which removes the iodine atom this is known as "*outer ring deiodination*." DIO3 converts T4 to the inactive reverse T3 (rT3). It does this by removing the iodine atom from the inner ring and this is known as "*inner ring deiodination*." DIO1 is a special case where it can perform both inner and outer deiodination. Due to the specificity of DIO2 it has a 700-fold greater efficiency than DIO1 at converting T4 to T3 (Maia et al., 2011).

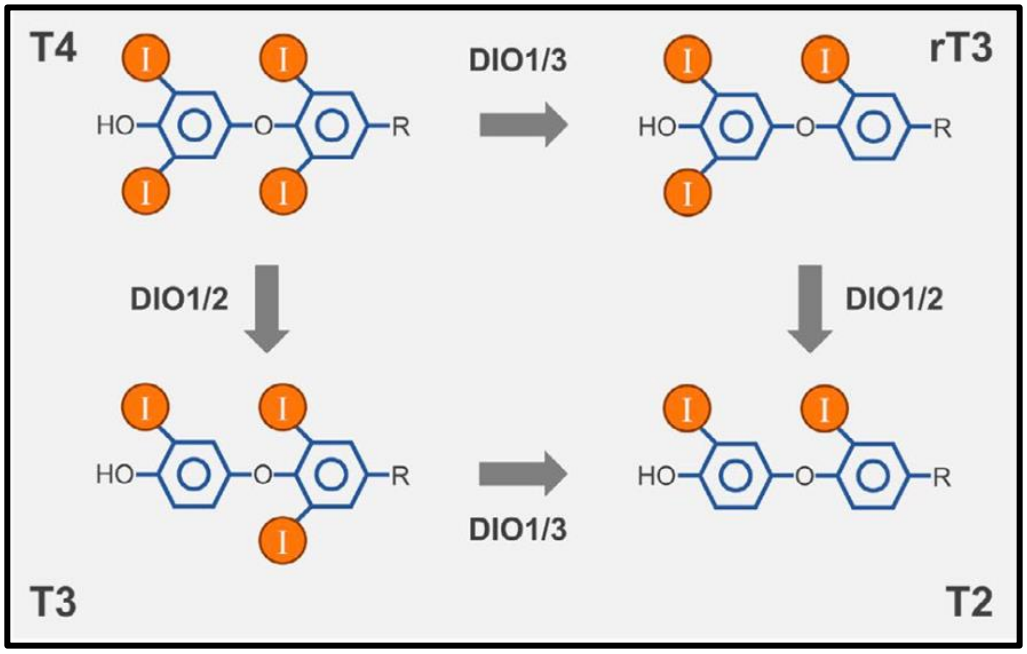

Figure 7 Diagram of the reaction pathways of the DIO enzymes.

(Kojima et al., 2019).

In circumstances where the levels of T4 become in excess, T4 will covalently bind to DIO2 which blocks the active site and reduces the production of T3. This is because as the active site is more readily exposed this gives a chance for the small protein ubiquitin to bind to a lysine on DIO2 and form a K48 linkage which leads to proteasomal degradation (Russo et al., 2021).

DIO1 has a selenenyl-sulfide bond between the Cys 124 and Sec 126. Studies that substitute the Sec 126 for Cys note less activity in the protein. The Se in the Sec plays a role in attacking the iodine and forming a Se-I bond (Rodriguez-Ruiz et al., 2022). The active Sec residue is at amino acid position 133 in DIO2 protein (Köhrle et al., 2005) compared to amino acid position 144 in DIO3 protein. As with the other two enzymes a substitution of Sec with Cys in the active site lowers the enzymes activity substantially. The lowered activity with Cys substitution is due to the Se atom in Sec being more nucleophilic than the S in Cys.

DIO1 has been shown to have anti-tumour properties. Alfandari et al. (2024) investigated the expression levels of DIO1 using two ovarian cancer cell lines; ES-2 and Kuramochi plus normal human fallopian tube cells, FT282 and FT109 along with normal Chinese hamster ovarian cells, CHO-K1. It was shown that human ovarian cancer cells expressed lower levels of DIO1 compared to the normal human and hamster cells. It was also found that lower mRNA levels resulted in worse survival and knocking out the gene or inhibiting the protein increased ovarian cancer proliferation (Alfandari et al., 2024).

A study that used mouse models with the strain $Apc^{\Delta 716}$, where there was a stop codon introduced at amino acid position 716 to cause the *Apc* gene to truncate, was used to investigate the relationship between DIO2 and colorectal cancer. Mice were treated with either ioponaic acid, an inhibitor of DIO2 or chemically suppressing the thyroid gland with a mixture of 2-mercapto-1-methyl-imidazole and potassium perchlorate. It was found that both treatments reduced the

number of small intestinal polyps. As the number of polyps was reduced survival time also increased. RT-PCR analysis of the small intestine polyps showed that *DIO2* mRNA levels were elevated in the polyps. An analysis of the cancer genome atlas shows that *DIO2* is upregulated in colorectal cancer (Kojima et al., 2019).

It has been documented that cancer patients with higher expression of DIO3 have a lower survival rate. This is because the substrate which DIO3 acts upon, T3, has tumour suppressor properties. This led to a preclinical study that used an inhibitor of D3, DBM, which has Bromine present and has a higher affinity for DIO3 as opposed to the Iodine that is present on T3. The study found that ovarian cancer cells had induction of apoptosis, lower cell count and lower cell proliferation. They noted that these adverse effects were not present in the healthy control cells (Moskovich et al., 2021).

A clinical study conducted between 2017 and 2021 studied metastatic urothelial carcinoma patients undergoing immune checkpoint inhibitor treatment. Patients had their thyroid function analysed and compared the ratios of free T3 and free T4 (fT3/fT4) (Pierantoni et al., 2023). It was found that a low fT3/fT4 ratio led to a low survival rate and worse progression free survival and overall survival, compared to patients that had a higher ratio of fT3/fT4 that showed a greater response to treatment and had higher survival rates (Pierantoni et al., 2023). A complementary study was conducted between April 2018 and May 2023 where they compared the fT3/fT4 ratio in advanced non-small cell lung cancer patients. These findings were similar to that of the previous study in that a higher fT3/fT4 ratio led to a better outcome for the patient's undergoing treatment. It was noted that there was an increase in fT3 and a decrease in fT4. fT3 is the biologically active hormone compared to the inactive fT4 (Nelli et al., 2024). The findings from these clinical studies could suggest that with a greater DIO activity, and thus Se, could improve patient outcomes with immunotherapy treatments.

1.3.6 Selenoprotein P

Selenoprotein P (SelP) was first discovered in 1973. It is one of the major Selenoproteins found in plasma. SelP has two main functions to; (1) transport Se to the cells throughout the body and (2) reduce phospholipid hydroperoxide like GPx. There are three SelP receptors that have been identified; (1) Low-Density Lipoprotein (LDL) Receptor Related Protein 8 (LRP8) is found in the neurons (2) LDL Receptor Related Protein 2 (LRP2) found in the kidneys and brain and (3) LDL Receptor Related Protein1 (LRP1) in skeletal muscle (Saito, 2021). These receptors are used by cells to uptake SelP and release Se as selenocysteine to the cells.

SelP is used widely in Se supplementation studies as a biomarker of Se status. SelP is used as a biomarker as it reflects the Se bioavailability and the saturation of functional Se transport and utilisation pathways. Total Se plasma levels will rise indefinitely however SelP levels have a plateau that once met indicates that Se-dependent enzymes for example glutathione peroxidase are fully saturated. This plateau has been widely accepted as a functional biomarker of adequate Se supply. Different Se compounds will vary in how efficiently they raise SelP levels.

Past studies have noted that 5-7 mg SelP/L is the maximum concentration achieved. However, a study in 2020 hypothesised that this was not the maximum limit as they used samples from two clinical trials that utilised a high selenite dosage. Patients that were receiving Selenite supplementation intravenously (IV) had a much higher level of SelP in their plasma, with some levels were higher than 10 mg/mL exceeding the previously reported 5-7 mg/L ceiling (Brodin et al., 2020).

The next section will provide a more in-depth insight into the progress of Se supplementation in human cancer clinical trials.

1.4 Human Se Supplementation Clinical Trials

With regards to Se research, two main approaches can be distinguished. The first involves supplementation trials which examine nutritional doses aimed at preventing cancer and improving overall health. The second involves high-dose supranutrational trials that investigate whether Se can improve cancer outcomes and reduce the toxicity of cancer treatments. A 2016 meta-analysis investigating the relationship between Se and cancer identified 69 published studies (Cai et al., 2016).

1.4.1 Supplement Trials

One notable study is the Nutritional Prevention of Cancer (NPC) trial, conducted between September 1983 to January 1993 in the Eastern and Southern states of the United States of America (USA). The trial included 1,312 patients at high risk for non-melanoma skin cancer, who were given 200 μg/day of selenised yeast tablets. The results showed no statistically significant relationship between Se supplementation and the risk of basal cell carcinoma. However, the study did indicate an elevated risk of cutaneous squamous cell carcinoma. Despite this, the overall incidence of cancer was lower in the treatment group compared to the placebo group, suggesting that Se supplementation may have some cancer prevention effects. Interestingly, the results of the NPC trial were inconsistent with previous studies that reported an association between Se plasma levels and protection from non-melanoma cancer (Duffield-Lillico et al., 2003; Reid et al., 2008). Further analysis of the NPC trial found that men with a baseline PSA concentration >4 ng/mL had a lower incidence of prostate cancer, as did those with baseline plasma Se concentrations < 123 ng/mL (Duffield-Lillico et al., 2003).

The next major Se supplementation trial was conducted between March 1986 through to May 1991 investigating the population in Linxian, China. This region was chosen due to the rates of squamous oesophageal and adenomatous gastric cardiac cancers. Participants were given an oral capsule containing 50 μg Se, 30 mg vitamin E, and 15mg of β-carotene this compound mixture was called "*factor D*." They observed the Se serum levels of the participants and noted that participants that had baseline levels of serum Se in the higher quartiles had a lower incidence of the two cancers that were being examined. Benefits were mainly observed up to a certain Se concentration. No further risk reduction was noted above these levels which indicates a plateau (Mark et al., 2000). A ten year follow up showed that participants on factor D had a reduced mortality by 5% and reduced gastric cancer mortality by 11%. These benefits were persistent 10 years after the supplementation trial ended. These protective effects were concentrated in participants <55 years old. Some limitations with these findings are that factor D is a combination of Se, vitamin E, and β-carotene. It is hypothesized that the sustained benefits were from Se and vitamin E as β-carotene has been linked to harm in other trials (Qiao et al., 2009).

The Selenium and Vitamin E cancer prevention trial (SELECT) study investigated how Se, vitamin E, or both, could be used to protect men from developing prostate cancer. They recruited 35,533 men across three countries; USA, Canada, and Puerto Rico. They were given 200 μg/day of Se in the form of SLM. No relationship was identified showing that Se reduced the risk of developing prostate cancer (Rataan et al., 2022). The SELECT trial was abandoned 5 years before the end date due to the concerns that participants that were on the Se only dose were at risk of developing Type II diabetes (El-Bayoumy, 2009; Ledesma et al., 2011).

1.4.2 Supernutrition Trials

Many preclinical trials have been conducted on Se compounds to investigate their use as a selective modulator in chemotherapy. Studies have focused on the dose and scheduling of administering the Se compounds. One study found that administering MSC and SLM seven days before chemotherapy yielded greater antitumor benefits than administering the compounds on the first day of chemotherapy. Based on these findings the trial is being moved to a Phase 1 clinical trial at Roswell Park that used SLM as the chosen Se compound at doses of 2,500, 3,000, 4,000, and 5,000 μg with the chemotherapy drug axitinib (Zakharia et al., 2019). Another preclinical trial investigated the use of SS as a co treatment with gemcitabine in pancreatic cell lines. It was found that SS demonstrated efficacy of increasing survival both alone and in combination with gemcitabine (Doello, 2021).

In a 2009 commentary article by Professor Karam El-Bayoumy, Penn State Centre for Research on Tobacco and Health, USA, he argued that Se should not be discredited and rather examine more closely regarding dosages and types of Se being used (El-Bayoumy, 2009). Thus, a 2017 supranutitional clinical trial was conducted by Marshall et al. investigated more closely the relationship between SLM and MSC. Their reasoning was that the SELECT trial used pure SLM as opposed to the NPC trial which used a yeast which usually contains a mix of SLM and MSC and this is probable as to why the SELECT trial did not give the desired results. They conducted a double-blind trial on 29 Se replete healthy men and used the two compounds SLM and MSC. They found that participants that were on the SLM drug achieved a much higher level of plasma Se than those on MSC. This higher Se plasma levels is due to SLM being able to non-specifically incorporate into proteins in place of methionine. This allows Se to be stable in plasma allowing for a longer half-life, three weeks (Nilsen et al., 2020) as opposed to SelP which has been shown to have a half-life of about four hours in rat studies which are commonly extrapolated to humans (Burk & Hill, 1994). However, this is slow and inefficient at generating active anticancer activity. MSC will exhibit lower Se plasma levels when compared with SLM due to the efficient β-lyase

metabolism into methylselenol. This metabolite is considered a key anticancer metabolite. (Marshall et al., 2017). This could account for the higher toxicity seen in the SELECT trial which used pure SLM as opposed to the selenised yeast which has a mix of both SLM and MSC. The findings of this investigation strengthens the use of both MSC and SLM in this trial.

A preclinical trial conducted in 2018, led by Dr Michael Jameson, Waikato Hospital, NZ, compared Se concentrations expected to be achieved in a planned Phase 1 trial using supernutrition Se dosages. The study investigated dose efficacy, toxicity in malignant versus normal cells, and the impact on pharmacodynamic mechanisms. The malignant human leukaemia monocyte cell line THP-1 and normal peripheral blood mononuclear cells (PBMCs) were used. Both were treated with methylselenic acid (MSA) at three different concentrations: 2.5 μM, 5 μM, and 15 μM. Additional treatments included 2GY radiation and the chemotherapy drugs arabinoside and doxorubicin (Lobb et al., 2018).

MSA was found to induce apoptosis in THP-1 cells through caspase-8 activation, whereas Caspase-8 expression was decreased in PBMCs. Intracellular glutathione (GSH) levels showed opposite trends between the two cell types: they increased in a dose-dependent manner in PBMCs but decreased in THP-1cells. When radiation or chemotherapy drugs were added, GSH levels remained elevated in PBMCs and suppressed in THP-1 cells. The 2.5 μM concentration provided the greatest protective benefit in PBMCs (Lobb et al., 2018).

At higher MSA concentrations 15 μM, DNA damage in PBMCs increased. However, when combined with radiation or chemotherapy drugs, MSA reduced DNA damage in PBMCs. These findings suggest that achieving Se plasma concentrations between 2.5 μM and 5 μM is optimal for achieving levels that enhance efficacy while reducing the toxic side effect of radiation. Notably, higher Se concentrations appeared safe when combined with chemotherapy. This work supported the initiation of the subsequent Phase 1 clinical trial (Lobb et al., 2018).

This led to a Phase one randomised double-blinded study that evaluated the safety, pharmacokinetics, and pharmacodynamics of the three Se compounds; SLM, MSC, and SS in 24 chronic lymphocytic leukaemia (CLL) or metastatic solid cancer patients from Waikato Hospital. In this trial they used Se dosages of 400 μg/day. They found that all three compounds were well tolerated and non-genotoxic. This was the first clinical trial to directly compare the three compounds MSC, SLM, and SS in a population (Evans, 2020).

Long-Run Real Time Polymerase Chain Reaction-Based DNA-Damage Quantification (LORD-Q) was used to assess DNA damage in the patient cohort. It was also discovered that there was no detrimental DNA damage at the dose of 400 μg (Evans, 2019). At the Se dose used no substantial changes to Se plasma concentration of vascular endothelial growth factor-α (VEGF-α), expression of proteins associated with ER stress or in intracellular total glutathione in PBMC were observed. The four ER stress proteins that were studied were; Glucose regulating protein 78 (GRP78), Caspase 8, Eukaryotic initiating factor 2 alpha (eIF2α), and spliced X-box binding protein (sxBP1). The chronic lymphocytic leukaemia cohort had significantly higher baseline of total glutathione at 12.31 nM/mg than the solid tumour cohort at 7.4 nM/mg. Changes of total glutathione at each time point from the baseline visit were not significant in either group. These results were to be expected as the purpose of this study was to study a dose that was unlikely to strongly activate the PD pathways before proceeding to a higher dose (Evans, 2020).

Del Castillo Busto et al. (2024) reported on the Se plasma content of the trial. It was reported that patients on the SLM compound exhibited higher changes in total Se plasma concentrations, an increase from 90.9 μg/kg to 208.1 μg/kg. Increases in Se plasma concentrations were observed in both MSC and SS at 95. μg/Kg to 125.9 μg/kg and 94.1 μg/kg to 116.7 μg/kg, respectively. Analysis of the distribution of Se species in plasma found that 45% of the Se increase observed in

the SLM group was from SeMet non-specific substitution of Met into proteins, primarily albumin forming selenoalbumin (non-regulated). This was shown by analysing the bound Se to albumin within the three compound groups. The increase from baseline to end of trial for SLM was 288% whereas it was approximately 25% for the MSC and SS groups. The higher Se plasma concentration observed in the MSC group when compared to the SS group is attributed to the efficient metabolism of MSC into the Selenoprotien metabolite hydrogen selenide. This study also noted that patients were deficient for Se due to full expression not being met at the 400 μg/day dose (del Castillo Busto et al., 2024). Thus, an extension of the clinical trial led by Dr Jameson, Waikato Hospital, NZ, investigates the use of a higher Se dose to determine if the higher dose will yield a higher level of total Se plasma expression and investigate changes in protein expression in the unfolded protein response. Which has become the focus of this thesis.

1.5 The Unfolded Protein Response

The endoplasmic reticulum (ER) is an organelle found in the cell and is responsible for the folding of about one third of proteins in humans. It also transports synthesised proteins to the Golgi apparatus using vesicles (Almanza et al., 2019). When misfolded or unfolded proteins accumulate in the ER this causes the GRP78 protein to unbind from the membrane and bind to the misfolded protein. However, when there is too much of a build up the ER will issue an unfolded protein response (UPR) (Ryoo, 2016). The UPR plays a crucial role in the stabilising cellular processes. However, if homeostasis cannot be restored, the pathway initiates cell death (Xia et al., 2021).

Glucose regulated protein 78 (GRP78) was first discovered in the 1970s by starving cells of glucose and is currently known as Heat Shock Protein Family A (Hsp70) member 5[1]. Under normal conditions, the GRP78 protein remains bound to the three transmembrane domains; IRE1, PERK, and ATF6 (**Figure 8**).

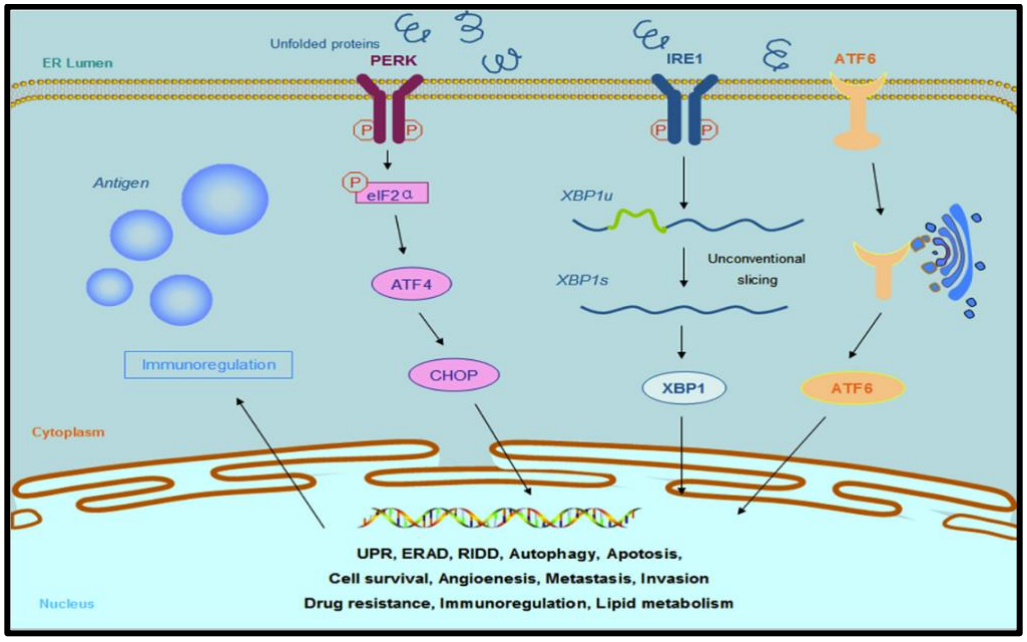

Figure 8 Overview of the ER pathways.

The three transmembrane receptors are shown; PERK (purple), IRE1 (blue) and ATF6 (orange) (Chen et al., 2020).

[1] Other alternative names: immunoglobulin heavy chain binding protein (BiP), along with GRP58 and GRP94

Under ER stress - caused by factors such as hypoxia, nutrient deficiency, oxidative stress, calcium depletion, and certain viral infections - misfolded or unfolded proteins accumulate. In response, the GRP78 protein detaches from these domains and binds to the unfolded proteins, helping to maintain them in a foldable state (Xia et al., 2021). This in turn triggers the activation of the three UPR pathways (**Figure 8**).

1.5.1 PERK Pathway

After GRP78 unbinds from protein Kinase R-like ER Kinase (PERK), the receptor undergoes dimerisation, becoming active and enabling it to phosphorylate Eukaryotic Translation Initiation Factor 2 Subunit protein (eIF2α) at the serine residue (Ser51) (Almanza et al., 2019) (Humeau et al., 2020). This phosphorylation inhibits eukaryotic translation initiation factor 2B (eIF2B) leading to downregulation of protein expression (Almanza et al., 2019). As a result, overall translation is inhibited, except for genes involved in the UPR. This selective translation helps conserve cellular resources, allowing the cell to either restore homeostasis or undergo apoptosis. One example of a gene that continues to be transcribed is Activation Transcription Factor 4 (*ATF4*), that regulates genes aiding in the cellular response to ER stress. However, prolonged stress shifts the cells response to restoring homeostasis to initiating apoptosis (Almanza et al., 2019).

A key gene involved in this process is C/EBP homologous protein (CHOP)[2], which, when expressed at high levels, promotes caspase-mediated cell death (Jaud et al., 2020). CHOP, a transcription factor was discovered in 1992 by David Ron and Joel Habener, Massachusetts' General Hospital, USA (Ron & Habener, 1992). CHOP facilitates apoptosis by enhancing the transcription of pro-apoptotic genes such as *BIM* and *PUMA* while repressing the transcription of

[2] Other alternative names: DNA Damage Inducible Transcript 3 (DDIT3), Growth Arrest And DNA Damage-Inducible (GADD153), CHOP-10.

anti-apoptotic genes from the BCL-2 family (Almanza et al., 2019). Additionally, Protein Phosphatase 1 Regulatory Subunit 15A (PPP1R15A or previously known as GADD34) plays a role in a negative feedback loop by dephosphorylating eIF2a, helping to restore normal translation levels (Almanza et al., 2019).

1.5.2 IRE1α Pathway

The second pathway activated when GRP78 binds to unfolded proteins is the activation of IRE1α, a transmembrane protein kinase inositol-requiring enzyme. Upon activation, IRE1α cleaves 26 nucleotides from the intron of X-Box Binding Protein 1mRNA (*xBP1)*, resulting in the production of two spliced transcripts; *xBP1s* and *xBP1u*. xBP1s contains a basic leucine zipper (bZIP) domain, which enables it to bind to DNA and also acts as a nuclear localisation signal, facilitating its translocation to the nucleus. After nuclear entry, xBP1s binds to the cis-elements of UPR-related genes, including RESE, ERSE-II, and the unfolded protein response element (Park et al., 2021). *HLA-DRA* is a gene that encodes the alpha chain of the HLA-DR (class II) protein that xBP1 forms a heterodimer with. HLA-DRA plays an important role in the immune response by displaying a foreign peptide that will in turn trigger an immune response, that enhances protein folding trafficking and increased protein degradation via ER associated degradation (Chen et al., 2020).

Although xBP1u lacks transcriptional activity it acts as a negative regulator of xBP1s. Through partial translation of the N-terminal, xBP1u can recruit its own mRNA to the ER membrane (Almanza et al., 2019). XBP1s has also been shown to play a role in cancer metastasis. xBP1s will recruit histone deacetylase (HDAC2) and Enhancer of Zeste 2 Polycomb Repressive Complex 2 Subunit (EZH2) on the promoter region of ΔNp63, which is a suppressor of metastasis, which in

turn suppresses Np63 transcription and promotes metastasis. This has been shown in breast cancer (Chen et al., 2024).

1.5.3 ATF6α Pathway

The third pathway involves the activation of ATF6α through release of GRP78. Upon activation, ATF6a relocates to the Golgi apparatus, where it undergoes cleavage by the Golgi protease membrane bound transcription factor peptidase site 1 (*MBTPS1*), resulting in the removal of approximately 400 nucleotides. This cleavage generates the transcriptionally active form, ATF6p50 (Namba et al., 2007). This cleaved ATF6p50 is responsible for promoting the transcription of genes that enhance xBP1 expression and increase ER capacity (Jaud et al., 2020).

1.6 Rationale to Study Selected Proteins

The chosen ER proteins for this study are GRP78, CHOP, eIF2α, and sXBP1. These were the candidates used in the phase 1 clinical trial as markers of the UPR.

GRP78 has been shown in previous studies to be a promising biomarker in cancer research. Comparing normal lung tissue with lung cancer tissues mRNA and protein levels of GRP78 are significantly overexpressed in lung cancer tissues. This overexpression has been closely related to the differentiation and development of lung cancer (Lee, 2007). Additionally, studies have been shown that patients with higher GRP78 levels in their serum have shorter survival time (Xia et al., 2021).

A 2021 study used Oleandrin, a cardiac glycoside, that was exposed to the human in vitro breast cancer cell lines MDA-MB-231, MCF-7 and T47D and the mouse mammary cell EMT6. It was found that Oleandrin induced ER stress via the PERK and IRE1 pathways. This was shown by the stronger western blot signals in the PERK pathway proteins p-PERK, p-eIF2a, ATF4, and CHOP when compared to the IRE1 pathway proteins. p-IRE1 and XBP1 Furthermore, when PERK and IRE1 were inhibited PERK inhibition had a stronger effect than when IRE1 was inhibited. This shows evidence that ER stress induced form Oleandrin is mainly through the PERK pathway (Li et al., 2021). This study shows that not all ER stress pathways will activate equally and that one pathway could be the key driver and another pathway play a secondary role. This is why when analysing ER stress, it is vital to have a diverse range of biomarkers.

A 2010 study was undertaken to investigate the apoptotic response between three Se compounds (MSC, SeMet, and SS) in relation to the UPR. They used four human in vitro cancer cell lines HSC-3 (tongue), HSC-4, A549 (lung), and MCF-7. It was found that higher levels of

phosphylated eIF2α were increased in SS treated cells, which is consistent with ER stress mediated apoptosis. P53 mediated apoptosis was observed in SeMet however no induction of ER stress markers, GRP78 and CHOP was observed. It was noted that low upregulation in CHOP and GRP78 expression were observed with MSC treatment. The authors attributed this low protein expression because these cells are in vitro, and cell culture is low in β-lysase which is an integral enzyme needed to convert MSC to the active metabolite methylselenol which leads to inefficient conversion and lowered activity (Suzuki et al., 2010).

1.7 Aims, Objectives and Hypotheses

This research was part of a phase 1b clinical trial led by Dr Michael Jameson, Waikato Hospital, NZ. The primary objective of the trial was identifying the safest and most effective Se dose and form for combination with anticancer therapies. Secondary objectives included assessing clinical and laboratory safety, plasma pharmacokinetics, DNA damage in PBMCs, and exploring pharmacodynamic markers.

This research project aim had the following two objectives:

1.) Evaluate the level of DNA damage via the LORD-Q assay; and
2.) Investigate the pharmacodynamic effects of Se by evaluating the protein expression levels of four proteins CHOP, EIF-2a, GRP78, and sXBP1 via western blotting.

The results of these two objectives will then form the basis of which Se compound and which concentration will be used in a further phase 2 clinical trial.

Yakes and Van Houten, 1997 they noted a three times higher damage rate in mitochondrial DNA (mtDNA) than nuclear DNA (nDNA). This is due to the proximity of mtDNA which is next to sources of ROS and the lack of DNA repair machinery (Yakes & Van Houten, 1997). mtDNA lack nuclear base repair which is the main repair system that repairs pyrimidine dimers which are caused by UV-C. Taking this into consideration and the previous clinical trial by Evans et al. 2020, two research hypothesises have been proposed:

1.) Dose-dependent changes are expected in the UPR proteins due to which chemical pathway is being activated; and
2.) MSC will likely exhibit less genotoxicity and less adverse events than the other two compounds SLM and SS.

Chapter 2 Methods

2.1 Human Ethics Approval

Human Ethics approval was given by the NZ Northen A Health and Disability ethics committee (ref 13/NTA/127/AM07) and was endorsed the University of Waikato (UoW) Human Ethics Committee to conduct a phase 1b clinical trial.

2.1.1 Study Design

This was a double-blinded randomised trial. Nine patients were randomised to be given either SLM, MSC, or SS visually identical capsules with each compound group enrolling three patients (*n*=3). Due to small sample size statistical inference is limited and findings are exploratory. Statistical tests were carried out to explore potential trends and to provide preliminary insights. On hospital visit Day 0 (V1), patients signed their informed consent, filled out a questionnaire, and had their baseline blood samples taken by a nurse. Patients were asked to keep a diary of any side effects that they experienced while on this trial. Patients were given an Identification number (ID) between 25-33 this was to ensure the double-blind status of the trial.

Blood samples were taken at Days 1, 2, 29, 30, 57, and 84 by a nurse (**Table 2**). Bloods were taken before doses on Day 1 and Day 29 as these were when the dosages started, 1600 mcg/day for Day 1 and 6400 mcg/day for Day 29 so this gives a baseline before a change in concentration. Bloods were taken four hours after dose on Day 2 and Day 30 to capture peak concentration of the Se compounds. Peripheral Blood Mononuclear Cells (PBMCs) were extracted from the blood samples within 6 hours of being taken. Patients took their Se compound containing elemental Se 1600 mcg/day for 28 days and then increased to 6400 mcg/day on Day 29 for another 28 days.

These Se dosages are based on findings of tolerability from Evans et al. (2020) where 400 mcg/day doses were used. No trial medication was taken between Days 57 and 84.

2.1.2 Recruitment of Informed Consented Participants

Potential participants were identified through their oncologist and provided with a Participant Information Sheet. This sheet would give them a clear outline of the study, the reason for the study, and relevant contact information. Nine consented cancer patients from Waikato Hospital, Hamilton, NZ were recruited and were screened on Hospital Visit (V) Day 0.

Table 2 Dose and Blood extraction timeline.

Waikato Hospital visit number and the dose escalation of the given Se compound for the phase 1b clinical trial. V = visit day, Q+A = Questions and Answers.

<table>
<tr><th colspan="8">Waikato Hospital Visit</th></tr>
<tr><th>V1</th><th rowspan="3">Randomisation</th><th>V2</th><th>V3</th><th>V4</th><th>V5</th><th>V6</th><th>V7</th></tr>
<tr><td rowspan="2">Q+A

Informed consent

Blood samples taken</td><td>Day 1

Before dose bloods</td><td>Day 2

4 hours after dose bloods</td><td>Day 29

Before dose bloods</td><td>Day 30

4 hours after dose bloods</td><td>Day 57

Before dose bloods</td><td>Day 84

Bloods</td></tr>
<tr><td colspan="3">1600 mcg/day capsule Days 1-28</td><td colspan="3">6400 mcg/day capsule Days 29-56</td></tr>
<tr><td colspan="2">14 days</td><td colspan="5">56 Days</td><td>28 Days</td></tr>
</table>

2.2 Extraction of PBMCs from Human Blood

PBMC extraction was carried out in a Physical Containment Level 2 laboratory at the UoW. The protocol used was the same protocol used by (Evans et al., 2016). In the biological safety cabinet, 6mL of the inform-consented donated blood was transferred into a 50mL Falcon® tube and made up to a final volume of 15 mL with 1x Phosphate Buffered Saline (PBS, pH 7.4). The 15mL blood PBS mixture was then transferred to a 50 mL Falcon® tube containing 15mL of Histopaque®, centrifuged at 400g at room temperature (RT) for 30 mins with the brake off. The PBS layer was removed, and the cell layer was transferred to a new 15mL Falcon® tube containing 10 mL of 1x PBS pH 7.4. The tube was centrifuged at 250 g for 15 mins at 4°C. The supernatant was

discarded, and the cells were washed with 1x PBS pH 7.4 two more times. Depending on the visit day (**Table 3**), 2.5 mL or 3.5 mL of freezing media was added to the tube, and the cell pellet was resuspended in the media. A cell count was taken by pipetting 20 µL of the cell sample and adding 20µL of 0.4% Trypan Blue then transferring 10 µL to both ends of a dual-chamber disposable counting slide (Bio Rad cat n# 1450011). The slide was then carefully inserted into the Bio Rad TC10™ Automated cell counter to obtain a cell count reading. The remaining cell lysate solution was aliquoted into the appropriate 2mL cryovial tubes to be snap frozen in liquid Nitrogen and stored at -80°C for downstream applications; western blots and LORD-Q.

Table 3 PBMC aliquot amounts.

PBMC sample aliquots that are taken and processed at each visit.

Waikato Hospital Visit Number							
Preparation of Samples for Future Analyses	**1** Baseline	**2** Day 1	**3** Day 2	**4** Day 29	**5** Day 30	**6** Day 57	**7** Day 84
Snap Frozen PBMC Speciation (LGC)		3 x 300µL		3 x 300µL		3 x 300µL	
Snap Frozen PBMC DNA rep Surrey		2 x 300µL		2 x 300µL		2 x 300µL	
Plasma Speciation		3 x 300µL		3 x 300µL		3 x 300µL	
Cryopreserved	1 x 1000µL						
Plasma for VegF	2 x 500µL						
Snap Frozen PBMC for Westerns	3 x 300µL						
Snap Frozen PBMC for Glutathione	1 x 300µL						

2.2.1 Cryopreservation of PBMCs

PBMCs were resuspended in sterile freezing media (10% dimethyl sulfoxide (Merck, Germany), 40% RPMI 1640 medium (Gibco, USA), 50% Foetal Bovine Serum (Gibco, USA) (FBS)) and transferred to a 2 mL cryovial. They were incubated overnight in a Coolcell® container at -80°C before moving to a new storage box in the -80°C freezer.

2.3 Western Blotting

Western blotting was a method conceived in 1979 (Renart et al., 1979). Briefly, this method allows the identification and quantification of proteins through the use of antibody detection by resolving proteins according to size using polyacrylamide gel electrophoresis (PAGE), transferring the separated proteins onto PVDF or nitrocellulose paper, blotting with a specific antibody pairing and detecting the resulting protein expression signal using chemiluminescence. Eight proteins of interest are being investigated in this clinical trial and focus are involved in angiogenesis and ER stress. For the purposes of this research thesis, the ER stress protein expression changes in response to Se over time will be investigated and angiogenesis markers will be reported separately.

Before patient samples were lysed and analysed through western blotting current on hand antibodies were validated prior to being used on patient samples. Protein lysates from three mammalian invitro cell lines; A549, HeLa (cervix) and MDA-MB-456 were used, cell lines were provided by C.Turnbull, (UoW). Antibodies that were tested were CHOP, GRP78, and sXBP1.

Cell pellets obtained from the PBMC extraction were lysed with 200 μL lysis buffer and 200 μL of protease inhibitor cocktail mix. Samples were left in the -80°C freezer overnight. Protein concentrations were determined by the Bradford assay as recommended by the manufacturer (BCA protein assay kit Pierce Biotechnology Rockford, IL, USA. 23225). Briefly, 100 μL of Bradford dye was added to the wells of a 96-well flat bottom plate. One μL of bovine serum albumin (BSA) standard (0 mg/mL to 10 mg/mL) was added to each well in triplicate and then 1μL of patient sample was added to additional wells (n=3). The plate was left to incubate for 10

mins at RT in the dark and then the samples were measured at a wavelength of 540 nm using a plate reader (Multiskan GO, Thermo Fisher Scientific, Ratastie, Finland).

The BSA absorbance values (n=3) were then plotted on a line graph (Excel) and a line of best fit was drawn and the R squared (R^2) value calculated. An R^2 value between 0.7 and 0.99 was denoted as acceptable. Next the protein concentrations were determined by plotting the samples against the BSA standard curve.

2.3.1 Sodium Dodecyl Sulphate Polyacrylamide Gel Electrophoresis Gel

Protein samples were prepared, denatured and then loaded onto a denaturing Sodium Dodecyl Sulphate (SDS) PAGE gel. Firstly, each sample had 5 µL of 4X Laemmli dye and diluted with 1x PBS pH 7.4 to a total volume of 20 µL in a 1.5 mL boil proof tube. Protein samples were then denatured at 95°C for 5 mins in the thermomixer. A gel apparatus (Hoefer™ Mighty Small IISE250/SE260 electrophoresis system (Hoefer, USA)) was set up with premade gel casts (surePAGE™, Bis-Tris, 10x8 cm, 10%, Lot number M00666, Genscript, USA) and 1x Tris- MOPS buffer (Express gel running buffer powder Lot number M00138, Genscript, USA) was used to carry out the electrophoresis. A protein ladder (Precision Plus Protein™ Dual Colour Standards, Thermofisher #1610374, 5 mL) was placed in position one of the SDS-PAGE gel for molecular weight comparison. The gel was then run for 30mins at 140V at RT.

2.3.2 Protein Transfer

The eBlot protein transfer system (Genscript L03010) instrument and kit were used to transfer the electrophoresed protein from the gel to the PVDF membrane. Firstly, the PVDF membrane (Merc Millipore) kwas cut to the appropriate size using scissors and activated in 10mL of 100%

Methanol for 15 seconds and then soaked in equilibrium buffer. eBlot™ Protein Transfer System instrument was then used to transfer the protein from the gel to the PVDF membrane. The anode pad was placed down first and then the activated membrane was placed on top. The pre-run SDS-PAGE gel was placed on top of the membrane and a window was placed to prevent the anode and cathode pads from sticking together. The cathode pad was placed on top last. The eBlot was then run for 7mins at RT. Protein transfer was confirmed by the presence of the protein ladder bands or Ponceau S staining by immersing the membrane in Ponceau S solution and gently agitating the membrane for 10mins at RT. The membrane is then washed with acetic acid (5%) until red bands are clearly visible. To use the membrane after Ponceau S staining the membrane was washed in 1x TBST (TBS with Tween 20) for 10mins for three washes until the stain has disappeared.

The membrane was then washed in three washes of 1x Tris Buffered Saline (TBS, pH 7.4) for 3 mins and then blocked for one hour in 5% Blocking Solution (25 mL 1x TBST with 1.25 g of Woolworths skim milk powder, NZ). Then, the membrane was incubated with the appropriate primary antibody (**Table 4**) suspended in the blocking solution, overnight at 4°C. To reduce and conserve the primary antibody solution, rather than using containers, the antibody was added to a membrane in a sealed plastic bag and incubated on an orbital shaker at high speed.

Table 4 Antibodies used in project.

Antibodies and dilution factors used during western blot process.

Antibody	Host	Dilution	Supplier	Catalog number	Molecular Weight (KDa)	Type
GAPDH	Rabbit	1:5000	Antibodies	A92889	37	Primary
GRP78	Mouse	1:5000	Santa Cruz	Sc-166490	78	
CHOP	Rabbit	1:500	GeneTex	GTX-109226	31	
sXBP1	Rabbit	1:200	Santa Cruz	Sc-7160	40	
eIF2a	Rabbit	1:200	Santa Cruz	Sc-11386	36	
HRP	Goat	1:5000	Abcam	AB97051	N/A	Secondary
HRP	Goat	1:5000	Abcam	AB97023	N/A	

After the overnight incubation the membrane was washed in 1x TBST for 15 mins three times and then incubation with the secondary antibody (**Table 4**) for one hour in 5% blocking solution. To remove unbound secondary antibody the membraned was washed three times in 1x TBST for 15 mins followed by a 1hr wash in 1x TBST at RT and a final wash in 1x TBS for 15 mins. The membrane as then developed using the ECL substrate (SuperSignal™ West Pico PLUS chemiluminescent Substrate 34577) for 5mins in the dark and imaged using the Invitrogen iBright™ Imaging System to detect the chemiluminescence signal using the white tray. The file was saved as a TIFF file for analysis using western blot densitometry (**Section 2.4.4**).

The PVDF membranes were stored at 4°C in 1x TBS until they were stripped of antibodies to allow reprobing with a different antibody (see **Table 4**). Depending on the affinity of the previous primary antibody there are two ways of stripping the membrane; (1) for low affinity antibodies, wash membrane for 5 min in 1x TBS, incubate in striping buffer for 30 mins, washed twice in 1x TBS for 5 mins and then reprobed with appropriate primary antibody (2) for membranes that were probed with high affinity primary antibodies this follows the same wash patterns but is conducted at 37°C.

2.3.3 Western Blot Densitometry

The TIFF files from the western blot images were imported into the open-source image processing software ImageJ (https://imagej.net/ij/). The band intensity of the loading reference protein and protein of interest was measured by selecting the precise band regions of interest (ROI) using the rectangle tool available in the ImageJ toolbar. Next, the analyse tool was selected to analyse the ROI in the representative peaks and measure the respective intensities. **Equation 1** was used to calculate the normalised density to the loading control.

Equation 1 Western blot calculation to normalise target protein expression.

$$\textit{Normalised density of loading control} = \frac{\textit{Target Protein X Loading Control}}{\textit{Loading of visit}}$$

Next, the fold difference between the normalised density of the target protein to the normalised density of the baseline visit was calculated (**Equation 2**).

Equation 2 Western blot calculation to find fold density of protein of interest.

$$\textit{Fold Density} = \frac{\textit{Normalised Density of Loading Control}}{\textit{Normalised Density of Loading Control of Baseline}}$$

2.5 Long-Run Real Time Polymerase Chain Reaction-Based DNA-Damage Quantification

The Comet assay was developed in 1984 by Ostling and Johanson to identify the genotoxicity of chemicals by measuring DNA breaks in eukaryotic cells (Langie et al., 2015). However, this is a very labour-intensive method with a low throughput (Langie et al., 2015). Lehele et al. 2014 was the first to develop a protocol to overcome these constraints using a molecular PCR-based assay that is much more sensitive. To induce DNA damage, they exposed in vitro mammalian cells to UVC radiation and cytotoxic agents (Lehle et al., 2014).

Due to the semi-quantitative nature of the Comet assay, the need to analyse nDNA and mtDNA, and the high volume of samples that will be analysed with the time constraints it was decided to use a modified LORD-Q PCR protocol published by Evans et al. 2019 for this clinical trial. Briefly, the in vitro human A549 and THP-1 cells were used as positive controls to validate that the assay was successfully run. These cells were either treated with 20 mJ/cm^2 or 100 mJ/cm^2 UVC radiation to induce DNA damage or were left non-treated to serve as a control. DNA was then extracted from the positive control and the patient samples and then the LORD-Q assay was

run. Based on previous troubleshooting the A549 line was used for the mitochondrial assay and THP-1 was used for the nuclear assay. These two cell lines were chosen for this assay as they have been previously validated by (Evans et al., 2016).

2.4.1 Culturing in vitro Human lung A549 cells

A549 cells were ascertained from the UoW Cell Culture Liquid Nitrogen inventory at Passage 10 and were revived according to Invitrogen Cell Culture Basics (Thermo Fisher Scientific, 2020). Briefly, the cryovial was thawed for 1min in a 37°C water bath and then the vial of cells was transferred to a biological safety hood where the cells were transferred to a 15mL conical tube. Nine mL of warm complete media (10% FBS, 1x Penicillin/Streptomycin, F12K media (Gibco Lot 2522683)) was added; this was to dilute the DMSO which is added to the freeing media which is toxic to cells at RT. The conical tube was then centrifuged at 300xg for 5 mins to pellet the cells at the bottom of the tube. The DMSO solution was then removed and then 10mL of warm media was then added to the tube to resuspend the cells. The cell mixture was then transferred into a T25 surface-treated flask (Greiner Bio-One T25) and incubated at 37°C with 5% CO_2.

The cells were passaged for at least two times prior to the experimental assays. Media was changed twice a week. Cells were passaged when they reached 90% confluency. The media was removed, and the cells were washed using 1x PBS and then adding pre-warmed at 37° 0.25% trypsin-EDTA phenol red solution (Thermofisher 25200056) and incubating the cells for 10 minutes at 37°. The trypsin was neutralised by the addition of an equal volume of complete media and then the sample was transferred to a 15 mL Falcon® tube and spun for 200xg at RT for 5 min. The pellet was resuspended in 1mL of complete media. The A549 cell concentration was determined by Bio-Rad TC10™ automated cell counter, if required. Cells were either used or transferred to new surface-treated T25 flasks or expanded into a T75 flask.

2.4.2 Preparation of UV Damaged DNA for Positive Template Control

A A549 cell concentration of 2.5-5x10^5 in a final volume of 2 mL was seeded into three non-treated 6-well plates (Plate 1 = Non-irradiated - no UVC; Plate 2 - 20mJ/cm^2 UVC and 3 = 100mJ/cm^2 UVC). Each plate contained three replicates of 2.5-5x10^5 cells plus one well had complete cell media only (2mL) to serve as a negative control (to detect for any microbial contamination). Plates 2 and 3 were irradiated in the Bio-link BXL-254 cross-linker (Gibco, USA) with 20 mJ/cm^2 or 100 mJ/cm^2 UV light. The next step was to extract the DNA from the cell samples in the three 6-well plates.

DNA extraction from the non-irradiated (Plate 1) and irradiated cells (Plates 2 and 3) was carried out using the protocol recommended by the manufacturer, Zymo Research (Ngaio Diagnostics, NZ). Firstly, genomic lysis buffer was added to the irradiated cell sample to a 4:1 ratio, mixed, and left at RT for 10 mins to allow cell lysis. Next, the sample was transferred to a spin column that was in a collection tube and then centrifuged at 10,000x g for 1min at RT. The solution collected in the collection tube was discarded. The spin column was transferred a new collection tube and 200 µL of DNA pre-wash buffer was added to the column. Centrifugation was repeated at 10,000xg for 1min at RT. Next, 500 µL of g-DNA wash buffer was added to the spin column and again spun at 10,000xg for 1min at RT. The spin column was transferred to a sterile 1.5 mL centrifuge tube with 50 µL of 65°C prewarmed elution buffer added to the column. Following a 5 min incubation at RT, the DNA was then eluted by centrifugation at 14,000x g for 30 sec. To improve the yield, the elution step was repeated a second time. The quality and quantity of extracted DNA was measured using the DeNovix DS-11 Spectrophotometer. The A269/280 ratio was used as a measure of DNA quality and a value between 1.8 and 2.2 was considered pure. We

aimed to achieve DNA concentrations greater than 12.5 μg/mL. After spectrophotometer analysis the DNA aliquots were stored at -20°C.

In some cases, DNA was further purified using the Zymo DNA Clean and Concentrator kit as either the DNA was less than 10 ng/μL and/or as a 260/280 ratio out of the range of 1.7-2.2. A 2:1 volume of DNA binding buffer to the DNA sample was prepared and mixed using vortexing (10sec). This solution was transferred to a Zymo spin column inside a collection tube and centrifuged for 30sec at 13,000x g at RT. The spin column was transferred to a clean 2 mL collection tube and then added 200 μL of DNA wash buffer to the column and spun again for 30sec at 13,000xg. This was repeated to remove any impurities. Finally, 25 μL of pre-warmed 65°C elution buffer was added to the column and incubated at RT for 1min. The elution step was repeated once more. Finally, the eluted DNA was measured using the DeNovix DS-11 Spectrophotometer and stored at -20°C.

2.4.3 Testing for Mycoplasma Contamination using PCR

To ensure there was no bacterial contamination of Mycoplasma in cultured A549 cells, a PCR test was applied according to universal Mycoplasma detection kit (ATCC cat no. 30-1012K) protocol. Experiments carried out with mycoplasma-infected cells may yield false, misleading and non-reproducible results. Briefly, the presence of Mycoplasma is detected by the observation of a 500 bp band on an agarose gel. If cells were cleared of mycoplasma contamination, then they were able to continue to be used for this thesis project.

Table 5 Mycoplasma PCR set-up

PCR Tube Set-up for Mycoplasma Contamination Assay

Tube N#	DNA Composition
1	UVC Cell Assay Negative Control (No UV treatment - Media only, no cells)
2	UVC Cell Treated Assay (100mJ/cm^2 irradiated Cells and media)
3	UVC Cell Assay Negative Control + PCR Positive control
4	UVC Cell Treated Assay + PCR Positive control
5	PCR Positive control (Mycoplasma DNA)
6	PCR Negative control (Water only)
Second Mycoplasma Assay	
Tube N#	**DNA Composition**
1	PCR Negative control (Water only)
2	Non-irradiated A549 cells
3	PCR Positive control (Mycoplasma DNA)
4	Non-irradiated A549 cells + PCR Positive control

A PCR master mix was set up in 1.5 mL centrifuge tube as outlined in **Table 6** below. The master mix (17.5 µL) was aliquoted into Axygen® 0.2mL thin wall clear flat cap PCR tubes on ice with 2.5 µL of DNA template or sterile MQ water added (**Table 6)**. Following a short spin 10sec spin, the tubes were transferred to Bio-Rad T100 thermal cycler and run according to the cycling parameters listed in **Table 7**.

Table 6 Mycoplasma master mix recipe.

Components	Individual Volume (µL)	Master Mix Volume (µL)
Universal PCR mix	15	97.50
Universal Primers	2.5	16.25
Cell line DNA	2.5	
Total volume	20	113.75

Table 7 Mycoplasma PCR cycling conditions.

Cycle Step	Temperature (°C)	Time	Cycle number
Initial denaturation	94	1.5 min	1
Denaturation	94	30 sec	20
Annealing	70 (-0.5/ cycle)	30 se	
Elongation	72	45 sec	
Denaturation	94	30 sec	12
Annealing	60	30 sec	
Elongation	72	45 sec	
Final Elongation	72	4 min	1

2.4.4 Agarose Gel Electrophoresis

Following traditional PCR or LORD-Q PCR, 5 µL of amplified DNA was mixed with 2 µL 6X Loading Dye (0.25% bromophenol blue dye, 0.25% xylene cyanol FF and 30% glycerol) with 5 µL being loaded onto the appropriate agarose gel against an appropriate DNA ladder. For long primer amplified products, a 0.8% 1x TAE agarose gel (0.4g HyAgarose™ powder to 50mL 1x TAE buffer) was made, whereas for short primers a 3% 1x TAE gel (1.5g HyAgarose™ powder to 50 mL 1x TAE). The 50 mL agarose gel was heated until dissolved using 800W microwave, cooled to 50°C and then supplemented with a final concentration of 1x Thiazole Orange to allow the visualisation of DNA visible under UV light. Gels were run at 90V for 40 minutes at RT and then photographed on the Invitrogen iBright™ Imager under UV light.

2.5 LORD-Q

To avoid contamination issues, LORD-Q reactions were set up in the ESCO Airstream® PCR cabinet. This cabinet is designated as a template dsDNA-free area; therefore, components of the master mix-including $MgCl_2$, Buffer solution, molecular-grade water (including negative control water), Taq DNA Polymerase, dNTPs, S Solution- were prepared within it. These master mix consumables were sourced from Solis BioDyne, Estonia. Primers were prepared in a separate biological safety hood. Primers and DNA were added to the PCR tubes in the general laboratory space; however, all PCR reactions were performed in a dedicated area reserved specifically for PCR assay using dedicated LORD-Q pipettors. All equipment used for PCR- such as pipettes, pipette filter tips, and PCR tubes-were sterilised under UVC light for 20 min in the hood prior to use.

Six primers (**Table 8**) were selected for the LORD-Q assay that had been used from two previous studies. The mitochondrial primers were from Evans et al 2016; and the nuclear primers were from Lehel et al 2014 (Evans et al., 2016; Lehle et al., 2014). They were ordered from IDT, NZ, resuspended in TE Buffer (pH 8) and amplify a long nucleotide fragment; nDNA (*TP53* gene; 3,075 bp) or mtDNA (3,723 bp) or a short fragment nDNA (*TP53* gene; 45 bp) or mtDNA 55 bp). To provide an indication of DNA damage, both sets of primers are used, and it is expected to observe more evidence of DNA damage in the amplicons generated with the long primers as there will be more likelihood of DNA breaks due to the length of the strands in the longer strands. Both nDNA and mtDNA are used to provide a comprehensive view of potential DNA damage, as they have distinct repair processes and respond to damage in different ways.

Table 8 LORD-Q PCR Primers.

Primer Name	**Tm (°C)**	**Sequence (5'-3')**	**Product Size (bp)**	**Ta (°C)**
TP53 long forward	55.61	CATAACCGCAAATGGGAAAC	3,075	64.5
TP53 long reverse	57.56	CGGGACGTGAAAGGTTAGAA		
TP53 short reverse	56.10	CGTCCTTTTGATGGCCTTT	45	60
Mitochondrial long forward	63.60	CGCCTCACACTCATTCTCAA	3,723	63
Mitochondrial long reverse	62.90	AATGTATGGGATGGCGGATA		
Mitochondrial short reverse	62.90	CAAGGAAGGGGTAGGCTATG	55	63

LORD-Q assay was set up in Axygen® 0.2 mL thin wall clear flat cap PCR tubes on ice. **Table 9** and **Table 10** shows the PCR master mix for preparing the four sets of primers. LORD-Q was run

on the Corbett Research Ltd Roto-Gene™ with the cycling conditions shown in **Table 11**. Each patient sample was run twice on two independent PCR runs for a total of four PCR runs.

Table 9 Master mix recipe for mitochondrial long, P53 short, and P53 long primers.

Components	Individual Volume (µL)	Master Mix Volume (µL)
5 U/µL HOTFIRE Taq Pol	0.1	3.3
10x B2 Buffer	1.0	33.0
25 mM $MgCl_2$	1.0	33.0
20 mM dNTPs	0.1	3.3
10 µM F/R Primer	0.4	13.2
5 µM SYTO 82 (Thermo fisher S11363)	0.01	0.33
Sterile MQ water	6.39	210.87
Total Volume	9.0	297.0

Table 10 Master mix recipe for mitochondrial short primers.

Components	Individual Volume (µL)	Master Mix Volume (µL)
5U/µL HOTFIRE Taq Pol	0.1	3.3
10x B2 Buffer	1.0	33.0
25 mM $MgCl_2$	1.0	33.0
20 mM dNTPs	0.1	3.3
10 µM F/R Primer	0.4	13.2
10x S Solution	0.5	16.5
5 µM SYTO 82 (Thermo fisher S11363)	0.01	0.33
MQ water	5.89	194.37
Total Volume	9.0	280.50

Table 11 LORD-Q Cycling Conditions.

PCR was run using the Corbett Research Ltd Roto-Gene™. The specific annealing temperature used for each specific primers set can be found in **Table 2.7**.

Step	Temp (°C)	Time (Sec)	Cycle number
Initial Denaturation	95	900	1
Hot start	95	10	10
	65(-0.5(°C)/Cycle)	10	
	72	240	
Amplification	95	15	35
	60 - 64.5	15	
	72	240 (acquire cycle A- yellow)	
	82	10 (acquire cycle B- yellow)	

Melt Curve	Ramp from 64 to 95 (Hold for 90 seconds on the first temp then 5 seconds for the others)	1

After each run the melt curved was analysed to determine if there is no negative contamination and to make sure there are no extra peaks in the control samples or patient samples and that the correct peaks were noted at the expected melting temperature (T_m). Small peaks may have been noted at lower temperatures, and these were deemed to be primer dimers.

When appropriate, the amplified LORD-Q samples were run on an agarose gel **Section 2.5.5** to confirm amplicon size, absence of DNA in the negative control, and/or the presence of primer dimers.

After the melt curve was analysed the quantification report was generated to give the C_q values that are used in the equation to calculate the number of lesions present in the DNA. The C_q value is known as the threshold cycle or quantification cycle and represents the PCR cycle number at which the reaction curve intersects the threshold line. The reaction report was exported into excel where the **Equation 3** was calculated. This equation was modified by Evans et al. (2016) from (Lehle et al., 2014).

Equation 3 Determination of DNA Damage.

$$\textit{Lesions per 10kb} = [(E_L^{Cql(Sample)} \times E_S^{-Cqs(Sample)} / E_L^{Cql(Control)} \times E_S^{-Cqs(Control)})^{1/a} - 1] \times 10{,}000$$

E_L and E_s is the average amplification efficiencies from the large and short products. C_p values are the crossover values given by the Roto-Gene™ software where C_{ql} is the long product and C_{ps} is the short product and a is the number of base pairs in the long fragment. This equation was calculated using a spreadsheet in Microsoft Excel.

To calculate the DNA damage in the control samples (A549 and THP-1) the change in Cq values using the averages of the long and short Cq was calculated using **Equation 4**.

Equation 4 Change in threshold cycle

$$\Delta C_q = C_{qlong} - C_{qshort}$$

C_q is the threshold cycle, C_{qlong} is the long product and C_{pshort} is the short product.

Next, **Equation 5** was used to calculate the Relative Integrity (RI). The lower the RI, the more damage that has been inflicted to the DNA.

Equation 5 Relative integrity of DNA

$$RI = 2^{-\Delta Cq}$$

Finally, the lesions per 10kb using the non-irradiated cell lines as the negative control and the irradiated cell lines as the sample were calculated suing **Equation 6**.

Equation 6 Calculation of lesions in DNA per 10kb

$$Lesions/10kb = 1/Lx\ (1 - (RI_{sample}/RI_{control})\ x\ 10{,}000$$

Lx in this equation was the product length of the long primer products for the nDNA - 3,075 and for the mtDNA it was 3,723. These values were taken from **Table 8**.

A standard curve was also determined using the DNA from the undamaged THP-1 cells using the primers sets listed in **Table 8**. A ten-fold serial dilution was made from both the undamaged A549 and THP-1 DNA using Molecular grade water (n=3). A master mix as prepared as outline in **Table 9** and **Table 10,** and they were finally run on the Corbett Research Ltd Roto-Gene™ as outlined in **Table 11**.

2.6 Statistical analysis

Statistical analysis for LORD-Q was calculated with using the commercial scientific 2D graphing and statistics software programme Graphpad Prism V 10.5.0. A Shapiro-Wilks test was performed on patient samples to determine if the data was normally distributed. The null hypothesis states that data are taken from normal distributed population. Thus, a p value of > 0.05 means the samples are normally distributed whereas a p value of <0.05 means the samples have deviated from normal distribution. This test is suitable for small sample sizes (<50 samples) if samples are normally distributed a mixed-effects analysis was performed on those groups (Mishra et al., 2019) If sample group are not normally distributed the Friedman test which is for non-parametric groups was applied. For all statistical tests applied a p value of <0.05 means there is a statistical significance in the group

Chapter 3 Results

The following results section will describe the recruitment and evaluation of patients for the Phase 1b clinical trial, culturing of A549 cells, mycoplasma testing, western blots, and the LORD- Q PCR assay.

3.1 Recruitment of Patients

Nine patients with informed consent were recruited for this Phase 1b clinical trial, they were divided into three Se treatment groups; MSC, SLM, and SS. **Table 12** shows a summary of these participants with their previous and current cancer treatment(s). The overall age range was 62- 80 years with a mean age of 73 years. Each treatment group included patients with prior therapy, including chemotherapy, targeted therapy, or both. All patients in the MSC and SS groups were concurrently receiving cancer treatment (Pembrolizumab or Exemestane). In contrast within SLM group, only one patient was receiving treatment (Pembrolizumab). It was also noted that three males were randomised for SLM whereas the other two treatment groups, MSC and SS had both sexes represented.

Table 12 Summary of informed-consented participants.

Summary of informed-consented participants and their previous and current cancer treatment.

Characteristics	**MSC (*n*=3)**	**SLM (*n*=3)**	**SS (*n*=3)**	**Combined**
Mean age, years (range)	78 (76-80)	69 (62-73)	72 (66-78)	73
Male	1	3	2	6
Female	2	0	1	3
Prior Treatment				
Chemotherapy	1	0	1	2
Targeted Therapy	1	0	1	2
Both	0	2	0	2

Characteristics	MSC (*n*=3)	SLM (*n*=3)	SS (*n*=3)	Combined
Nil	1	1	1	1
Current Treatment				
Pembrolizumab	2	1	2	5
Exemestane	1	0	1	2
Nil	0	2	0	2

Table 13 below outlines the 15 potential adverse events (AE) observed during the trial. Grade 1 AE are non-serious and do not significantly impact daily activities, whereas Grade 2 AE may interfere with the ability to perform daily tasks. The numbers shown are the numbers of patients with the relevant AE Grade. Relevant AEs are highlighted in bold.

Table 13 Adverse events reported in the Phase 1b clinical trial.

	Adverse event frequency (number of patients)					
	Methylselenocysteine		Sodium Selenite		Seleno-L-methionine	
Grade	**1**	**2**	**1**	**2**	**1**	**2**
Abdominal Cramping	1	0	0	0	0	0
Low phosphate	0	1	0	0	0	0
Foot pain	0	0	1	0	0	0
Diarrhoea	1	0	0	0	2	0
Loose Stools	0	0	2	0	2	0
Bloating	0	0	1	0	0	0
Urinary frequency	1	0	0	0	0	0
Headaches	0	0	1	0	0	0
Nausea	1	1	0	1	0	0
Vomiting	1	0	0	1	0	1
Skin Rash	0	0	1	0	0	0
Encephalopathy	0	0	0	0	0	1
Fatigue	0	0	1	0	0	1
Reduced appetite	0	0	0	0	0	1
Dizziness	0	0	0	0	1	1

The data indicates that the MSC compound has been the safest during this trial with seven AEs, two of which were Grade 2 (nausea and low serum phosphate). Of the remaining two compounds, SS was the next safest, with nine AEs, seven of which were Grade 1 and two Grade 2 (nausea and vomiting). For SLM ten AEs were reported, five of which were Grade 2, including

encephalopathy. Encephalopathy is brain dysfunction and can present as confusion, disorientation and even cause seizures or coma in more serious cases. This AE was subsequently attributed to endocrine dysfunction related to pembrolizumab, and not related to Se. Two patients withdrew from the trial, one was in the SLM group, and the other was in the SS group. They withdrew at the higher dose point. An independent doctor assessed that the illness were unrelated to the Se compound. Their final recorded visits were treated as Day 84.

3.2 Culturing of A549 Cells

A549 lung cells were revived from frozen liquid Nitrogen storage and grown until they were 90% confluent. **Figure 9** below shows the cell morphology of the cell line used for the purposes of this study and agrees with (Ren et al., 2015) who reported a pebble-like shape cell morphology with close cell–cell adhesion.

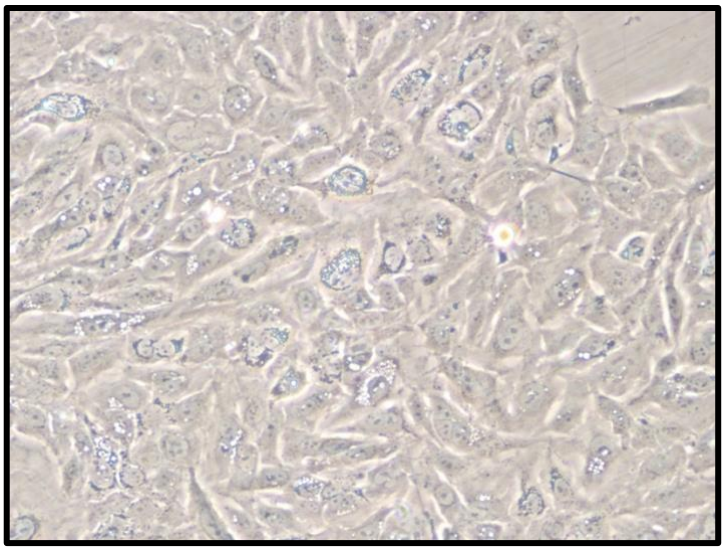

Figure 9 Morphology and appearance of cultured in in vitro A549 cells,

Cells were cultured in a surface-treated T25 flask. The photograph was captured using a camera fitted to a Nikon Eclipse TS100 microscope under 10X lens and normal bright light.

3.2.1 Mycoplasma contamination validation

The Mycoplasma PCR Contamination Assay demonstrated that the A549 cells used in this study were free of detectable mycoplasma contamination due to the absence of bands at ~500bp in Lane 3 on the agarose gel (**Figure 10**, TOP). Also, the internal DNA amplified at 500 bp for the negative template control (Lane 4), test A549 cell sample (Lane 5), and positive control (Lane 6). Thus, the possibility of false negative results was ruled completely out as this showed that the primers and all other components of the PCR were performing as expected.

A second assay was run with undamaged A549 DNA as a template to show no Mycoplasma contamination and rule out that the possibility of UVC destroying any detectable Mycoplasma. **Figure 10** (Bottom) shows the no product at ~500bp in the negative control (Lane 2) and the undamaged A549 sample (Lane 3). The positive control (Lane 4) and the positive control and sample (Lane 5) had product observed at ~500bp. This data shows that the control samples used were free of any mycoplasma DNA that would cause interference in the assay.

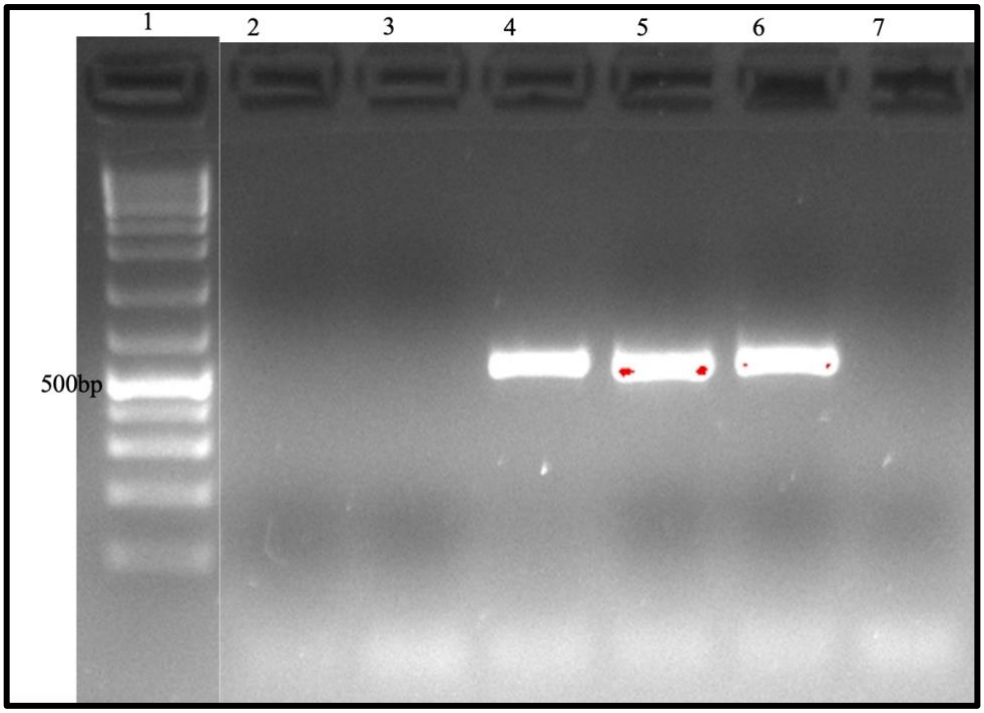

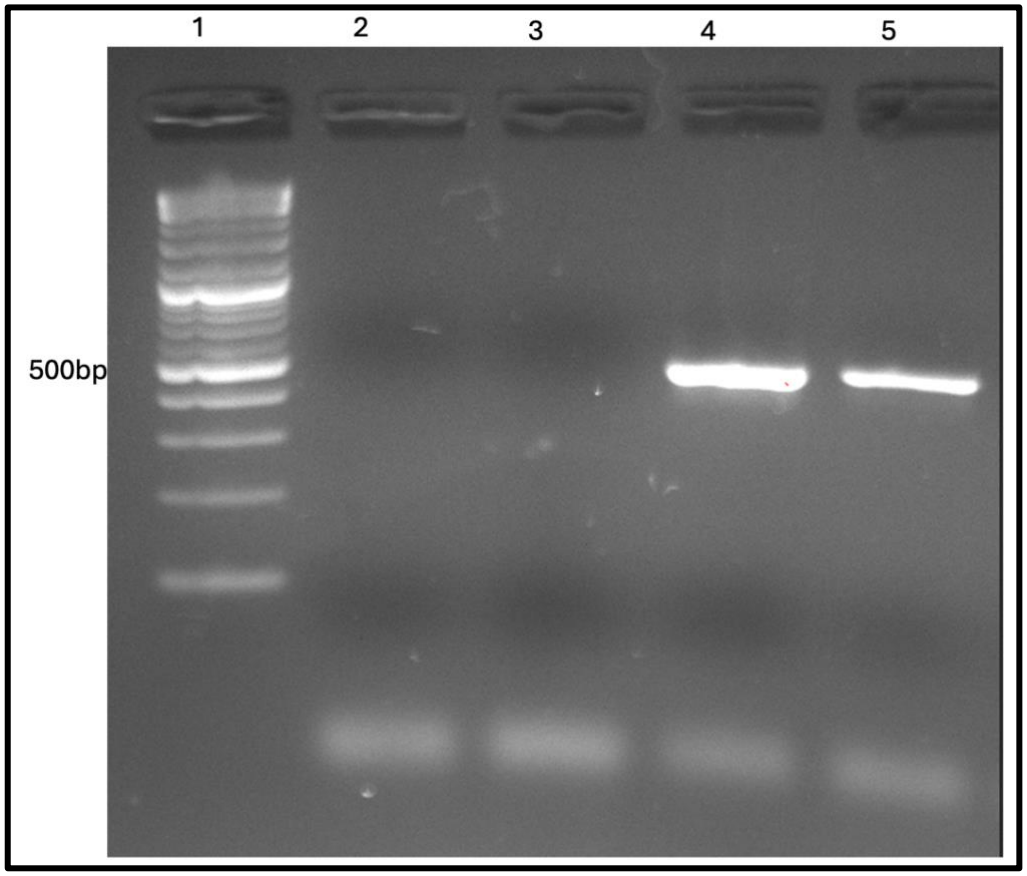

Figure 10 3% Agarose gel showing the Mycoplasma PCR Contamination Assay.

TOP: Lane 1 = DNA Ladder 1kb Plus Ladder was cropped from the same gel. Lane 2 = Media only. Lane 3 =A549 cells 100mJ/cm^2 damage. Lane 4 = Media only with positive control. Lane 5 = A549 cells 100mJ/cm^2 damage with positive control. Lane 6 = Positive control Lane 7 = Negative control (water). **BOTTOM:** Lane 1 = DNA Ladder 1kb Plus ladder. Lane 2 = Negative Control (water) Lane 3 =A549 cells undamaged. Lane 4 = positive control. Lane 5 = A549 cells undamaged with positive control.

3.3 Protein Extraction and Quantification

A total of 58 blood samples from nine patients were received and processed for PBMCs. These cells were snap frozen and later lysed so that the whole protein lysate could be measured using the Bradford assay to ensure equal loading of the protein of each sample into the wells of the SDS-PAGE gels for western blotting analyses. A representative example of Bradford Assay Standard Curve is shown in **Figure 11**. There was one negative protein sample (0 ng/mL BSA) and nine BSA standard readings ranging from 0.1 to 10 mg/mL (*n*=1). The accuracy of the standard curve was assessed by reviewing the distribution of data points along the best-fit line and the correlation coefficient R^2 value. In this representative example, this was in the acceptable high range (0.98).

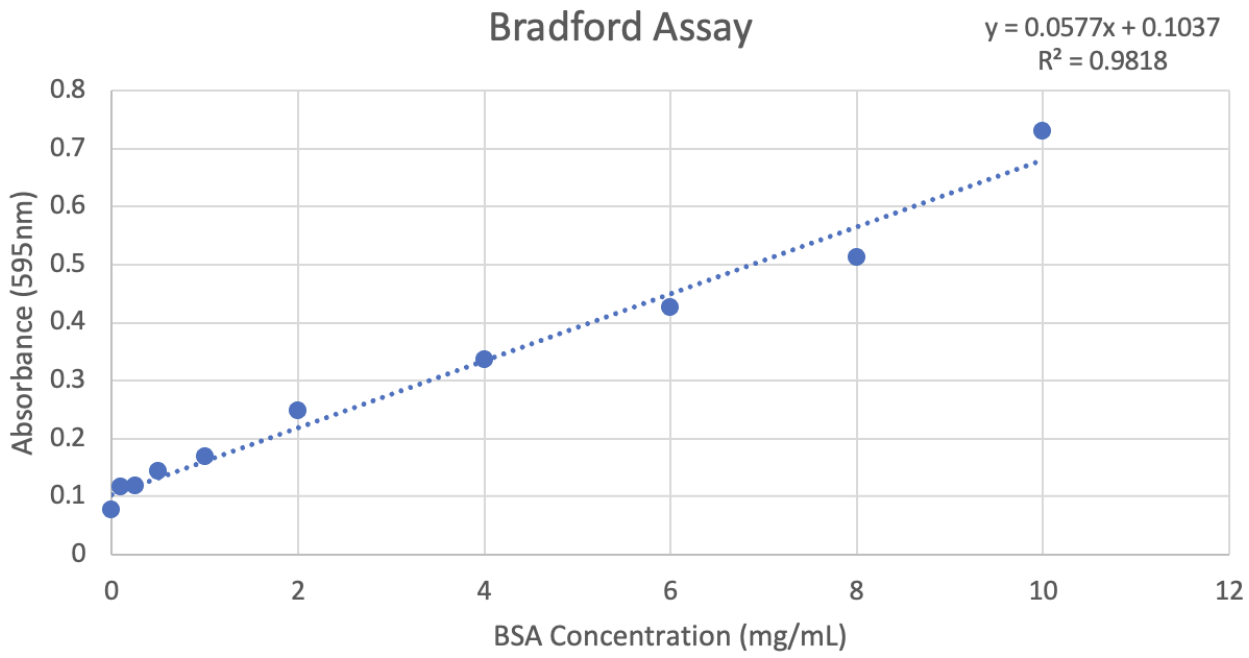

Figure 11 Representative Standard Curve of a Bradford Assay.

Ten BSA standards ranging from 0 - 10 mg/mL were plotted (*n*=1).

Table 14 shows the overall summary of the estimated protein concentrations from the Bradford Assay for patients 25-33 across seven hospital visits. The protein range was 1.0- 10 mg/mL. The mean was 3.66 mg/mL. If we review the protein yield and range across each patient, patients 28 and 30 have the largest protein concentration range; 1-10 mg/mL and 3-10 mg/mL, respectively.

Table 14 Protein Concentration.

Nine Patient Lysed PMBC as determined by the Bradford Assay.

SLM	
Pt and visit number	Protein Concentration (mg/mL)
Pt 27 V1	1.5
Pt 27 V2	4
Pt 27 V3	5
Pt 27 V4	4
Pt 27 V5	5
Pt 29 V1	3
Pt 29 V2	2
Pt 29 V3	5
Pt 29 V4	2
Pt 29 V5	2
Pt 29 V6	6
Pt 29 V7	3
Pt 33 V1	3
Pt 33 V2	1.5
Pt 33 V3	1.5
Pt 33 V4	1
Pt 33 V5	3
Pt 33 V6	2.5
Pt 33 V7	2

MSC	
Pt and visit number	Protein Concentration (mg/mL)
Pt 25 V1	6
Pt 25 V2	10
Pt 25 V3	10
Pt 25 V4	10
Pt 28 V1	1.5
Pt 28 V2	1
Pt 28 V3	3
Pt 28 V4	5
Pt 28 V5	1
Pt 28 V6	10
Pt 28 V7	5
Pt 32 V1	2
Pt 32 V2	3
Pt 32 V3	1.5
Pt 32 V4	2.5
Pt 32 V5	4
Pt 32 V6	4
Pt 32 V7	3

SS	
Pt and visit number	Protein Concentration (mg/mL)
Pt 26 V1	6
Pt 26 V2	2
Pt 26 V3	3
Pt 26 V4	2
Pt 26 V5	1
Pt 26 V6	2
Pt 26 V7	1
Pt 30 V1	10
Pt 30 V2	4
Pt 30 V3	N/A
Pt 30 V4	3
Pt 30 V5	4
Pt 30 V6	6
Pt 30 V7	4
Pt 31 V1	3
Pt 31 V2	4
Pt 31 V3	1
Pt 31 V4	5
Pt 31 v5	3
Pt 31 v6	2
Pt 31 V7	3.5

3.4 Western Blot Densitometry

Western blot analysis was carried out on nine patient samples using four primary antibodies which were normalised against the housekeeping loading control, GAPDH. Prior to testing, the current antibodies that were available in the laboratory were tested against A549, HeLa, and MDA-MB-456 protein cell extracts. **Figure 12** shows the western blot of five protein lysates samples against 1:200 sXBP1 antibody. It is expected to observe a 40kDa protein (**Table 4**) and this sized band was observed for the A549 cell line investigated. The inactive uXBP1 was also observed at the 22kDa mark. However, non-specific bands were observed, and the protein ladder (Lane 1) was over exposed and did not easily depict 10 recombinant proteins. This membrane was stripped and reprobed with CHOP and GRP78 (data not shown).

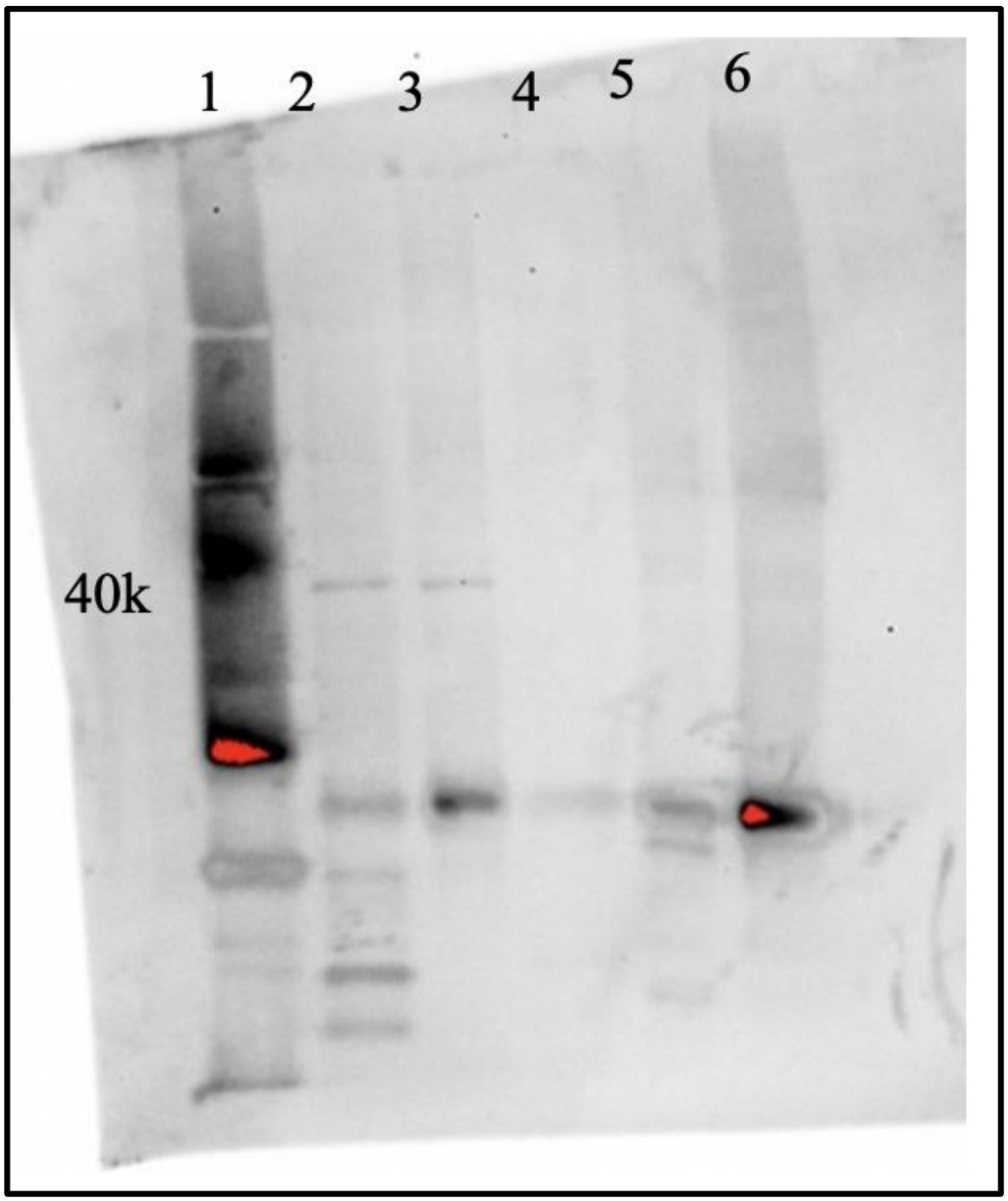

Figure 12 Validating the sXBP1 antibody using a western blot.

Lane 1= Ladder Bio Rad Precision Plus; Lane 2=A549 protein; Lane 3= A549-BP protein; Lane 4= HeLa protein; Lane 5= MDA-MB 456 protein; Lane 6= MDA-MB-456 protein. Red band = signal intensity is too high.

Since bands of the correct size were observed on the western blot we proceeded to use this antibody for analysis but introduced more washing steps to removed non-specific antibody binding. The antibodies for CHOP or GR78 did not show bands so a new batch of antibodies was ordered. Next, the antibody specificity and equal loading was determined by running a western blot to ensure the detection of single black band at the expected molecular weight (**Table 4**). Due to time constraints and limited resources only two western blots for eIF2a and sXBP1 and

one western blot for GRP78 are presented in this thesis. The remaining western blots will be carried out and analysed at a later date. For the purposes of this thesis, I have been unblinded to allow analysis of the western blots and LORDQ PCR data.

3.4.1 Relative Expression of eIF2α

Two membranes blotted with the eIF2α antibody recognised a single 37 kDa band (**Figure 13 A and B**) from hospital visits 2-6 for patients 32 and 33. It was noted that even though the baseline (V1) showed evidence of protein in the Bradford Assay, it was hardly visible on the western blot compared to the other protein extracts. Thus, it was determined not to use that data point in the results. However, this result will still be shown in the following membrane images but will not be represented in the western blot analysis. It was decided since the baseline samples were taken at the pre-clinical checks and the D1 (V2) sample was taken before treatment had begun on D1, the V2 sample was deemed appropriate as an initial starting point. A simple *t*-test were carried out on patient 32 and patient 33 comparing V2 GAPDH with the protein of interest V2 through to V7, with both being statistically significant with *p* values of 0.0002 and 0.0025, respectively.

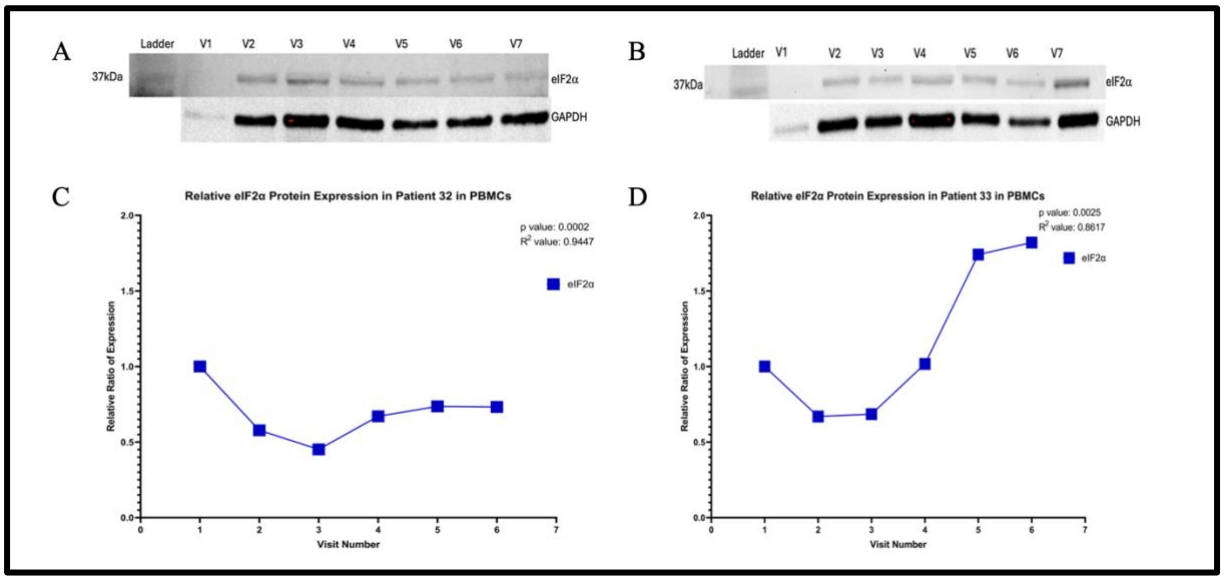

Figure 13 Western blot from patients 32 and 33 showing eIF2α protein bands against housekeeping protein GAPDH.

A.) Patient 32 western blot V=hospital visit. **B.)** Patient 33 western blot V=hospital visit. **C.)** Relative expression of eIF2α in Patient 32. Visit number 1= D1, Visit number 2= D2, Visit number 3=D29, Visit number 4=D30,

Visit number 5=D57, Visit number 6=D84 **D.)** Relative expression of eIF2α in Patient 33 Visit number 1= D1, Visi number 2= D2 Visit number 3=D29 Visit number 4=D30 Visit number 5=D57 Visit number 6=D84.

Patient 32 shows are more stable protein expression (**Figure 13A, C)**, whereas patient 33 shows an increase in relative eIF2α protein expression notably at the higher dosage point. (F**igure 13B, D**). The decrease in eIF2a expression could mean that the PERK pathway is not being activated. Whereas the increase in eIF2a could show that the PERK pathway is being activated.

3.4.2 Relative Expression of sXPB1

The membranes that were analysed for the 40 kDa protein sXBP1 are shown in **Figure 14 A** and **B**. Patient 32 (taking MSC) shows a decrease in relative protein expression and then a small increase when the Se dosage is increased then the expression lowers. This could be showing the lower dose being a better dosage at reducing ER stress with the lower sXBP1 expression (**Figure 14**). Patient 33 (taking SLM) shows a decrease in relative expression notably at the lower dosage point. With a small increase as dosage increases and then levels out near the end of treatment. A simple t-test were carried out comparing GAPDH from Day 1 (Visit 2) to the protein of interest, sXBP1, on patient 32 and patient 33 with patient 33 being statistically significant with a *p* value of 0.0212 and patient 32 not being statistically significant with a *p* value of 0.0752.

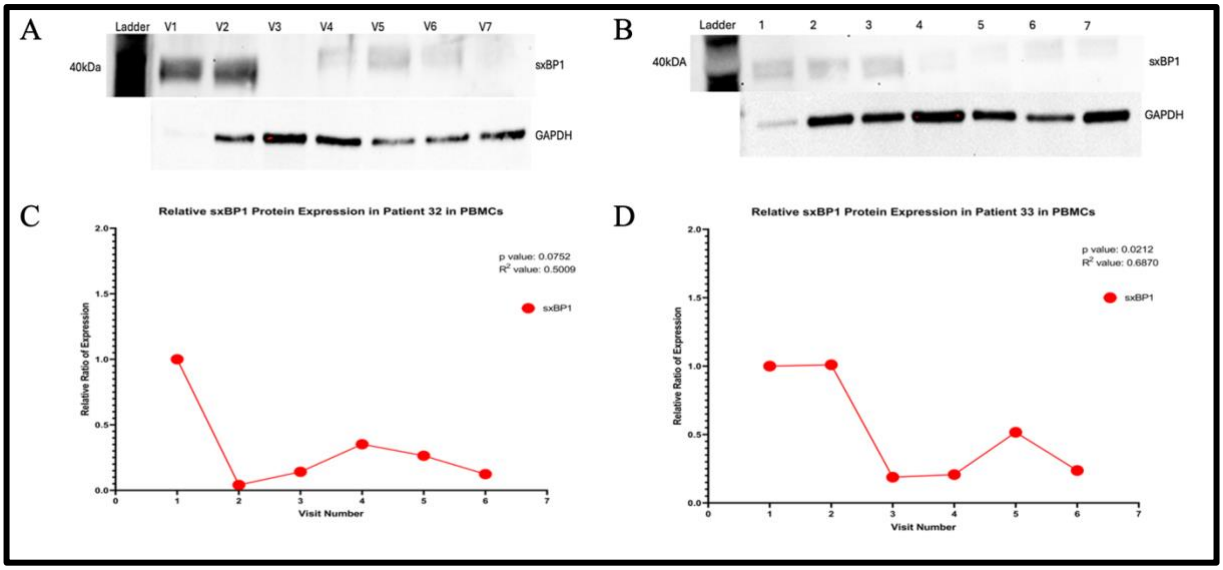

Figure 14 Western blot from patients 32 and 33 showing sXBP1 protein bands against housekeeping protein GAPDH.

With graph showing relative ratio of protein expression. **A.)** Patient 32 western blot V=hospital visit. **B.)** Patient 33 western blot V=hospital visit. **C.)** Relative expression of eIF2α in patient 32. Visit number 1= D1, Visit number 2= D2, Visit number 3=D29, Visit number 4=D30, Visit number 5=D57, Visit number 6=D84. **D.)** Relative expression of sXBP1 in Patient 33. Visit number 1= D1, Visit number 2= D2, Visit number 3=D29 Visit number 4=D30 Visit number 5=D57, Visit number 6=D84.

3.4.3 Relative Expression of GRP78

The membrane that was analysed for the 78 kDa protein GRP78 is shown in **Figure 15 A**. The expression of GRP78 decreases during the lower dose phase and then increases during the higher dose phase. Near the end of the higher dose the expression of GRP78 starts to decline showing a decline in ER stress. A simple t-test was carried out comparing GAPDH from Day 1 (Visit 2) to the protein of interest, GRP78, on patient 32 which gave a *p* value of 0.007 which shows this value is statistically significant.

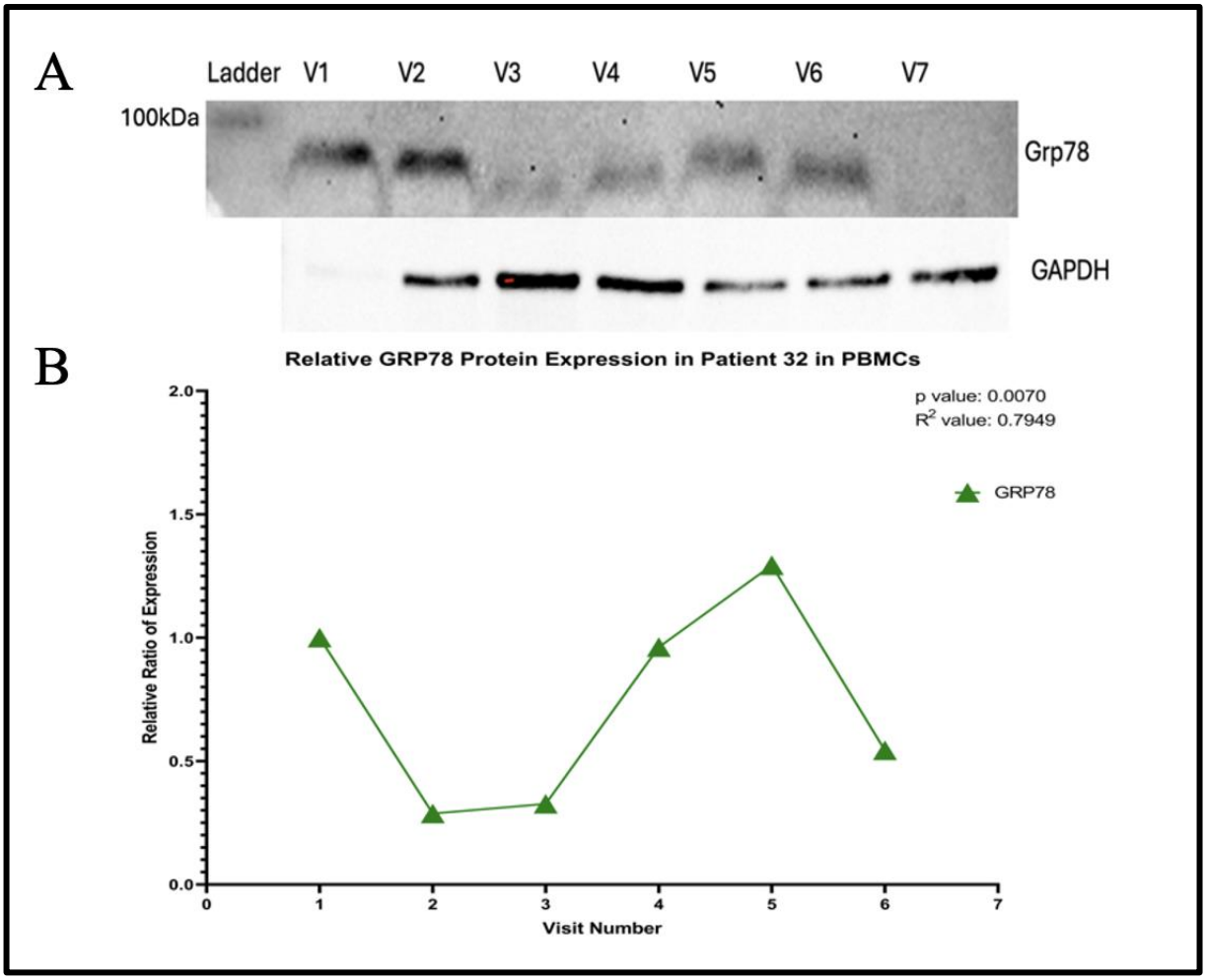

Figure 15 Western blot from patient 32 showing GRP78 protein bands against housekeeping protein GAPDH.

With graph showing relative ratio of protein expression. **A.)** Patient 32 western blot V=hospital visit. **B.)** Relative expression of GRP78 in patient 32. Visit number 1= D1, Visit number 2= D2, Visit number 3=D29, Visit number 4=D30, Visit number 5=D57, Visit number 6=D84.

3.4.4 Relative Expression of CHOP

No CHOP bands were detectable on the western blot membrane during the project. There could be three reasons for this. The first reason could be that the antibody is of poor quality, the second reason could be due to further refinements of the protocol used or the third reason is that the patient is not expressing that protein due to that pathway not being activated.

3.5 DNA Extraction from A549 Cells and Patient Blood Samples

3.5.1 A549 DNA Extraction

DNA was extracted from UVC-irradiated and non-irradiated A549 cells. **Table 15** shows the Denovix spectrophotometer concentration and quality of six DNA samples (*n*=2) that were extracted from Plates 1-3 (non-irradiated, 20 mJ/cm^2, and 100 mJ/cm^2). Due to the low concentration (<12.5 ng/μL) and quality of DNA samples 4 and 5 ($A_{260/280}$ <1.8), it was determined to do a clean and concentrate step to improve the yield and purity for downstream applications. Following purification, the yield 13.7 – 34.75 ng/μL and purity improved ($A_{260/280}$ > 1.8). However, the $A_{260/230}$ reading was not in the expected range of 2.0-2.2 before or after purification except for purified sample S6.

Table 15 A549 extracted DNA spectrophotometer results.

Spectrophotometer Data of DNA extracted of A549 before and after a clean and concentrate.
S = sample. A = Absorbance.

	DNA conc (ng/µL)	A260	260/230	260/280	Clean and Concentrate DNA samples	DNA conc (ng/µL)	A260	260/230	260/280
S1 No UVC	7.087	0.1417	0.181	1.912		34.750	0.6506	2.743	1.826
S2 No UVC	10.913	0.2183	0.176	1.777		13.784	0.4757	3.473	1.912
S3 20 mJ/cm^2	2.047	0.0409	0.09	1.801		24.961	0.4992	3.985	2.046
S4 20 mJ/cm^2	2.865	0.0573	0.128	1.385		25.123	0.5025	1.382	2.11
S5 100 mJ/cm^2	3.178	0.0636	0.061	1.621		19.709	0.3842	4.9113	2.263
S6 100 mJ/cm^2	5.752	0.115	0.103	2.059		25.151	0.503	2.075	2.07

3.5.2 Patient Sample Extraction

Table 16 shows the average DNA concentration that was extracted from blood samples of the nine patients, three patients did not have all seven visits. Patient 25 had visits 1, 2, 4, and 7, patient 27 had visits 1, 2, 3,4, and 7, and patient 30 had visit 1, 2, 4, 5, 6, and 7. The average range was 21- 76ng/µL with a mean of 43ng/µL. The $A_{260/280}$ quality was greater than 1.8 (data not shown). The resulting DNA was then used as a template for the LORD-Q.

Table 16 Average DNA concentrations (ng/µL) extracted from patient's blood.

Average DNA concentrations (ng/µL) extracted from patient's blood.

Patient	Average DNA concentration (ng/µL)
Pt 25	29.09
Pt 26	76.50
Pt 27	21.06
Pt 28	33.86
Pt 29	62.71
Pt 30	51.55
Pt 31	40.96
Pt 32	49.04

Pt 33	29.32

3.6 LORD-Q

3.6.1 Method Development and Validation

Prior to running the LORD-Q assay, the published primers sets (**Table 8**) were validated via traditional PCR to ensure all DNA templates amplified to the correct product size with no contamination in the negative control (no DNA template). A representative melt curve from PCR run is shown below (**Figure 16 A**) and shows three high sharp peaks at 85-90 degrees for the amplified undamaged A549 (Olive peak) and irradiated A549 DNA (20 mJ/cm^2 (Blue peak) and 100 mJ/cm^2 (Purple peak)). Additional broader peaks were observed around 65-80 degrees and represent primer dimers. The agarose gel (**Figure 16 B**) shows the results of six PCR reactions with the expected size of 3723 bp observed as a sharp white band in Lanes 3-5 and 7. However, smearing was also observed, indicating non-specific amplification plus a primer dimer was observed, running around the 100 bp ladder. All the samples that were extracted from the A549 cells, non-treated and UVC irradiated amplified. A sharp band around 4000 bp was observed for patient 33 (visit 2) with a faint band for patient 29. The negative control in Lane 2 also showed a primer dimer which is consistent with the melt curve data (**Figure 16 A**).

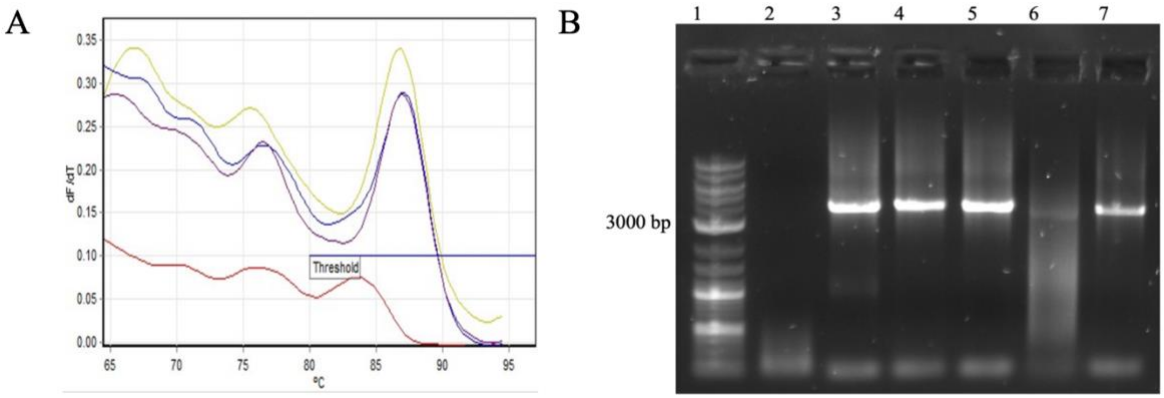

Figure 16 Validation of mitochondrial long run PCR Primers for patients 29 and 33.

A.) melt curve from PCR run on the 27.5.2025 long Mito run. Red= negative control; Olive= Undamaged; Blue=20mJ/cm^2; Purple=100 mJ/cm^2 **B.)** 0.8% agarose gel; Lane 1= DNA Ladder; Lane 2= Negative; Lane 3= No UVC damage; Lane 4= 20 mJ/cm^2 damage; Lane 5= 100 mJ/cm^2 damage; Lane 6= Patient 29 Visit 4; Lane 7= Patient 33 Visit 2.

Figure 17 A shows the melt curve for a PCR run validating the short mitochondrial primers. Two high peaks from 76-84 degrees were observed for undamaged A549 DNA (olive) and irradiated DNA (purple). However, a small narrow peak for negative control (red) and a 20 mJ/cm^2 irradiated damaged DNA sample. A 3% agarose gel (**Figure 17 B**) was run to determine if this was contamination or a primer dimer. It was found in the gel that there was no product or primer dimer formation (Lanes 2 and 4). This small peak could have been caused by dye interference. Thus, it was decided to use a different 20 mJ/cm^2 A549 damaged DNA sample for the following runs.

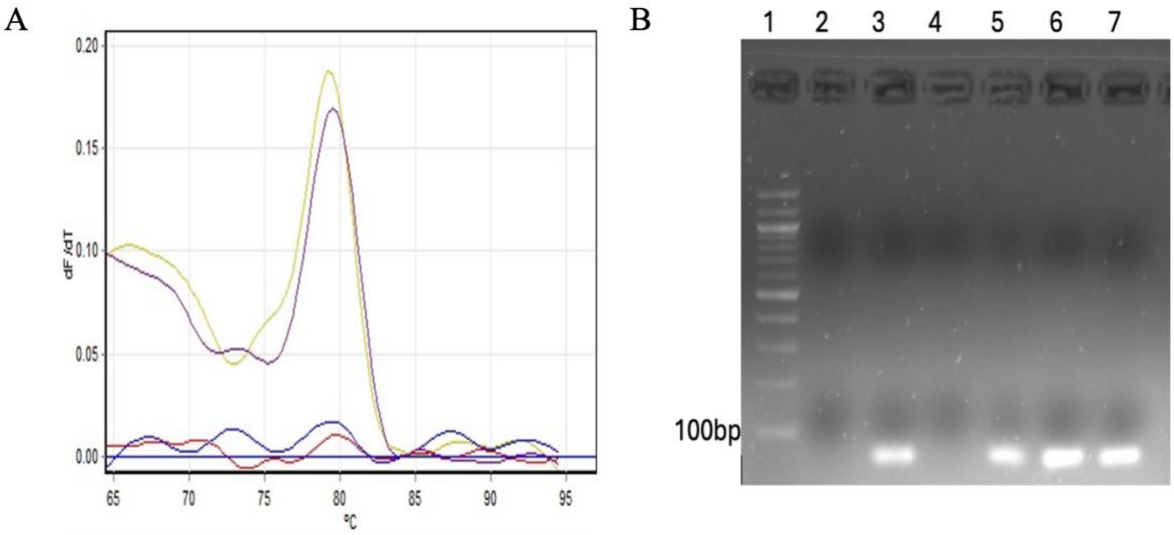

Figure 17 Validation of mitochondrial short run PCR Primers for patients 26 and 31.

A.) Melt Curve from PCR run on the 10.6.2025 Short Mito run. Red= negative control; olive= undamaged; Blue=20 mJ/cm^2; Purple=100 mJ/cm^2; **B.)** 3% Agarose Gel. Lane 1= DNA Ladder 100 bp; Lane 2= negative control; Lane 3= undamaged; Lane 4= 20 mJ/cm^2; Lane 5= 100 mJ/cm^2; Lane 6= pt 26 V1; Lane 7= pt 31 V1.

Figure 17 B also shows that the observation of the expected amplicon size, 45 bp, using the small mitochondrial primer set. Lanes 3, 5, 6 and 7 show a band running below the 100 bp ladder (Lane 1) and represents the amplified A549 undamaged and UV damaged (100mJ/cm^2) and two patient's samples, 26 and 31from hospital visit 1. No contamination was observed in the negative control (Lane 2).

Melt curves for the nDNA run are shown in figure 3.10. These runs show no contamination during the PCR run evident by no peaks visible in the negative control (red).

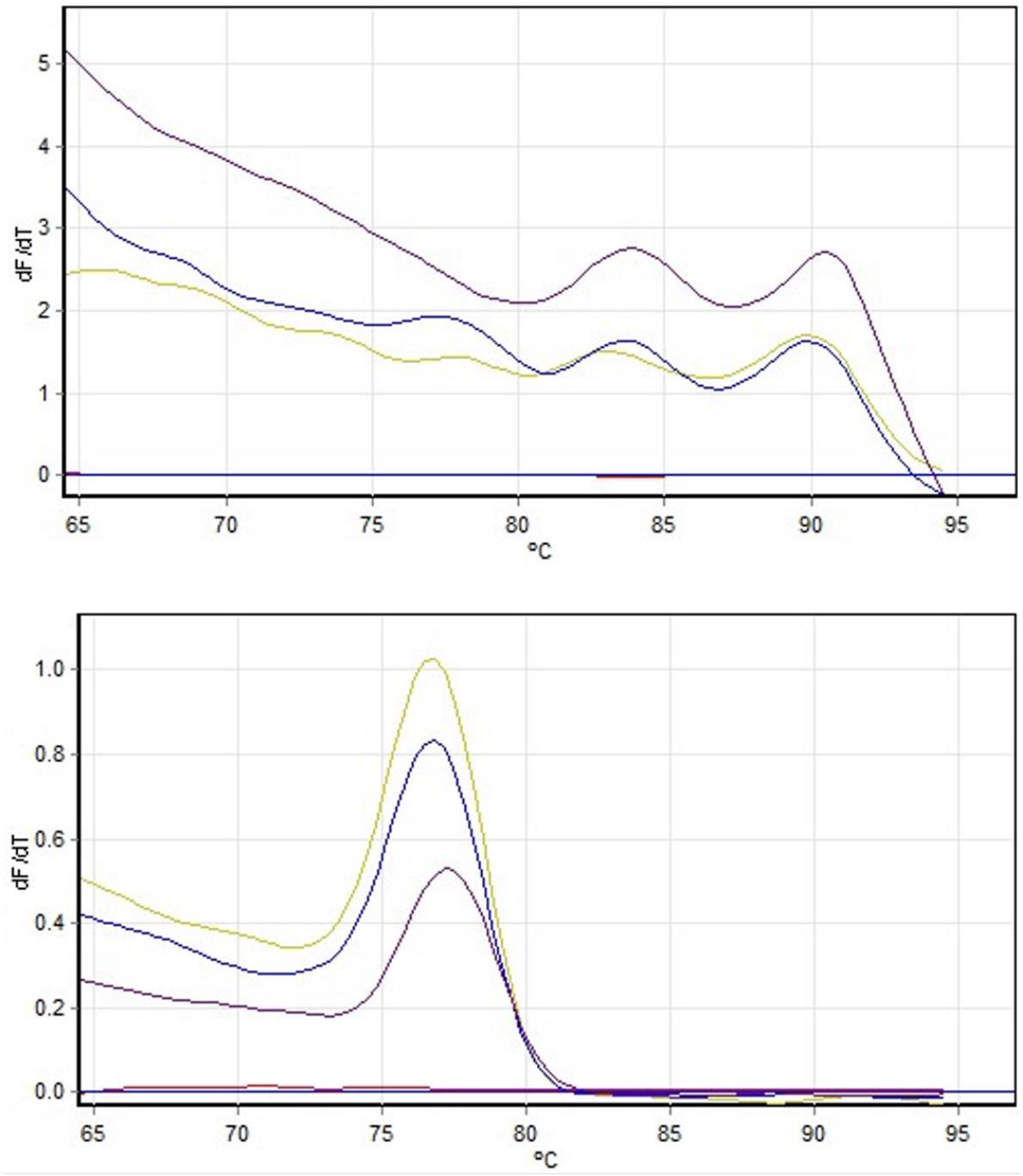

Figure 18 Validation of nDNA short and long run PCR Primers

TOP: Long Primer run: red= negative control; olive= undamaged; blue=20 mJ/cm^2; purple=100 mJ/cm^2
BOTTOM: Short primer: red= negative control; olive= undamaged; blue=20 mJ/cm^2; purple=100 mJ/cm^2

Based on the validation assay data, LORD-Q was set up using DNA as outlined in **Table 9** for mtDNA long, and the nDNA short and long and **Table 10** for mtDNA short , run under PCR

conditions outlined in **Table 11** and the quantification report was taken from each run and the C_q values were then used to calculate the lesions in the examined material using **Equation 2** in **Section 2.6**. The calculations are available in the Supplementary Electronic Appendix.

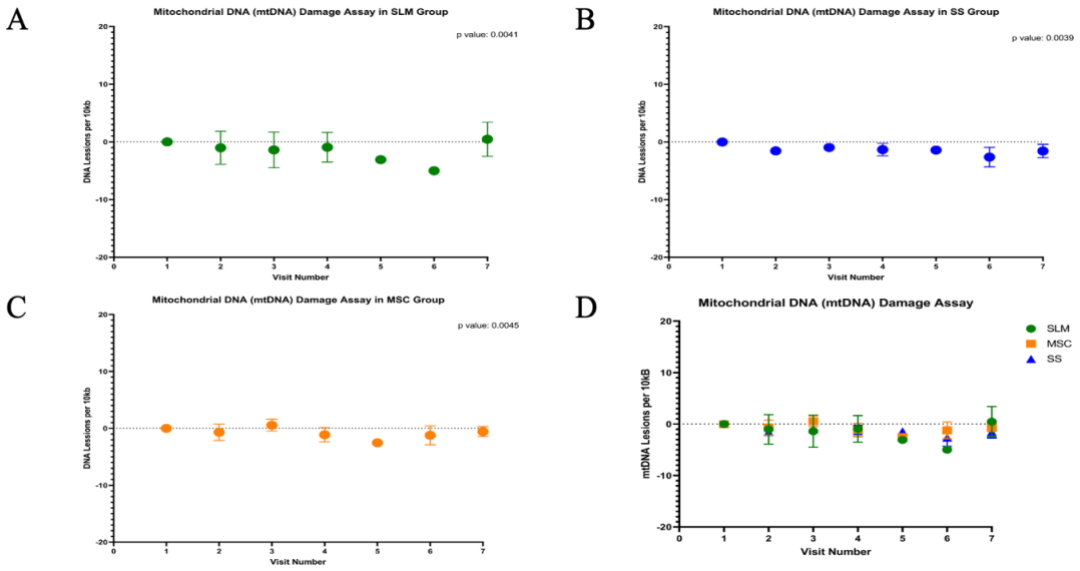

Figure 19 Comparing mtDNA damage between Se compound groups.

A.) SLM; **B.)** SS; **C.)** MSC: **D.)** Average mtDNA damage between the three Se compounds.

3.6.2 Mitochondrial DNA (mtDNA) Damage

No adverse genotoxicity was observed in all three compounds. All three compounds have shown sustained relative mtDNA protection or repair during the trial. SLM (**Figure 19 A)** shows a downward trend, seen especially from visit 3 onward. Error bars increase from the later visits; this could be due to a patient removing themselves from the trial. SS (**Figure 19 B**) shows the strongest downward trend. Error bars are smaller showing less variability. MSC (**Figure 19 C**) has the smaller downward trend. The error bars are smaller than SLM which suggests a consistent effect across patients. The Shapiro-Wilks test was used to determine the normality of the sample groups. Under this test the SLM, MSC, and SS groups were all found to be normal with *p* values of 0.3680, 0.8607, and 0.5359, respectively. An analysis using the mixed-effects analysis method

in the SLM, MSC, and SS compound groups shows statistically significant changes in mtDNA within each treatment group, with *p* values of 0.0041, 0.0045, and 0.0039, respectively.

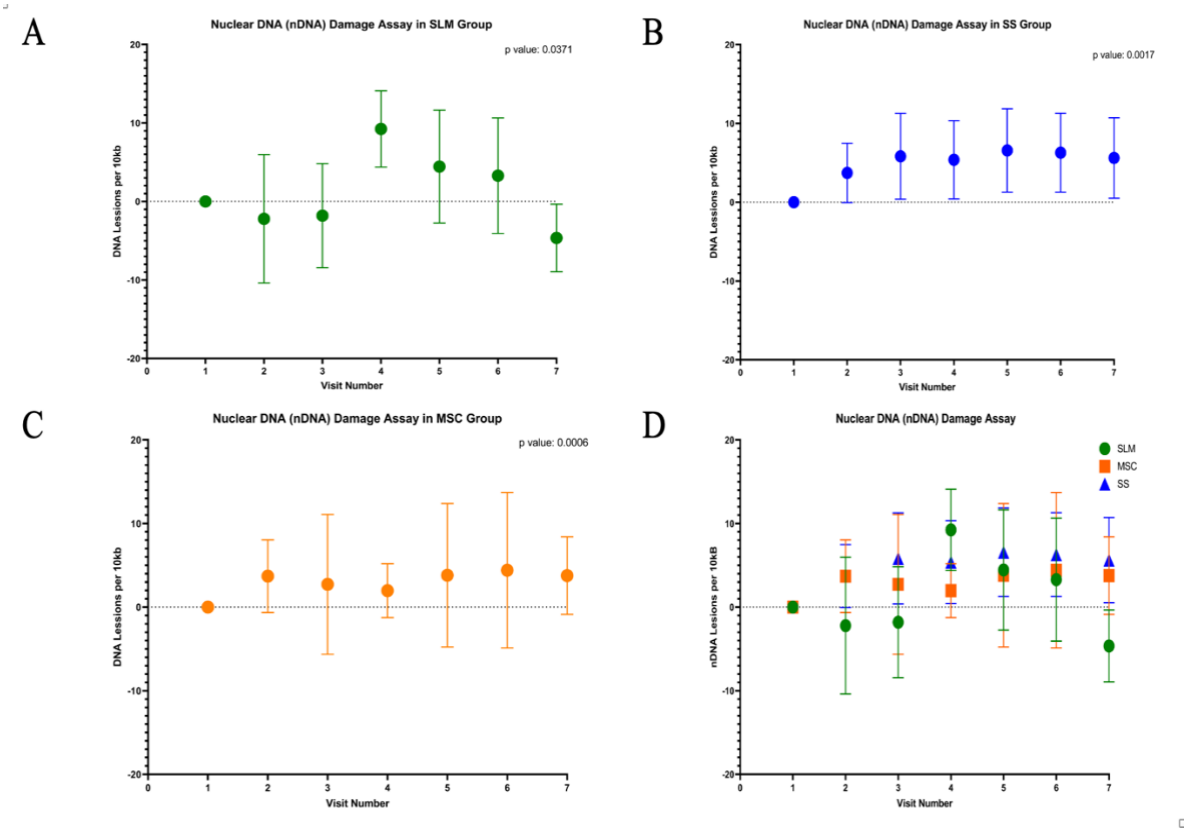

Figure 20 Comparing nuclear DNA damage between Se compound groups,

A.) SLM; **B.)** SS; **C.)** MSC; **D.)** Average genomic DNA damage between the three Se compounds. *n* =3. Results are presented as mean ±SE.

3.6.3 Nuclear DNA (nDNA) Damage

No adverse genotoxicity was observed in the three Se compounds. The SLM compound group (**Figure 20 A**) shows fluctuating lesions with an initial decrease in the lower dose visits and then an increase in the higher dose with no lesions or higher nDNA repair relative to the control group in the final visit. Error bars are large which indicates higher sample variability. This could be due to patient 27 removing themselves from the trial at the half-way point, also there was no long

product for V4 and sparce amplification for V3 and V7 for patient 27, and the DNA yield was also low: V4 was 11.58 ng/μg and V7 yield being 7.16 ng/μg.

The SS compound group (**Figure 20 B**) remains above zero which shows consistent relative nDNA damage to the control group. Error bars show moderate variability in the data set. The MSC compound group (**Figure 20 C**) shows a similar pattern to the SS compound group. Wide error bars could suggest subject-dependent responses. The Shapiro-Wilks test was used to determine the normality of the sample groups. Under this test the SLM and MSC groups were found to be normal with *p* values of 0.7746 and 0.1587, respectively. The SS group were found to not be normally distributed with a *p* value of 0.0207.

Under a statistical analysis using the mixed-effects analysis the MSC and SLM compounds in nDNA gave a *p* value of 0.0006 and 0.0371, respectively which means there is a significant relationship. Under a statistical analysis using the Friedman test the SS group gives a *p* value of 0.0017 which also means a statistically significant relationship. However, the large standard deviation bars show that there is high variability with the response to the Se compounds between the patients. This is caused by outliers, notably Patient 27, as discussed above.

3.6.4 Cell Line DNA Damage

The C_q values were taken from the averages of the non-irradiated A549 and THP-1 cells and were compared with the 20mJ/cm^2 and 100mJ/cm^2 averages of each LORD-Q run to validate that damage has occurred in these samples. The change in C_q was calculated using **Equation 4**. The RI was calculated using **Equation 5** and finally the lesions per 10kb was calculated using **Equation 6**. **Table 17** shows the results of the relative integrity of the DNA and the estimated lesions per 10kb. The A549 cell line shows the most damage in the 20mJ/cm^2 (1.53kb) group when the non-irradiated cells are used as a reference. Whereas the THP1 cell line shows less damage in the 100mJ/cm^2 (-8.78kb) group than non-irradiated cells.

Table 17 DNA lesions caused by UV treatment against cell lines that were not UV treated.

Cell line and Treatment	Relative Integrity (RI)	Lesions per 10kb
A549 non-irradiated	0.00450	0.00
A549 20 mJ/cm^2	0.00193	1.53
A549 100 mJ/cm^2	0.00389	0.36
THP-1 non-irradiated	0.03900	0.00
THP-1 20 mJ/cm^2	0.02900	0.84
THP-1 100 mJ/cm^2	0.14300	-8.78

The A549 cell line was used for the mtDNA assay and the THP-1 cell line was used for the nDNA assay, as during the validation process A549 had a greater amplification with the mtDNA primers and the THP-1 had a greater amplification with the nDNA primers. **Table 17** shows a low RI for the A549 and THP-1 non-irradiated cell lines. This is not unexpected due to both cell lines being a cancerous where there is genomic instability, increased rates of mutation, and greater oxidative stress. The lesions per 10kb increase with irradiation in the A549 cell line validated that UV-C damage did occur. The THP-1 cell line shows an increase in nDNA damage at the 20 mJ/cm^2 which is to be expected. However, there is a decrease in nDNA damage when the non-irradiated nDNA is compared with the 100 mJ/cm^2 this is unexpected and should follow a pattern of greater nDNA damage.

Chapter 4 Discussion

4.1 Evaluation of Compound Safety

For safety, three evaluations were used: AEs were used as a short-term response, ER stress as a medium-term response, and the LORD-Q PCR assay was used for long-term response and to assess genotoxicity.

In this Phase 1b clinical trial no AEs above Grade 2 were observed in any of the Se compound groups, indicating that all Se compounds were adequately tolerated at the administered doses of 1600mcg/day and 6400mcg/day. The most common AEs recorded were gastrointestinal (GI) related AEs, most commonly loose stools and diarrhoea. These GI AEs were predominantly Grade 1 and all resolved without intervention.

MSC showed the most favourable safety profile, with the only AEs recorded above Grade 1 being nausea and low phosphate. Mild abdominal cramping, diarrhoea, urinary frequency, nausea, and vomiting were observed. Similarly, AEs with SS were predominantly Grade 1, with two Grade 2 AEs limited to loose stools. However, SLM was less well tolerated, with Grade 2 events of loose stools, vomiting, dizziness, fatigue, and reduced appetite. Of note, two patients withdrew from the trial one in the SLM and one in the SS group withdrew during the lower dose phase of the trial; however, this withdrawal was assessed as unrelated to the treatment by the oncologist. Some of the AEs were unrelated to the compound or dosage but were related to the other AEs occurring.

This safety data is consistent with what has been noted in previous clinical trials. In Marshall et al. 2017. there were no Grade 2 or higher AEs with MSC and SLM at doses of 400 µg and 800 µg. It is of note that this study was conducted on healthy men (Marshall et al., 2017). This is something

to keep in mind when evaluating Se compounds for thus trial as the participants will be undergoing chemotherapy and/or radiotherapy. A 2015 trial on cancer patients was conducted by Brodin et al 2015,. used SS at doses three times higher than doses used in this clinical trial (Brodin et al., 2015). Grade three and four AEs were observed in this trial with fatigue being the stand out AE with six instances. In the Phase 1a clinical trial Evans et al. (2019) noted that SLM was the only compound showing an AEs of Grade 3 (Evans, 2019).

Analysis of data from previous trials and the Phase 1a clinical trial, preliminary evidence suggest that MSC, showing the fewest AEs at all three dosages, can be deemed the safest of the three Se compounds. However, a larger cohort will be needed to better assess this claim.

4.2 Evaluation of Protein Expression Biomarkers

The baseline samples from patients 32 and 33 showed elevated levels of sXBP1(Figure 3.6A and B). Patient 32 also exhibited elevated expression GRP78 expression at baseline (Figure 3.7). Interestingly, GAPDH expression at baseline was much lower than that of both sXBP1 and GRP78. For this reason, the baseline visit was excluded from the western blot analysis, as GAPDH loading was uneven and the Se compound treatment had not yet commenced.

In this study, four UPR markers, sXBP1 ,eIF2a, GRP78, and CHOP, were evaluated to investigate how supranational Se influences ER stress signalling in cancer patients. At the 400 mcg/day level, sXBP1 expression was consistently suppressed across MSC, SLM and SS treatment groups, suggesting that Se broadly attenuates IRE1a mediated signalling. In contrast, single patient western blot data revealed more nuanced and compound specific effects. In patient 33, who was in the SLM group, eIF2a expression increase markedly by Day 84, indicating activation of the PERK pathway and suggesting that SLM may promote more sustained stress response due to its longer half-life and capacity for nonspecific protein incorporation. Patient 32, who was in the MSC group, showed a similar biphasic pattern in GRP78 expression, with an initial decrease followed by a pronounced increase at later time points, consistent with the induction of unresolved ER stress. Given that GRP78 induction reflects compensatory activation of the UPR and dissociation from ER stress sensors, this pattern supports the notion that MSC, though rapidly metabolised, can trigger late-stage stress signalling through PERK and GRP78. Interestingly, CHOP, a pro-apoptotic UPR effector downstream of PERK, was undetectable in the samples that were tested, suggesting that while Se treatment altered early and adaptive UPR markers, it did not drive a detectable terminal UPR within the timeframe studied. Taken together, these findings suggest that Se does not uniformly suppress ER stress but instead redistributes signalling away from the IRE1a pathway towards the PERK pathway, with compound specific kinetics shaped by differences in

Se metabolism. This may reflect a dose-dependent switch in Se activity, from protective antioxidant effects at lower exposures to pro-oxidant stress induction at higher exposures.

In this study, total eIF2α expression was used as a measure of ER stress; however, this approach is limited because it is the phosphorylated form of eIF2a that is functionally activated during ER stress (Costa-Mattioli & Walter, 2020). A more informative metric is the ratio of total eIF2α to phosphorylated eIF2α, accounts for the variability in protein loading and expression and provides a clearer indication of ER stress signalling. For example, Han et al. applied this method to study ER stress during adipogenesis in mouse cells, demonstrating that the PERK pathway, rather than the IRE1α pathway, was primarily responsible for suppressing adipogenesis based on pathway-specific marker expression, as indicated by the expression levels of pathway-specific markers (Han et al., 2013). Applying a similar strategy in the present study would allow a more detailed characterisation of UPR activation in response to different Se compounds and could clarify whether distinct pathways are preferentially engaged. This supports the original hypothesis that an increase in Se compounds will see an increase in proteins that are responsible for UPR and SLM will have a greater increase due to the nature of its longer half life in the human body.

One possible explanation for the absence of a CHOP signal is that CHOP was not expressed in these patient samples. Alternatively, some commercial antibodies are known to be unreliable, potentially due to storage or transportation conditions. The detection of CHOP by traditional western blot methods is known to be challenging. For instance, Turpin et al. (2020) explored improving CHOP detection using an immunofluorescence assay in A549 cells treated with thapsigargin to activate ER stress and fixed with glutaldehyde (Turpin et al., 2020). Another study reported issues with commercial CHOP antibodies when assessing ER stress in patients with diabetes- although a different disease context, the underlying principles are comparable (Haataja et al., 2008). Furthermore, Brodin et al. (2020) compared an in-house SelP antibody with a

commercial SelP antibody and found that the in-house antibody detected more bands. This finding suggested there is indeed a degree of variability in how effectively different antibodies detect target protein, highlighting the importance of careful selection for future studies (Brodin et al., 2020).

4.3 Se Plasma Levels

Total plasma Se was measured by Canterbury Health Laboratories, NZ using mass spectrometry. In the SLM treatment group, an increase of approximately 30 µmol/L was observed from baseline by Day 57. This trend is consistent with findings reported by Evans et al., where plasma Se levels of around 3 µmol/L were observed in the SLM group. The difference in magnitude is likely due to dose escalation in the current trial, as higher doses produced nearly a ten-fold increase in plasma Se compared to lower dosing regimens.

SelP concentrations were assessed by ELISA, performed by C. Turnbull (University of Auckland). Analysis of SelP levels revealed that SS produced the highest plasma concentrations, followed by SLM, with MSC showing the lowest. These findings highlight the compound-dependent differences in Se speciation. The higher proportion of total Se observed in the SLM group is likely attributable to its ability to substitute for methionine and incorporate into proteins such as albumin. In contrast, the lower SelP levels with MSC suggest alternative metabolic fates: while a portion of MSC undergoes demethylation to form methylselenol, the key intermediate for selenoprotein synthesis, some is methylated into excretable forms, leading to urinary and respiratory elimination.

Despite dose escalation, SelP plateaued at approximately 7 mg/L, consistent with a regulatory ceiling reported in earlier trials (Hurst et al., 2010). Such saturation points suggest that SelP may

be regulated independently of total Se plasma concentrations once a threshold is reached. However, this is not consistent with the hypothesis stated by Brodin et al. (2020) where SelP concentrations of 7 mg/L were considered intermediates and not the plateau (Brodin et al., 2020). This contradictory result would be due to the delivery method of SS, intravenously, and the collection time points. The samples in that study were collected daily and not over an extended period as in this trial where samples were collected at the 28-day mark.

These differences in Se compound metabolism and distribution are particularly relevant when considering safety and does-escalation studied. As this trial is set out to identify which Se compound to use as a co treatment with chemotherapy and/or radiotherapy it is important to keep in mind that the dose and compound we add does not add unwarranted toxicity to the patient. So there are a few key points to keep in mind when evaluated the Se plasma levels. SLM incorporating albumin prolongs its half-life and can lead to accumulation (Nilsen et al., 2020), creating the potential for chronic toxicities with repeated dosing. SS remains low in total Se plasma. However, it has been linked to stronger oxidative stress and has higher variability in bioavailability. In contrast, MSC is metabolised and excreted more rapidly, which likely provides a wider safety margin over extended treatment durations. Linking this back to the observations made in AEs and the LORD-Q PCR assays this could explain the higher number of AEs observed in both SLM and SS when compared to MSC. The slow releasing and prolonged activity could also explain the increase relative nDNA damaged observed in the SLM group in the LORD-Q PCR assay.

4.4 DNA Damage

No evidence of adverse genotoxicity was observed in the LORD-Q data. Protective effects were apparent across all three Se compound groups at the level of mtDNA, with relative damage remaining below baseline throughout the trial. In contrast, nDNA damage showed a compound and dose-dependent pattern. For SLM, protective effects were evident at the 1600mcg/day dose; however, at the initiation of the 6400 mcg/day dose and increase in relative nDNA damage was observed. By Day 84, these levels had returned to baseline. This may suggest that SLM is being stored in the albumin and Se is accumulated in the plasma which can magnify the genotoxicity of Se. For both MSC and SS, nDNA damage remained relatively stable across the study, paralleling the consistent plasma Se concentration observed with these compounds. These findings align with previous results from the Phase 1a trial, further supporting the relationship between plasma Se pharmacokinetics and genotoxic outcomes.

A 2025 case-control study investigated DNA damage in gastric cancer patients. LORD-Q PCR was used in this study to identify DNA lesions. Comparing results found in that study and results from this project the MSC and SS profiles closely relate to what was observed in the control group of that study. The SLM results are close to what was observed in the gastric cancer patients. This further backs the claim that SLM exhibits higher genotoxicity than the MSC and SS compound groups (Mahjabeen et al., 2025)

Validation of DNA damage caused by UVC radiation confirmed that mtDNA lesions occurred in the A549 cell. In contrast, the THP-1 cell line, which measures nDNA damage, showed a negative result in the 100mJ/cm^2 sample compared to the non-irradiated control. This suggests that the non-irradiated THP-1 cells had more detectable lesions than the irradiated ones. A possible explanation is that robust nDNA repair mechanisms rapidly resolved UVC-induced lesions before DNA extractions. Literature on this specific comparison is limited; however, Evans et al. (2016) used both A549 and THP-1 cell lines in their study and observed a similar pattern - mtDNA exhibited

more persistent damage than nDNA. Additionally, the lower RI value observed in the non-irritated A549 cells indicates that these cells were already damaged. This could explain the apparent negative lesion values in mtDNA, as this sample was used as the reference for calculating lesion frequency.

4.5 Future Directions

Several limitations were identified during this clinical trial. The sample size was small, with only nine patients, three per compound. This restricted the statistical power of the study and made the data set fragile, as the loss of a single participant or deviations from the dosing schedule could cause major variability that could not be treated as outliers.

Technical challenges were also encountered in the western blot analyses. In particular, signal detection of CHOP proved problematic. This is consistent with previous reports that CHOP detection by standard western blot methods is difficult. For example, Turpin et al. (2020) optimised CHOP detections in A549 cells by employing immunofluorescence (Turpin et al., 2020), while Haataja et al. (2008) noted unreliable performance of commercial CHOP antibodies in diabetes related ER stress studies (Haataja et al., 2008). Similarly, Brodin et al. (2020) demonstrated that an in house SelP antibody outperformed a commercial antibody, emphasising variability in antibody performance and the importance of careful antibody selection in future work (Brodin et al., 2020).

Low baseline signals were another limitation, complicating data interpretation. A coomassie stain was not performed to assess protein integrity because of the limited PAGE gel availability.

Instead, Ponceau S staining after protein transfer revealed a banding smear that included high molecular weight proteins (data not shown). For future experiments, the use of a protein concentrator kit, such as the Vivaspin® 500 centrifugal concentrator with a polyethersulfone membrane (Sartorius), suitable for small sample volumes (approximately 300 μL) is recommended to improve protein concentration and ensure more consistent loading

Further work on Se speciation is also warranted. For example, urinary analysis could provide insight into MSC metabolism, while mass spectrometry of selenoalbumin could clarify the incorporation of SLM into albumin and its contribution to plasma Se. This is vital information that can yield a clearer interpretation of pharmacodynamic biomarkers. Tests similar to del Casillo Busto, 2024 would be sufficient (del Castillo Busto et al., 2024).

Finally, the LORDQ PCR assay would benefit from improved controls. At present, DNA damage is assessed relative to patient baseline samples, but this does not account for damage introduced during PBMC extraction or freeze thaw cycles. Including untreated PBMCs as an experimental control would enable normalisation for background damage unrelated to the Se treatment, thereby strengthening the interpretation of the data. In the 2025 case-control study, Mahjabeen et al. (2025) used a control group of healthy participants to normalise the DNA damage observed in the gastric cancer patient cohort. Using a similar control group would allow us to normalise the DNA damage and eliminate any background damage (Mahjabeen et al., 2025).

Based on the results from this Phase 1b clinical trial and the previous Phase 1a clinical trial it is recommended that the MSC compound be taken to a Phase 2 trial with a dose escalation of 1600 mcg/day to 3200 mcg/day and then a final dose of 6400 mcg/day. In addition, suggest a larger sample size of about 50 patients to increase the statistical power of the results plus a healthy

control cohort of similar ages of the patients in the treatment group so to use the PBMCs extracted from that group too normalise against. Finally, keep the LORD-Q PCR assay as a tool for observing gDNA damage but consider a more robust method of analysing ER stress proteins such as ELISA or mass spectrometry.

5. Conclusion

Based on the preliminary findings discussed in this thesis, I would recommend that MSC be selected as the compound that is used in a future Phase 2 clinical trial. In contrast, the Se plasma levels that are exhibited by SLM are of concern. Total Se in plasma is too high in SLM as it incorporates into albumin and can give toxicities further along the trial. MSC also exhibited less AE when compared with SLM and SS. The biochemical pathway that MSC undertakes is also advantageous, as the metabolite methylselenol is an anticancer agent. Further analyses need to be completed including processing western blot data for all nine patients, before a final definite recommendation can be given.

References

Alfandari, A., Moskovich, D., Weisz, A., Katzav, A., Kidron, D., Beiner, M., Josephy, D., Asali, A., Hants, Y., Yagur, Y., Weitzner, O., Ellis, M., Itchaki, G., & Ashur‐Fabian, O. (2024). The selenoenzyme type I iodothyronine deiodinase: a new tumor suppressor in ovarian cancer. *Molecular Oncology*, *18*(9), 2298–2313. . https://doi.org/10.1002/1878-0261.13612

Almanza, A. C., A., Chintha, C., Creedican, S., Doultsinos, D., Leuzzi, B., Luís, A., McCarthy, N., Montibeller, L., More, S., Papaioannou, A., Püschel, F., Sassano, M., L, S., J., Agostinis, P., Belleroche, J., Eriksson, L. A., Fulda, S., & Gorman, A. M., … Samali, A. (2019). Endoplasmic reticulum stress signalling – from basic mechanisms to clinical applications. *The FEBS Journal*, *286*(2), 241-278. https://doi.org/10.1111/febs.14608

Ames, B. N., Gold, L. S., & Willett, W. C. (1995). The causes and prevention of cancer. *Proceedings of the National Academy of Sciences - PNAS*, *92*(12), 5258–5265. https://doi.org/10.1073/pnas.92.12.5258

Bleys, J., Navas-Acien, A., & Guallar, E. . (2008). Serum selenium levels and all-cause, cancer, and cardiovascular mortality among US adults. *Archives of internal medicine*, *168*(4). https://doi.org/10.1001/archinternmed.2007.74

Boutelle, A. M., & Attardi, L. D. (2021). p53 and tumor suppression: it takes a network. *Trends in Cell Biology*, *31*(4), 298–310. https://doi.org/10.1016/j.tcb.2020.12.011

Brodin, O., Eksborg, S. W., M., Asker-Hagelberg, C., Larsen, E., Mohlkert, D., Lenneby-Helleday, C., Jacobsson, H., Linder, S., Misra, S., & Björnstedt, M. (2015). Pharmacokinetics and toxicity of sodium selenite in the treatment of patients with carcinoma in a phase I clinical trial: the SECAR study. *Nutrients*, *7*(6), 4978–4994. https://doi.org/10.3390/nu7064978

Brodin, O., Hackler, J., Misra, S., Wendt, S., Sun, Q., Laaf, E., Stoppe, C., Björnstedt, M., & Schomburg, L. (2020). Selenoprotein P as biomarker of selenium status in clinical trials with therapeutic dosages of selenite. *Nutrients*, *12*(4). https://doi.org/10.3390/nu12041067

Bulteau, A. L., & Chavatte, L. (2015). Update on selenoprotein biosynthesis. *Antioxidants & Redox Signaling*, *23*(10), 775-794. https://doi.org/10.1089/ars.2015.6391

Burk, R. F., & Hill, K. E. (1994). Selenoprotein P. a selenium-rich extracellular glycoprotein. *The Journal of Nutrition*, *124*(10), 1891-1897. https://doi.org/10.1093/jn/124.10.1891

Cai, X., Wang, C., Yu, W., Fan, W., Wang, S., Shen, N., Wu, P., Li, X., & Wang, F. (2016). Selenium exposure and cancer Risk: an updated meta-analysis and meta-regression. *Scientific Reports*, *6*(1). https://doi.org/10.1038/srep19213

Chen, H., Peng, F., Xu, J., Wang, G., & Zhao, Y. (2023). Increased expression of GPX4 promotes the tumorigenesis of thyroid cancer by inhibiting ferroptosis and predicts poor clinical outcomes. *Aging (Albany, NY.)*, *15*(1), 230-245. https://doi.org/10.18632/aging.204473

Chen, H., Yu, S., Ma, R., Deng, L., Yi, Y., Niu, M., Xu, C., Xiao, Z., & X, J. (2024). Hypoxia-activated XBP1s recruits HDAC2-EZH2 to engage epigenetic suppression of ΔNp63α expression and promote breast cancer metastasis independent of HIF1α. *Cell Death and Differentiation*, *31*(4), 447-459. https://doi.org/10.1038/s41418-024-01271-z

Chen, S., Chen, J., Hua, X., Sun, Y., Cui, R., Sha, J., & Zhu, X. (2020). The emerging role of XBP1 in cancer. *Biomedicine & Pharmacotherapy*, *127*. https://doi.org/10.1016/j.biopha.2020.110069

Cheng, Q., Sandalova, T., Lindqvist, Y., & Arnér, E. S. J. (2009). Crystal structure and catalysis of the selenoprotein thioredoxin reductase 1. *The Journal of Biological Chemistry*, *284*(6), 3998-4008. https://doi.org/10.1074/jbc.M807068200

Combs, G. F. (2001). Selenium in global food systems. *British Journal of Nutrition*, *85*(5), 517-547. https://doi.org/10.1079/BJN2000280

Copeland, P. R., & Howard, M. T. (2021). Ribosome fate during decoding of uga-sec codons. *International Journal of Molecular Sciences*, *22*(24), 13204. https://doi.org/10.3390/ijms222413204

Costa-Mattioli, M., & Walter, P. (2020). The integrated stress response: from mechanism to disease. *Science (American Association for the Advancement of Science)*. https://doi.org/10.1126/science.aat5314

del Castillo Busto, M. E., Ward-Deitrich, C., Evans, S. O., Rayman, M. P., Jameson, M. B., & Goenaga-Infante, H. (2024). Selenium speciation studies in cancer patients to evaluate the responses of biomarkers of selenium status to different selenium compounds. *Springer Science and Business Media LLC.*

Doello, K., Mesas, C., Quiñonero, F., Perazzoli, G., Cabeza, L., Prados, J., Melguizo, C., & Ortiz, R. (2021). The Antitumor Activity of Sodium Selenite Alone and in Combination with Gemcitabine in Pancreatic Cancer: An In Vitro and In Vivo Study. *Cancers*, *13*(13). https://doi.org/10.3390/cancers13133169

Duffield-Lillico, A. J., Slate, E. H., Reid, M. E., Turnbull, B. W., Wilkins, P. A., Combs, G. F., Park, H. K., Gross, E. G., Graham, G. F., Stratton, M. S., Marshall, J. R., & Clark, L. C. (2003). Selenium supplementation and secondary prevention of nonmelanoma skin cancer in a randomized trial. *JNCI : Journal of the National Cancer Institute,*, *95*(19), 1477-1481. https://doi.org/10.1093/jnci/djg061

Duffield‐Lillico, A. J., Dalkin, B. L., Reid, M. E., Turnbull, B. W., Slate, E. H., Jacobs, E. T., Marshall, J. R., & Clark, L. C. (2003). Selenium supplementation, baseline plasma selenium status and incidence of prostate cancer: an analysis of the complete treatment period of the nutritional prevention of cancer trial. *BJU International*, *91*(7), 608-612. https://doi.org/10.1046/j.1464-410X.2003.04167.x

El-Bayoumy, K. (2009). The negative results of the SELECT study do not necessarily discredit the selenium-cancer prevention hypothesis. *Nutrition and Cancer*, *61*(3), 265-286. https://doi.org/10.1080/01635580902892829

Evans, S. O., Jacobson, G. M., Goodman, H. J. B., Bird, S., & Jameson, M. B. . (2019). Comparative safety and pharmacokinetic evaluation of three oral selenium compounds in cancer patients. *Biological Trace Element Research,*, *189*(2), 395-404. https://doi.org/10.1007/s12011-018-1501-0

Evans, S. O., Jacobson, G. M., Goodman, H. J. B., Bird, S., & Jameson, M. B. . (2020). Comparison of three oral selenium compounds in cancer patients: Evaluation of differential pharmacodynamic effects in normal and malignant cells. . *Journal of Trace Elements in Medicine and Biology*, *58*, 126446. https://doi.org/10.1016/j.jtemb.2019.126446

Evans, S. O., Jameson, M. B., Cursons, R. T., Peters, L. M., Bird, S., & Jacobson, G. M. (2016). Development of a qPCR method to measure mitochondrial and genomic DNA damage with application to chemotherapy-induced DNA damage and cryopreserved cells. *Biology*, *5*(4). https://doi.org/10.3390/biology5040039

Gurney, J., Stanley, J., McLeod, M., Koea, J., Jackson, C., & Sarfati, D. (2020). Disparities in Cancer-Specific Survival Between Māori and Non-Māori New Zealanders. *JCO Global Oncology*, *6*(6), 766–774. . https://doi.org/10.1200/GO.20.00028

Haataja, L., Gurlo, T., Huang, C., & Butler, P. C. (2008). Many commercially available antibodies for detection of CHOP expression as a marker of endoplasmic reticulum stress fail specificity evaluation. *Cell Biochemistry and Biophysics*, *51*(2-3), 105-107. https://doi.org/10.1007/s12013-008-9019-2

Hadrup, N., & Ravn-Haren, G. (2023). Toxicity of repeated oral intake of organic selenium, inorganic selenium, and selenium nanoparticles: a review. *Journal of Trace Elements in Medicine and Biology,*, *79*, 127235-127235. https://doi.org/10.1016/j.jtemb.2023.127235

Han, J., Murthy, R., Wood, B., Song, B., Wang, S., Sun, B., Malhi, H., & Kaufman, R. J. (2013). ER stress signalling through eIF2α and CHOP, but not IRE1α, attenuates adipogenesis in mice. *Diabetologia*, *56*(4), 911-924. https://doi.org/10.1007/s00125-012-2809-5

Hanahan, D., & Weinberg, R. A. (2000). The hallmarks of cancer. *Cell*, *100*(1), 57-70. https://doi.org/10.1016/s0092-8674(00)81683-9

Hanahan, D., & Weinberg, R. A. (2011). Hallmarks of cancer: the next generation. *Cell 144*(5), 646–674. https://doi.org/10.1016/j.cell.2011.02.013

He, L., Zhang, L., Peng, Y., & He, Z. (2025). Selenium in cancer management: exploring the therapeutic potential. *Frontiers in Oncology*, *14*. https://doi.org/10.3389/fonc.2024.1490740

Hedström, E., Eriksson, S., Zawacka-Pankau, J., Arnér, E. S. J., & Selivanova, G. (2009). p53-dependent inhibition of TrxR1 contributes to the tumor-specific induction of apoptosis by RITA. *Cell Cycle (Georgetown, Tex.)*, *8*(21), 3584-3591. https://doi.org/10.4161/cc.8.21.9977

Humeau, J., Leduc, M., Cerrato, G., Loos, F., Kepp, O., & Kroemer, G. (2020). Phosphorylation of eukaryotic initiation factor-2α (eIF2α) in autophagy. *Cell Death & Disease*, *11*(6). https://doi.org/10.1038/s41419-020-2642-6

Hurst, R., Armah, C. N., Dainty, J. R., Hart, D. J., Teucher, B., Goldson, A. J., Broadley, M. R., Motley, A. K., & Fairweather-Tait, S. J. (2010). Establishing optimal selenium status: results of a randomized, double-blind, placebo-controlled tria. *The American Journal of Clinical Nutrition*, *91*(4), 923-931. https://doi.org/10.3945/ajcn.2009.28169

Jackson-Rosario, S. E., & Self, W. T. (2010). Targeting selenium metabolism and selenoproteins: Novel avenues for drug discovery. *Metallomics*, *2*(2), 112-116. https://doi.org/10.1039/B917141J

Jaud, M., Philippe, C., Di Bella, D., Tang, W., Pyronnet, S., Laurell, H., Mazzolini, L., Rouault-Pierre, K., & Touriol, C. (2020). Translational regulations in response to endoplasmic reticulum stress in cancers. *Cells (Basel, Switzerland)*, *9*(3). https://doi.org/10.3390/cells9030540

Kalimuthu, K., Keerthana, C. K., Mohan, M., Arivalagan, J., Christyraj, J. R. S. S., Firer, M. A., Choudry, M. H. A., Anto, R. J., & Lee, Y. J. (2022). The emerging role of selenium metabolic pathways in cancer: New therapeutic targets for cancer. *Journal of Cellular Biochemistry*, *123*(3), 532-542. https://doi.org/10.1002/jcb.30196

Karunasinghe, N., Ng, L., Wang, A., Vaidyanathan, V., Zhu, S., & Ferguson, L. R. (2019). Selenium Supplementation and Prostate Health in a New Zealand Cohort. *Nutrients*, *12*(1). https://doi.org/10.3390/nu12010002

Kim, H.-Y., & Gladyshev, V. N. (2005). Different catalytic mechanisms in mammalian selenocysteine- and cysteine-containing methionine-R-sulfoxide reductases. *PLoS Biology*, *3*(12). https://doi.org/10.1371/journal.pbio.0030375

Köhrle, J., Jakob, F., Contempré, B., & Dumont, J. E. (2005). Selenium, the thyroid, and the endocrine system. *Endocrine Reviews*, *26*(7), 944-984. https://doi.org/10.1210/er.2001-0034

Kojima, Y., Kondo, Y., Fujishita, T., Mishiro-Sato, E., Kajino-Sakamoto, R., Taketo, M. M., & Aoki, M. (2019). Stromal iodothyronine deiodinase 2 (DIO2) promotes the growth of intestinal tumors in ApcΔ716 mutant mice. *Cancer Science*, *8*(110), 2520-2528. https://doi.org/10.1111/cas.14100

Krannich, F., Mücke, R., Büntzel, J., Schomburg, L., Micke, O., Hübner, J., & Dörfler, J. (2024). A systematic review of Selenium as a complementary treatment in cancer patients. *Complementary therapies in medicine*, *86*. https://doi.org/10.1016/j.ctim.2024.103095

Kuganesan, M., Samra, K., Evans, E., Singer, M., & Dyson, A. (2019). Selenium and hydrogen selenide: essential micronutrient and the fourth gasotransmitter? *Intensive Care Medicine Experimental,*, *7*(1). https://doi.org/10.1186/s40635-019-0281-y

Langie, S. A. S., Azqueta, A., & Collins, A. R. (2015). The comet assay: Past, present, and future. *Frontiers in Genetics*(6). https://doi.org/10.3389/fgene.2015.00266

Ledesma, M. C., Jung-Hynes, B., Schmit, T. L., Kumar, R., Mukhtar, H., & Ahmad, N. (2011). Selenium and vitamin E for prostate cancer: Post SELECT (selenium and vitamin E cancer prevention trial) status. *Molecular Medicine 17*(1-2), 134-143. https://doi.org/10.2119/molmed.2010.00136

Lee, A. (2007). GRP78 induction in cancer: therapeutic and prognostic implications. *Cancer Res*, *67*(8), 3496-3499. https://doi.org/10.1158/0008-5472.CAN-07-0325

Lee, S., R.Bar-Noy, S., Kwon, J., Levine, R. L., Stadtman, T. C., & Rhee, S. G. (2000). Mammalian thioredoxin reductase: oxidation of the C-terminal cysteine/selenocysteine active site forms a thioselenide, and replacement of selenium with sulfur markedly reduces catalytic activity. *Proceedings of the National Academy of Sciences - PNAS*, *97*(6), 2521-2526. https://doi.org/10.1073/pnas.050579797

Lehle, S., Hildebrand, D. G., Merz, B., Malak, P. N., Becker, M. S., Schmezer, P., Essmann, F., Schulze-Osthoff, K., & Rothfuss, O. (2014). LORD-Q: a long-run real-time PCR-based DNA-damage quantification method for nuclear and mitochondrial genome analysis. *Nucleic Acids Research*, *6*(42), 41. https://doi.org/10.1093/nar/gkt1349

Li, J., Fu, C., Feng, B., Liu, Q., Gu, J., Khan, M. N., Sun, L., Wu, H., & Wu, H. (2024). Polyacrylic Acid-Coated Selenium-Doped Carbon Dots Inhibit Ferroptosis to Alleviate Chemotherapy-Associated Acute Kidney Injury. *Advanced Science*, *11*(28). https://doi.org/10.1002/advs.202400527

Li, X., Zheng, J., Chen, S., Meng, F., Ning, J., & Sun, S. (2021). Oleandrin, a cardiac glycoside, induces immunogenic cell death via the PERK/elF2α/ATF4/CHOP pathway in breast cancer. *Cell Death & Disease*, *12*(4). https://doi.org/10.1038/s41419-021-03605-y

Liu, L., Yao, H., Zhou, X., Chen, J., Chen, G., Shi, X., Wu, G., Zhou, G., & He, S. (2022). MiR-15a-3p regulates ferroptosis via targeting glutathione peroxidase GPX4 in colorectal cancer. *Molecular Carcinogenesis*, *61*(3), 301-310. https://doi.org/10.1002/mc.23367

Lobb, R. J., Jacobson, G. M., Cursons, R. T., & Jameson, M. B. (2018). The interaction of selenium with chemotherapy and radiation on normal and malignant human mononuclear blood cells. *International Journal of Molecular Sciences*, *19*(10). https://doi.org/10.3390/ijms19103167

Mahjabeen, I., Hussain, M. Z., Haq, M. F. U., Mehmood, A., Haris, M. S., Khan, S. A., Chaudhry, A., Hakim, F., Abbasi, A. Z., & Kayani, M. A. (2025). Exploring the role of mitochondrial sirtuin 3 gene in gastric cancer risk based on SNP analysis and LORD-Q assay. *Biochemical Genetics*. https://doi.org/10.1007/s10528-025-11119-x

Maia, A. L., Goemann, I. M., Meyer, E. L. S., & Wajner, S. M. (2011). Type 1 iodothyronine deiodinase in human physiology and disease: Deiodinases: the balance of thyroid hormone. *Journal of Endocrinology*, *209*(3), 283-297. https://doi.org/10.1530/JOE-10-0481

Manta, B., Makarova, N. E., & Mariotti, M. (2022). The selenophosphate synthetase family: A review. *Free Radical Biology & Medicine*, *192*, 63-76. https://doi.org/10.1016/j.freeradbiomed.2022.09.007

Mark, S. D., Qiao, Y.-L., Dawsey, S. M., Wu, Y.-P., Katki, H., Gunter, E. W., Fraumeni, J. F., Blot, W. J., Dong, Z.-W., & Taylor, P. R. (2000). Prospective study of serum selenium levels and incident esophageal and gastric cancers. *JNCI : Journal of the National Cancer Institute,*, *92*(21), 1753-1763. https://doi.org/10.1093/jnci/92.21.1753

Marshall, J. R., Burk, R. F., Ondracek, R. P., Hill, K. E., Perloff, M., Davis, W., Pili, R., George, S., & Bergan, R. (2017). Selenomethionine and methyl selenocysteine: Multiple-dose pharmacokinetics in selenium-replete men. *Oncotarget*, *8*(16), 26312-26322. https://doi.org/10.18632/oncotarget.15460

Medicine, N. L. o. (2025). *Lyases*. Retrieved 13/1/25 from https://www.ncbi.nlm.nih.gov/mesh?Db=mesh&Cmd=DetailsSearch&Term=%22Lyases%22%5BMeSH+Terms%5D

Mehdi, Y., Hornick, J. L., Istasse, L., & Dufrasne, I. (2013). Selenium in the environment, metabolism and involvement in body functions. *Molecules (Basel, Switzerland)*, *18*(3), 3292-3311. https://doi.org/10.3390/molecules18033292

Minch, W. B. (2022). Selenium metabolism and biosynthesis of selenoproteins in the human body. . *Biochemistry Moscow*, *87*(1), 369-390. https://doi.org/10.1134/S0006297922140139

Mishra, P., Pandey, C., Singh, U., Gupta, A., Sahu, C., & Keshri, A. (2019). Descriptive statistics and normality tests for statistical data. *Ann Card Anaesth*, *22*(1), 67-72. https://doi.org/10.4103/aca.ACA_157_18

Mojadadi, A., Au, A., Salah, W., Witting, P., & Ahmad, G. (2021). Role for selenium in metabolic homeostasis and human reproduction. *Nutrients*, *13*(9), 3256. https://doi.org/10.3390/nu13093256

Moskovich, D., Finkelshtein, Y., Alfandari, A., Rosemarin, A., Lifschytz, T., Weisz, A., Mondal, S., Ungati, H., Katzav, A., Kidron, D., Mugesh, G., Ellis, M., Lerer, B., & Ashur-Fabian, O. (2021). Targeting the DIO3 enzyme using first-in-class inhibitors effectively suppresses tumor growth: a new paradigm in ovarian cancer treatment. *Oncogene*, *40*(44), 6248-6257. https://doi.org/10.1038/s41388-021-02020-z

Namba, T., Ishihara, T., Tanaka, K., Hoshino, T., & Mizushima, T. (2007). Transcriptional activation of ATF6 by endoplasmic reticulum stressors. *Biochemical and Biophysical Research Communications*, *355*(2), 543-548. https://doi.org/10.1016/j.bbrc.2007.02.004

National Cancer Institue. (2021). *What is Cancer?* Retrieved 27/4/2025 from https://www.cancer.gov/about-cancer/understanding/what-is-cancer

National institutes of Health. (2024). *Selenium* Retrieved 12/1/25 from https://ods.od.nih.gov/factsheets/Selenium-HealthProfessional/#en13

Nelli, F., Ruggeri, E. M., Schirripa, M., Virtuoso, A., Giannarelli, D., Raso, A., Remotti, D., & Fabbri, A. (2024). Longitudinal assessment of FT3 to FT4 conversion ratio in predicting the efficacy of first-line pembrolizumab-based therapy in advanced non-small cell lung cancer: a propensity-score matching analysis of data from the national drug monitoring agency. *Current Oncology*, *12*(31), 7647-7662. https://doi.org/10.3390/curroncol31120564

Nilsen, J., Trabjerg, E., Grevys, A., Azevedo, C., Brennan, S. O., Stensland, M., Wilson, J., Sand, K. M. K., Bern, M., Dalhus, B., Roopenian, D. C., Sandlie, I., Rand, K. D., & Andersen, J. T. (2020). An intact C-terminal end of albumin is required for its long half-life in humans. *Communications Biology*, *3*(1). https://doi.org/10.1038/s42003-020-0903-7

Obertová, Z., Scott, N., Brown, C., Stewart, A., & Lawrenson, R. (2015). Survival disparities between Māori and non-Māori men with prostate cancer in New Zealand. *BJU International*, *115*(S5), 24-30. https://doi.org/10.1111/bju.12900

Olivier, M., Hollstein, M., & Hainaut, P. (2010). TP53 mutations in human cancers: origins, consequences, and clinical use. *Cold Spring Harbor Perspectives in Biology*, *2*(1). https://doi.org/10.1101/cshperspect.a001008

Park, S. M., Kang, T. I., & So, J. S. (2021). Roles of XBP1s in transcriptional regulation of target genes. *Biomedicines*, *9*(7), 791-817. https://doi.org/10.3390/biomedicines9070791

Pei, J., Pan, X., Wei, G., & Hua, Y. (2023). Research progress of glutathione peroxidase family (GPX) in redoxidation. *Frontiers in Pharmacology*, *14*. https://doi.org/10.3389/fphar.2023.1147414

Pierantoni, F., Dionese, M., Basso, U., Lai, E., Cavasin, N., Erbetta, E., Mattana, A., Bimbatti, D., Zagonel, V., Lonardi, S., & Maruzzo, M. (2023). The prognostic Value of thyroid hormone levels in immunotherapy-treated patients with metastatic urothelial carcinoma. *Clinical Genitourinary Cancer*, *5*(21), 378-385. https://doi.org/10.1016/j.clgc.2023.04.006

Qiao, Y.-L., Dawsey, S. M., Kamangar, F., Fan, J.-H., Abnet, C. C., Sun, X.-D., Johnson, L. L., Gail, M. H., Dong, Z.-W., Yu, B., Mark, S. D., & Taylor, P. R. (2009). Total and cancer mortality after supplementation with vitamins and minerals: follow-up of the Linxian general population nutrition intervention trial. *JNCI : Journal of the National Cancer Institute,*, *101*(7), 507-518. https://doi.org/10.1093/jnci/djp037

Rataan, A. O., Geary, S. M., Zakharia, Y., Rustum, Y. M., & Salem, A. K. (2022). Potential role of selenium in the treatment of cancer and viral infections. *International Journal of Molecular Sciences 23*(2). https://doi.org/10.3390/ijms23042215

Rayman, M. P. (2012). Selenium and human health. *The Lancet 379*(9822), 1256-1268. https://doi.org/10.1016/S0140-6736(11)61452-9

Rayman, M. P., Winther, K. H., Pastor-Barriuso, R., Cold, F., Thvilum, M., Stranges, S., Guallar, E., & Cold, S. (2018). Effect of long-term selenium supplementation on mortality: Results from a multiple-dose, randomised controlled trial. *Free Radical Biology & Medicine*, *127*, 46-54. https://doi.org/10.1016/j.freeradbiomed.2018.02.015

Reid, M. E., Duffield-Lillico, A. J., Slate, E., Natarajan, N., Turnbull, B., Jacobs, E., Combs, G. F. J., Alberts, D. S., Clark, L. C., & Marshall, J. R. (2008). Nutritional prevention of cancer: 400 mcg Per day selenium treatment. *Nutrition and Cancer*, *60*(2), 155-163. https://doi.org/10.1080/01635580701684856

Ren, Z.-X., Yu, H.-B., Li, J.-S., Shen, J.-L., & Du, W.-S. (2015). Suitable parameter choice on quantitative morphology of A549 cell in epithelial–mesenchymal transition. *Bioscience Reports*, *35*(3). https://doi.org/10.1042/BSR20150070

Renart, J., Reiser, J., & Stark, G. R. (1979). Transfer of proteins from gels to diazobenzyloxymethyl-paper and detection with antisera: a method for studying antibody specificity and antigen structure.

Proceedings of the National Academy of Sciences - PNAS, *76*(7), 3116-3120. https://doi.org/10.1073/pnas.76.7.3116

Rodriguez-Ruiz, A., Braun, D., Pflug, S., Brol, A., Sylvester, M., Steegborn, C., & Schweizer, U. (2022). Insights into the mechanism of human deiodinase 1. *International Journal of Molecular Sciences*, *23*(10). https://doi.org/10.3390/ijms23105361

Ron, D., & Habener, J. F. (1992). CHOP, a novel developmentally regulated nuclear protein that dimerizes with transcription factors C/EBP and LAP and functions as a dominant-negative inhibitor of gene transcription. *Genes & Development*, *6*(3), 439–453. https://doi.org/10.1101/gad.6.3.439

Russo, S. C., Salas-Lucia, F., & Bianco, A. C. (2021). Deiodinases and the metabolic code for thyroid hormone action. *Endocrinology (Philadelphia)*, *162*(8). https://doi.org/10.1210/endocr/bqab059

Ryoo, H. D. (2016). Long and short (timeframe) of endoplasmic reticulum stress-induced cell death. *The FEBS Journal*, *238*(20), 3718-3722. https://doi.org/10.1111/febs.13755

Ryuta, T., Min-Hyuk, Y., Noelia, F., Carlson., B. A., Soledad, C., Gladyshev., V. N., & Hatfield, D. L. (2012). Thioredoxin reductase 1 deficiency enhances selenite toxicity in cancer cells via a thioredoxin-independent mechanism. *Biochem J*, *445*(3), 423-430. https://doi.org/10.1042/BJ20120618

Saito, Y. (2021). Selenium transport mechanism via selenoprotein P—its physiological role and related diseases. *Frontiers in Nutrition (Lausanne)*, *8*. https://doi.org/10.3389/fnut.2021.685517

Schrauzer, G. N. (2000). Selenomethionine: a review of Its nutritional significance, metabolism and toxicity. *The Journal of Nutrition*, *130*(7), 1653–1656. https://doi.org/10.1093/jn/130.7.1653

Seemann, S., & Hainaut, P. . (2005). Roles of thioredoxin reductase 1 and APE/Ref-1 in the control of basal p53 stability and activity. *Oncogene*, *24*(24), 3853-3863. https://doi.org/10.1038/sj.onc.1208549

Sekhar, K. R., Hanna, D. N., Cyr, S., Baechle, J. J., Kuravi, S., Balusu, R., Rathmell, K., & Baregamian, N. (2022). Glutathione peroxidase 4 inhibition induces ferroptosis and mTOR pathway suppression in thyroid cancer. *Scientific Reports*, *12*(1), 1-10. https://doi.org/10.1038/s41598-022-23906-2

Shetty, S. P., Kiledjian, N. T., & Copeland, P. R. (2022). The selenoprotein P 3' untranslated region is an RNA binding protein platform that fine tunes selenocysteine incorporation. *PloS One*, *17*(7). https://doi.org/10.1371/journal.pone.0271453

Sudhadevi, T., & Harijith, A. (2024). Thioredoxin: an antioxidant, a therapeutic target and a possible biomarker. *Pediatric Research*, *96*(5), 1117-1119. https://doi.org/10.1038/s41390-024-03370-6

Suzuki, M., Endo, M., Shinohara, F., Echigo, S., & Rikiishi, H. (2010). Differential apoptotic response of human cancer cells to organoselenium compounds. *Cancer chemotherapy and pharmacology*, *66*(3), 475-484. https://doi.org/10.1007/s00280-009-1183-6

TeWhatuOra. (2024). *Cancer Web Tool*. Retrieved 27/4/2025 from https://www.tewhatuora.govt.nz/for-health-professionals/data-and-statistics/cancer/data-web-tool

Thermo Fisher Scientific. (2020). *Cell Culture Basics Handbook*

Thomson, B. M., Vannoort, R. W., & Haslemore, R. M. (2008). Dietary exposure and trends of exposure to nutrient elements iodine, iron, selenium and sodium from the 2003–4 New Zealand Total Diet Survey. *British Journal of Nutrition*, *99*(3), 614-625. https://doi.org/10.1017/S0007114507812001

Tobe, R., & Mihara, H. (2018). Delivery of selenium to selenophosphate synthetase for selenoprotein biosynthesis. *Biochimica et Biophysica Acta. General Subjects,*, *1862*(11), 2433-2440. https://doi.org/10.1016/j.bbagen.2018.05.023

Turpin, J., Frumence, E., El Safadi, D., Meilhac, O., Krejbich-Trotot, P., & Viranaïcken, W. (2020). Improvement of immunodetection of the transcription factor C/EBP homologous protein by western blot. *Analytical Biochemistry*, *601*, 113775-113775. https://doi.org/10.1016/j.ab.2020.113775

Wallenberg, M., Misra, S., & Björnstedt, M. (2014). Selenium cytotoxicity in cancer. *Basic & Clinical Pharmacology & Toxicology*, *5*(114), 377-386. https://doi.org/10.1111/bcpt.12207

Wang, P., Chen, B., Huang, Y., Li, J., Cao, D., Chen, Z., Li, J., Ran, B., Yang, J., Wang, R., Wei, Q., Dong, Q., & Liu, L. (2023). Selenium intake and multiple health-related outcomes: an umbrella review of meta-analyses. *Frontiers in Nutrition (Lausanne)*, *10*. https://doi.org/10.3389/fnut.2023.1263853

Weaver, K., & Skouta, R. (2022). The selenoprotein glutathione peroxidase 4: from molecular mechanisms to novel therapeutic opportunities. *Biomedicines*, *10*(4), 891. https://doi.org/10.3390/biomedicines10040891

Wright, D. E., & O'Donoghue, P. (2023). Biosynthesis, engineering, and delivery of selenoproteins. *International Journal of Molecular Sciences*, *25*(1), 223. https://doi.org/10.3390/ijms25010223

Xia, S., Duan, W., Liu, W., Zhang, X., & Wang, Q. (2021). GRP78 in lung cancer. *Journal of Translational Medicine*, *19*(1), 118. https://doi.org/10.1186/s12967-021-02786-6

Yakes, F. M., & Van Houten, B. (1997). Mitochondrial DNA damage is more extensive and persists longer than nuclear DNA damage in human cells following oxidative stress. *Proceedings of the National Academy of Sciences - PNAS*, *94*(2), 514–519. https://doi.org/10.1073/pnas.94.2.514

Yoo, M.-H., Xu, X.-M., Carlson, B. A., Gladyshev, V. N., & Hatfield, D. L. (2006). Thioredoxin reductase 1 deficiency reverses tumor phenotype and tumorigenicity of lung carcinoma cells. *The Journal of Biological Chemistry*, *281*(19), 13005-13008. https://doi.org/10.1074/jbc.C600012200

Zakharia, Y., Garje, R., Brown, J., Nepple, K., Bellizzi, A., Bonner, J., Parr, D., Born, J., Sieren, J., Park, J., Milhem, M., & Rustum, Y. (2019). Results of phase I clinical trial of high doses of seleno-l-methionine (SLM) in sequential combination with axitinib in previously treated and relapsed clear cell renal carcinoma (ccRCC) patients. *Annals of Oncology*, *30*. https://doi.org/10.1093/annonc/mdz249.048

Zeng, R., Farooq, M. U., Zhang, G., Tang, Z., Zheng, T., Su, Y., Hussain, S., Liang, Y., Ye, X., Jia, X., & Zhu, J. (2020). Dissecting the potential of selenoproteins extracted from selenium-enriched rice on physiological, biochemical and anti-ageing effects In vivo. *Biological Trace Element Resaerch 196*(1), 119-130. https://doi.org/10.1007/s12011-019-01896-z

Appendix 1 Reagents

All reagents were prepared with MQ water (18.2 MΩ·cm) unless otherwise stated. All glassware was cleaned in the dishwasher. Autoclaving was carried out at 121°C for 15 minutes.

10X Phosphate buffer saline (PBS), pH 7.4
40 g NaCl
1g KCl
5.75 Na_2HPO_4
1 g KH_2PO_4

Dissolve all the ingredients in 500 mL MQ water.
Adjust pH to 7.4 with concentrated HCl
Bring to volume of 1000 mL
Autoclave

1X PBS
100 mL 10X PBS pH 7.4
900 mL MQ water
Autoclave

10X Tris-buffered saline (TBS) pH 7.6
24 g Tris base
88 g NaCl

Dissolve all the ingredients in 500 mL MQ water.
Adjust pH to 7.6 with concentrated HCl
Bring to volume of 1000 mL

1X TBS
100 mL 10X TBS pH 7.4
900 mL MQ water

1X Tris-buffered saline with Tween20 (TBST)
100 mL 10X TBS pH 7.4
900 mL MQ water
1 mL Tween20

Mild Stripping Buffer
15 g glycine
1 g SDS
10 mL Tween20

Dissolve all the ingredients in 500 mL MQ water.
Adjust pH to 2.2 with concentrated HCl

Bring to volume of 1000 mL

Freezing media see below box

REAGENT	VOLUME	FINAL CONCENTRATION
100% DMSO	5mL	10%
100% RMPI	20mL	40%
100% FCS	25mL	50%
FINAL VOLUME	50mL	

Appendix 2 DNA Data Analyses

	Conc (ng/µL)	A260 `	260/230	260/280
PT 25				
V1	12.928	0.2586	3.996	1.770
V2	26.798	0.5360	3.930	1.876
V3	-			
V4	63.060	1.2612	2.121	1.815
V5	-			
V6	-			
V7	13.591	0.2718	3.872	1.788
P26				
V1	32.700	0.6450	3.031	2.141
V2	19.893	0.3979	1.581	2.046
V3	21.009	0.4022	2.068	2.006
V4	20.836	0.4167	9.3818	1.874
V5	203.242	4.0648	2.461	1.837
V6	63.477	1.2695	2.238	1.842
V7	174.341	3.4868	2.463	1.85
Pt27				
V1	49.519	0.9904	2.963	1.875
V2	15.811	0.3162	0.651	1.999
V3	21.232	0.4287	0.503	1.729
V4	11.584	0.2317	0.664	2.286
V5	-			
V6	-			
V7	7.158	0.135	0.176	2.257
Pt28				
V1	25.260	0.5052	3.128	1.927
V2	39.459	0.7892	2.848	1.901
V3	43.387	0.8677	2.875	1.983
V4	42.253	0.8451	4.199	2.148
V5	19.373	0.3875	0.875	1.787
V6	35.853	0.7171	11.484	2.402
V7	31.460	0.6292	6.331	2.236
Pt29				

V1	25.315	0.5063	2.965	1.801
V2	49.066	0.9813	2.043	1.907
V3	194.279	3.8856	0.749	1.643
V4	28.130	0.5626	3.736	2.085
V5	42.466	0.8493	2.715	2.036
V6	61.467	1.2293	3.276	2.06
V7	38.275	0.7655	2.69	1.93
Pt30				
V1	37.027	0.7405	1.704	1.767
V2	19.760	0.3952	3.875	2.021
V3	-			
V4	79.246	1.5849	2.751	1.869
V5	40.029	0.8006	2.568	1.87
V6	55.200	1.104	2.605	1.884
V7	78.056	1.5611	2.404	1.866
Pt31				
V1	34.061	0.6812	1.43	1.828
V2	26.928	0.5386	2.488	1.849
V3	58.067	1.1613	2.314	1.887
V4	37.190	0.7438	2.063	1.818
V5	46.379	0.9276	2.876	1.869
V6	39.919	0.7984	2.827	1.894
V7	44.199	0.884	2.769	1.88
Pt32				
V1	46.217	0.9243	0.83	1.675
V2	24.177	0.4835	3.341	1.93
V3	138.192	2.7638	1.574	1.78
V4	11.723	0.2345	1.696	2.023
V5	36.595	0.7319	2.558	1.856
V6	32.014	0.6403	2.484	1.857
V7	54.371	1.0874	1.987	1.818
Pt33				
V1	7.501	0.15	-8.784	2.129
V2	36.027	0.7205	2.747	1.85
V3	13.502	0.27	21.623	1.85
V4	40.524	0.8105	3.062	1.911
V5	11.609	0.2322	1.937	1.825
V6	37.123	0.7425	3.091	1.912

V7	58.971	1.1794	2.69	1.914

Appendix 3 Copyright Declaration